BIOMECHANICS AND ELECTROMYOGRAPHY IN ASSESSING FEMALE STRESS URINARY INCONTINENCE

A Dissertation

Presented to

the Faculty of the Department of Biomedical Engineering

University of Houston

In Partial Fulfillment

of the Requirements for the Degree

Doctor of Philosophy

In Biomedical Engineering

By

Yun Peng

December 2016

BIOMECHANICS AND ELECTROMYOGRAPHY IN

ASSESSING FEMALE STRESS URINARY INCONTINENCE

Yun Peng

Approved:

Chair of the Committee
Yingchun Zhang, Assistant Professor,
Department of Biomedical Engineering

Committee Members:

Timothy B. Boone, Professor,
Department of Urology
Houston Methodist Hospital

Kirill Larin, Professor,
Department of Biomedical Engineering

Nuri Ince, Assistant Professor,
Department of Biomedical Engineering

Ahmet Omurtag, Associate Professor,
Department of Biomedical Engineering

Suresh K. Khator, Associate Dean,
Cullen College of Engineering

Metin Akay, Professor and Chair,
Department of Biomedical Engineering

ACKNOWLEDGEMENT

Foremost, I would like to express the deepest appreciation to my PhD supervisor, Dr. Yingchun Zhang, for this continuous guidance and encouragement to me, which makes the completion of this dissertation possible. In retrospect, I have a very fruitful PhD career experience, both in academic achievements and personal development. I greatly appreciate this opportunity and am very grateful to him for his great trust to recruit me in his team.

I would like to thank my committee members, Dr. Timothy Boone, Dr. Kirill Larin, Dr. Nuri Ince and Dr. Ahmet Omurtag, for their advices and comments on this dissertation, as well as critical questions incented to widen my research from various perspectives.

I would also like to thank a number of our collaborators at local hospitals and institutes, Dr. Rose Khavari from Houston Methodist Hospital, and Dr. Ping Zhou and Dr. Sheng Li from University of Texas Health and many others, for their technical assistances in our collaboration experiments and insightful inputs to our data analysis and manuscript preparation.

I have received a great amount of support from my department, the Biomedical Engineering, as well as its enthusiastic and friendly staffs, who have always been very informative and helpful whenever I met difficulties during my PhD life. I also greatly appreciate Cullen College of Engineering and the graduate school at University of Houston, and the Simon Foundation, for their generous financial support for my academic travels.

My special thanks to all the friends that I made at Houston – my PhD life would never be so interesting without you.

Finally, and most importantly, my sincere thanks to my wife Tiantian Zhang, for her presence in my life, which I will always treasure.

BIOMECHANICS AND ELECTROMYOGRAPHY IN

ASSESSING FEMALE STRESS URINARY INCONTINENCE

An Abstract

of a

Dissertation

Presented to

the Faculty of the Department of Biomedical Engineering

University of Houston

In Partial Fulfillment

of the Requirements for the Degree

Doctor of Philosophy

in Biomedical Engineering

by

Yun Peng

December 2016

ABSTRACT

Introduction

Stress urinary incontinence (SUI), the involuntary urinary leakage associated with increases in intra-abdominal pressure, has a prevalence of 25–50% in U.S. women and the number of those who will undergo surgery will increase by half in the next forty years. SUI negatively affects the patient's quality of life and places a great burden to the society. The functional anatomy of the continence mechanism remains vaguely understood. Hence my dissertation aims at offering a complete description of the pelvic floor muscles (PFM), the key contributor to the continence, thorough biomechanical and neurophysiological approaches.

Methods

The biomechanical approach involves the development of a subject-specific finite element (FE) model of the female pelvic floor region. Subsequent computer simulations are targeted at finding the most contributive muscle to the urethral support function and evaluating current treatment strategies using a mini-sling. The neurophysiological approach involves the implementation of a novel surface electromyography (EMG) probe to acquire bioelectrical information of PFMs and the assessment of their innervations in healthy subjects and patients.

Results

An FE pelvic floor model was developed which incorporates 40+ anatomical structural in the pelvis, representing the most complete model in the field. Simulation results showed that the vaginal walls, puborectalis, and pubococcygeus are the most important structures and that mid-distal post-urethral implantation represents the optimal location. Innervation zones of PFMs have been successfully identified and described for multiple PFMs. An high-density surface EMG-based motor unit number estimation approach was developed, providing a novel tool to evaluate the condition of neurologically impaired PFM.

Conclusions

The combined information greatly advances our understanding of the physiology of PFM and would lay a firm foundation to novel, non-invasive, patient-specific interventional strategies in the future.

TABLE OF CONTENTS

LIST OF FIGURES

LIST OF TABLES

CHAPTER 1 – Introduction

1.1 Background

Urinary incontinence (UI) is defined as the complaint of any involuntary leakage of urine, according to the International Conference Society (Abrams et al., 2002). It is a worldwide problem that mainly affects women of all ages and across different cultures and races (Minassian, Drutz, & Al-Badr, 2003). Stress urinary incontinence (SUI), defined as the complaint of involuntary urinary leakage on effort or exertion, or on sneezing or coughing, is the most common subtype of UI. Survey data from the U.S. National Health and Nutrition Examination Survey showed that 49.6% of women reported UI, with 49.8% reporting pure SUI and 34.4% reporting mixed UI (Dooley et al., 2008). This concurs with another report that about 50% of women with UI reported SUI as the primary or sole symptom of incontinence (Hunskaar et al., 2005).

Though not a life-threatening condition, SUI not only places significant financial, social and psychological burdens on individual patients and cause a great burden to the health care system. A recent study reported an annual direct cost of $12 billion specifically for female incontinence annually, with SUI accounting for 82% of the total cost (Chong, Khan, & Anger, 2011). This exceeds that on breast cancer ($8.9 billion) and rivals that of osteoporosis ($13.8 billion).

Major recognized risk factors associated with SUI include mid-age, white race, obesity, pregnancy, and vaginal delivery (Imamura et al., 2010; Minassian, Stewart, & Wood, 2008; Nygaard & Heit, 2004; Rogers, 2008). Other potential risk factors include smoking, thyroid disease, diabetes, stroke, asthma, caffeine intake, and congestive heart failure (Minassian et al., 2008; Nygaard & Heit, 2004; Peyrat et al., 2002). The cause of SUI is thought to be multifactorial (Daneshgari & Moore, 2006). Over the last century, a number of theories have been proposed to describe the pathophysiology of SUI and signicantly improved its clinical management.

1.2 A Historical Overview of SUI Theories

A well-summarized historical review of these concepts can be found in recent works of Daneshgari and Moore (2006) and DeLancey (2010).

Early theories about SUI focused on a lack of urethral compression efforts associated with altered urethral position. In 1912, Kelly described the open vesical neck and reported successful results of an operation to plicate the vesical neck (Kelly & Dumm, 1914). A decade later, Bonney observed abnormal displacement of the anterior vaginal wall in incontinent women and proposed loss of urethral support as the cause of stress incontinence (Bonney, 1923), crediting the success of Kelly's operation to the improved urethral support instead of an enhanced vesical neck closure. These primitive concepts were later popularized in 1962 by Enhorning (Enhorning, 1961), who studied the intraurethral and intravesical pressures in continent and incontinent women and hypothesized that the urethra must be located above the pelvic floor to allow the pressure transmitted to the bladder to be equally transmitted to the urethra, leading to a compensatory increase in closure pressure and maintain continence. This pressure transmission theory led to a prevailing view that SUI is based on an alteration in urethral angles; however, the underlying mechanism responsible for the altered urethral angle remained unclear. The concept of "hypermobility", altered urethral angles caused by paravaginal defects, was introduced by Richardson (Richardson, Lyon, & Williams, 1976) and led to later surgical success (RICHARDSON, EDMONDS, & WILLIAMS, 1981).

The integral theory (Petros & Ulmsten, 1990), as illustrated in Figure 1.1, and the hammock hypothesis (DeLancey, 1994), as illustrated in Figure 1.2, represented the two most popular theories in the modern urology. These two theories are not mutually exclusive and in fact shared a lot in common – both supported that supportive structures surrounding the urethral are pivotal in persevering urinary continence. The former theory stressed on the role of paravaginal laxity in SUI, which may be caused by defects within the vaginal wall itself, or its supporting structures including ligaments, muscles, and their connective tissue insertions, while the latter one credited the urethral support to the endopelvic fascia and anterior vaginal wall, which are stabilized through lateral attachments with the arcus tendineous fascia and levator ani muscle – all together

formed a rigid support against which the urethra can be compressed under increased intra-abdominal pressure to properly close.

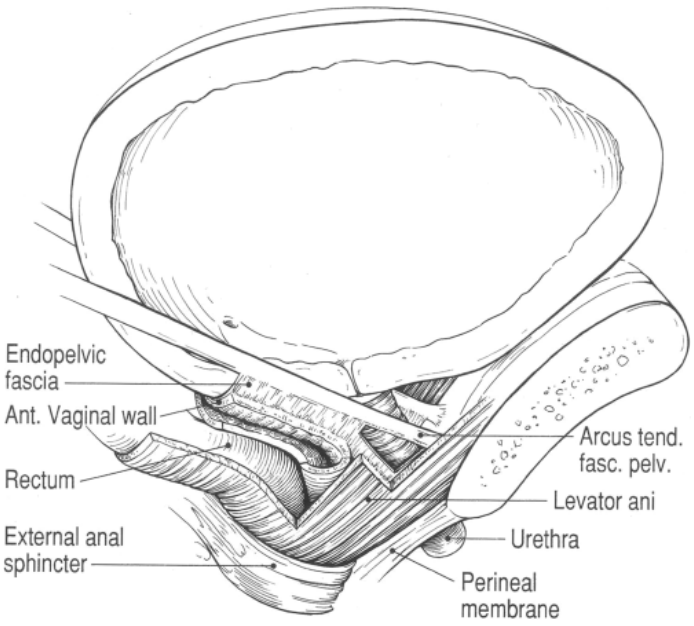

Figure 1.1 (The hammock theory) Lateral view of the components of the urethral support system. Reproduced from ASHTON-MILLER and DeLANCEY (2007), with permission of John Wiley and Sons.

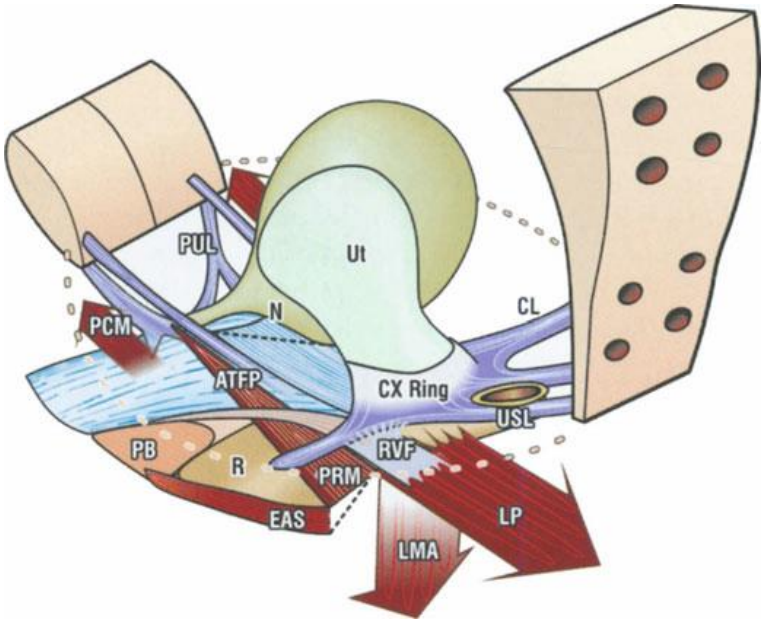

Figure 1.2 (The integral theory) Fascial attachments and tensioning mechanism. Reproduced from Petros (2011), with permission of Springer.

1.3 Current Approaches in SUI Research

Stress urinary incontinence has a clear definition and can be accurately diagnosed with the propose use of patient history, cystometry, urodynamics and pelvic floor examination (Garely & Noor, 2014). Although current theories have pointed out that paravaginal defects and intrinsic closure system defects are majorly responsible for SUI, there has been a lack of efforts to quantitatively assess the roles of relevant structures to the urethral support, possibly because of the complexity of female pelvis and thereby a lack of competent tools to non-invasively and comprehensively evaluate the interactions of multiple structures inside the female pelvis as well as their connection to SUI.

Traditional medical imaging techniques such as the magnetic resonance (MR) imaging (Derpapas, Digesu, Fernando, & Khullar, 2011; Itani et al., 2016) and ultrasonography (Derpapas et al., 2011; Hans Peter Dietz, 2010) have played a significant role in the diagnosis and treatment of a range of pelvic floor disorders. The strengths of these imaging tools are that they can provide a great amount of anatomical information that can be useful for investigating the relation between SUI and morphological abnormalities. For example, urethral mobility is often viewed as a useful marker for assessing weakened urethral support. When a urethra is well supported, any force applied to the urethra and bladder as a result of increased intra-abdominal pressure during activities can be effectively balanced by the posterior urethral support structures, leading to an effective urethral closure. The amount of mobility can be quantified by a simple cotton-swab test (or Q-tip test) with urethral mobility resulting in a straining angle of greater than 30° considered as hypermobile; however this test is often disliked by women because of the uncomfortable insertion (Garely & Noor, 2014). An alternative approach can be performed with the transperineal ultrasonography, which presents the advantage of allowing the visualization of the entire lower urogenital tract, including the pelvic floor and of guaranteeing a dynamic assessment of the pelvis during muscular contraction. A number of investigators have employed this approach to study the relation of urethral mobility to parity status (S. Costantini et al., 2005), reproducibility and the urethral mobility between control and SUI patients (Pregazzi et al., 2002), correlation between urodynamics and ultrasound (Minardi et al., 2007) and implanted sling performance (Kociszewski

et al., 2010; Kociszewski et al., 2008). Magnetic resonance imaging has also been widely used to study the relation of morphology of the levator ani muscle, endopelvic fascia and urethra in women with SUI (Heilbrun et al., 2010; Tunn et al., 2006). However, when the main limitation of medical imaging tools is that, to assess urethral hypermobility caused by isolated impairment of each specific urethral support structure and to compare components' relative contribution to urethral support function, it would require the recruitment of patients with only one impairment condition, which is clinically challenging to identify. Cross-subject differences in female pelvic floor anatomy also affect the objectivity of the comparison.

Electromyography (EMG) is a technique commonly used in neurophysiologic diagnosis. By recording the bioelectrical activities associated with action potentials during muscle fiber activation, it provides useful information in many aspects of the neurophysiology of the neuromuscular system. However, EMG has seldom been used in the routine assessment of pelvic floor muscle functions because of the invasive and painful nature of concentric needle EMG (Osman, Marzi, Cornu, & Drake, 2016). As an alternative, intravaginal or intrarectal surface EMG probes have been gaining an increasing popularity in urology practice. However, a recent review showed that currently available intravaginal probes had deficiencies in design parameters including probe geometry, electrode size, location, and/or configuration and called for the development of improved intravaginal EMG probes for research and clinical use (Keshwani & McLean, 2015).

1.4 Hypothesis and Specific Aims

Based on these considerations, the topics presented in this dissertation are majorly novel solutions to current research in urology as it relates to SUI. The central hypothesis of this dissertation is that the urethrovaginal support can be minimally invasively and quantitatively assessed and characterized using a subject-specific pelvic electromechanical modeling approach.

The first hypothesis is that the urethrovaginal support function in women can be non-invasively and quantitatively assessed using a subject-specific biomechanical pelvic modeling approach.

The second hypothesis is that the neuromuscular functions of pelvic floor muscles in women can be minimally invasively and quantitatively assessed using a subject-specific electrophysiological pelvic modeling approach. Two specific aims are proposed to test these hypotheses. The first specific aim is to develop a subject-specific biomechanical pelvic model based on high resolution MR images. Within this specific aim, the relative contribution of multiple urethral supporting structures will be assessed and compared and the dynamic behavior of an implanted suburethral mini-sling will be evaluated. The second specific aim is to develop a subject-specific electrophysiological pelvic model based on high-density surface EMG recordings of pelvic floor muscles. Within this aim, novel intravaginal and intrarectal EMG probes will be developed to describe the innervation of pelvic floor muscles and characterize their motor unit properties.

The proposed research is innovative because it represents the first effort to minimally invasively and quantitatively assess both urethral function and urethrovaginal support, common etiological factors associated with female SUI. With the successful completion of these two specific aims, new insights into the etiology of female SUI will be obtained and provide useful guidance for future diagnosis and management of this condition.

1.5 Arrangement of Chapters

Following the proposed hypotheses and specific aims, the rest of this dissertation is arranged as follows:

In the first part of the dissertation, chapter 1-3 describe the development of the subject-specific biomechanical pelvic model based on high-resolution MR images (Chapter 1) and its applications in single-incision sling treatment (Chapter 2) and young female athletic incontinence (Chapter 3).

In the second part of the dissertation, chapter 4-5 describe the development of the subject-specific electrophysiological pelvic model using novel intravaginal and intrarectal high-density surface EMG probes (Chapter 4) and the development of a novel motor unit number estimation approach (Chapter 5), which lays the foundation to further application to pelvic floor muscles.

Lastly, in Chapter 6, a summary of this dissertation is provided and suggestions for future research directions are made.

CHAPTER 2 – Development of a Subject-Specific Biomechanical Pelvic Model

2.1 Abstract

Introduction and Hypothesis: This study aims to assess the role of individual anatomical structures and their combinations to urethral support function. Methods: A realistic pelvic model was developed from an asymptomatic female subject's MR images for dynamic biomechanical analysis using the finite element method. Validation was performed by comparing simulation results with dynamic MR imaging observations. Weaknesses of anatomical support structures were simulated by reducing their material stiffness. Urethral mobility was quantified by examining the urethral axis excursion from rest to the final state (Intra-abdominal pressure = 100cmH2O). Seven individual support structures and five of their combinations were studied. Result: Among seven urethral support structures, weakening the vaginal walls, puborectalis muscle and pubococcygeus muscle generated the top three largest urethral excursion angles. A linear relationship was found between urethral axis excursions and intra-abdominal pressure. Weakening all three levator ani components together caused a larger weakening effect than the sum of each individually weakened component, indicating a nonlinearly-additive pattern. The pelvic floor responded to different weakening conditions distinctly: weakening the vaginal wall developed urethral mobility through collapsed vaginal canal while weakening the levator ani showed a more uniform pelvic floor deformation. Conclusions: The computational modeling and dynamic biomechanical analysis provides a powerful tool to better understand the dynamics of the female pelvis under pressure events. The vaginal walls, puborectalis and pubococcygeus are the most important individual structures in providing urethral support. The levator ani muscle group provides urethral support in a well-coordinated way with a nonlinearly-additive pattern.

2.2 Introduction

Lack of urethral support due to weakness in various components of the urethral support system (USS) has been considered as the main etiologic factor causing stress urinary

incontinence (SUI) (DeLancey, 1994). The “hammock hypothesis” describes support of the urethra by a coordinated action of fasciae and muscles, which provides a hammock onto which the urethra is compressed during increases in intra-abdominal pressure (IAP) (DeLancey, 1994). In a broad sense, the USS includes the levator ani muscle, vaginal wall and connective tissues that are extrinsic to the urethra, as well as the coccygeus muscle, obturator internus muscle, piriformis muscle and pelvic organs such as the rectum and uterus, as all these structures reside in the female pelvis and interact intimately during pressure events to support the urethra.

Many studies have investigated the pathophysiology of SUI through medical imaging techniques such as ultrasonography (Sendag et al., 2003), anatomical magnetic resonance (MR) imaging (Heilbrun et al., 2010) and dynamic MR imaging (Del Vescovo et al., 2014). To assess urethral hypermobility caused by isolated impairment of each specific USS component and to compare the components’ relative contribution to urethral support function would require the recruitment of patients with only one impairment condition, which is clinically challenging to identify. Cross-subject differences in female pelvic floor anatomy also affect the objectivity of the comparison. Computer modeling using MR images and simulation using the finite element method (FEM) have been widely used in biomedical research (Peng et al., 2014; S. Wang et al., 2014). This approach is able to conveniently simulate various impairment conditions and keep these comparisons based on the same subject (Y. Peng et al., 2015; Y. Zhang, Kim, Erdman, Roberts, & Timm, 2009). Several computer models developed from MR images have been reported recently in studies of female pelvic floor dysfunctions such as pelvic organ prolapse (Z. W. Chen et al., 2015; Luo, Chen, Fenner, Ashton-Miller, & DeLancey, 2015; Ren, Xie, Wang, & Rong, 2015), childbirth related levator ani muscle damages (D. Jing, J. A. Ashton-Miller, & J. O. DeLancey, 2012a) and ligament impairment (S. Brandao et al., 2015). However, the clinical application of these models and their comparisons to the true dynamic response of the pelvis is limited due to either 1) missing or simplified important anatomical structures (e.g., the bladder, rectum, vaginal canal, uterus are not included (Jing et al., 2012a); buffering fatty tissues are not included) or 2) less accurate realization of boundary conditions (e.g., direct inferior displacement is applied on the uterus (Z. W. Chen et al., 2015); intra-abdominal pressure is directly applied on

the muscle (S. Brandao et al., 2015) or vaginal wall (Luo et al., 2015) that are studied). A comprehensive pelvic model, which incorporates 44 anatomical structures in the female pelvis to maintain the integrity of the natural pelvic anatomy, was developed in this study to better understand the role of individual structures and their combination on urethral support in women.

2.3 Materials and Methods

A 21-year-old healthy female subject (nulliparous, non-smoker, BMI=22) was recruited according to a protocol approved by the Institutional Review Boards (IRBs) of the University of Minnesota and the University of Houston, for a high-resolution pelvic MRI scan in the supine position at rest with a 3T MRI scanner (Trio Tim, Siemens, Germany) (slice thickness 3mm; matrix 320 × 160; field of view 430mm; pixel size 1.344mm). For validation purposes, dynamic MR images were acquired in the mid-sagittal plane approximately every 1.5 second while the subject performed several Valsalva maneuvers.

Image segmentation was first performed on the axial MR images for each anatomical pelvic structure with the guidance of urologists using Mimics 11.0 (Materialise Group, Leuven, Belgium). The closed surfaces were reconstructed for each anatomical structure and exported in STL (Stereolithography) format. Those surfaces were imported into MAYA 8.5 (Autodesk, Inc., San Rafael, CA) and Rhinoceros 4.0 (McNeel North America, Seattle, WA) for artifact smoothing and intersecting surface correction and then converted into solid SAT (Standard ACIS Text) geometries. All solid geometries were discretized into finite element meshes with a total number of 126,378 tetrahedral elements in ABAQUS 6.12 (SIMULIA, Providence, RI). The final 3D pelvic model contains 44 anatomical parts including pelvic muscles, sphincteric muscles, ligaments, bones, fat, bladder, urethra, uterus, vagina, deep perineal pouch, colon, rectum and anus. In addition, a bodyfill part was created to fill the intra-abdominal space for pressure transmission. A stiff Q-tip swab part was placed in the urethra to simulate the Q-tip swab that has been frequently used in clinical diagnosis and research for SUI (Crystle, Charme, & Copeland, 1971; Ghoniem et al., 2008). Figure 2.1 illustrates the reconstructed 3D pelvic model. The bottom of the model was restrained from both translations and rotations. Two uniformly distributed pressures were applied

on the front and top surfaces of the bodyfill to simulate Valsalva. The IAP was calculated as the averaged contact pressure between the urine and inner bladder wall.

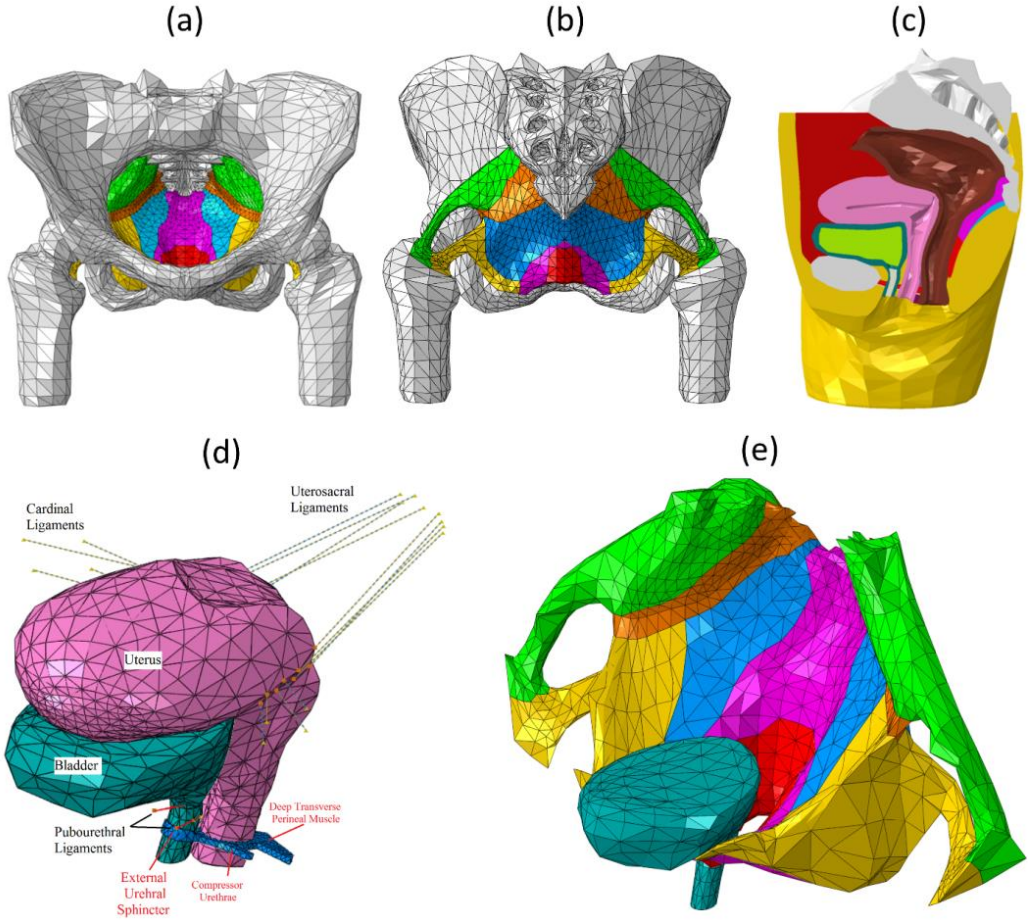

Figure 2.1 Illustrations of finite element pelvic floor models. Reproduced from Peng, Khavari, Nakib, Boone, and Zhang (2016), with permission of Springer.

Although soft tissues show viscoelastic behavior (Dai, Peng, Mansy, Sandler, & Royston, 2014; Q. Wang et al., 2014; Zhou, Peng, Bai, & Rosandich, 2014), a previous study found quasi-linear material property of urological soft tissues when the stress level is under 70% of the maximal stress value (Y. Zhang, Kim, et al., 2009). As such, soft tissues involved in the pelvic model were modeled as linear elastic solids using material properties from Young's moduli of the bladder, urethra, uterus, rectum, muscle, ligament and vaginal tissue (0.05, 0.03, 0.05, 0.1, 2.4, 1.2 and 7.4e-3 *MPa*) (Y. Peng et al., 2015). A soft material (Young's modulus of 0.04*MPa*) was assigned to the bodyfill part. Urine was modeled as an elastic liquid with a Young's modulus of

1.0e-3*MPa*. All soft tissues were considered incompressible considering that they contain abundant water. The bony pelvis was modeled as one rigid and fixed structure considering its negligible deformation under normal pelvic functions due to its much higher stiffness compared with soft tissues (S. Brandao et al., 2015). A simplifying condition was made to not include the voluntary contraction of the pelvic muscles, as it is often the case that, unless the female is trained using pelvic floor physical therapy, the female pelvic floor responds to acute increase of intra-abdominal pressure without voluntary contractions, such as during coughing or sneezing.

The general contact algorithm in ABAQUS was applied to mimic the natural interaction between parts that are in contact but anatomically independent, such as the bladder and uterus, the uterus and rectum, or the pelvic muscles and fatty tissues. Tie constraints in ABAQUS that binds two shared surfaces were used to couple motions of parts which are biologically connected (e.g., the coccygeus muscle and the coccyx) and to model the connecting effects of fasciae (e.g., the tendineous arch of levator ani muscle between the iliococcygeus muscle and the obturator internus muscle). Connector elements, with the ability to model connective tissues such ligaments (Luo et al., 2015), were employed in this study to model the uterosacral and cardinal ligaments. The Abaqus/Explicit solver was used for finite element method implementation.

A validation study was first performed by comparing the pelvic floor configurations achieved in computer simulation results with dynamic MR imaging observations along the mid-sagittal plane at both rest and maximal Valsalva maneuver (Figure 2.2). The subject was instructed on how to perform a Valsalva maneuver for the dynamic MR imaging and asked to hold each Valsalva maneuver for at least 2 seconds. During Valsalva maneuver, the abdominal muscles were contracted. Special attention was paid to the motions of the bladder, urethra, uterus and rectum. The results showed that the bladder, uterus and rectum slide in a posterior direction under the elevated IAP. It was also observed that the increased IAP led to bladder neck descent and clockwise rotation of the urethra, both of which are important landmarks commonly used in assessing urethral supports. The achieved consistency demonstrated the competence of the computer modeling and simulation method in characterizing pelvic floor responses to increased IAP.

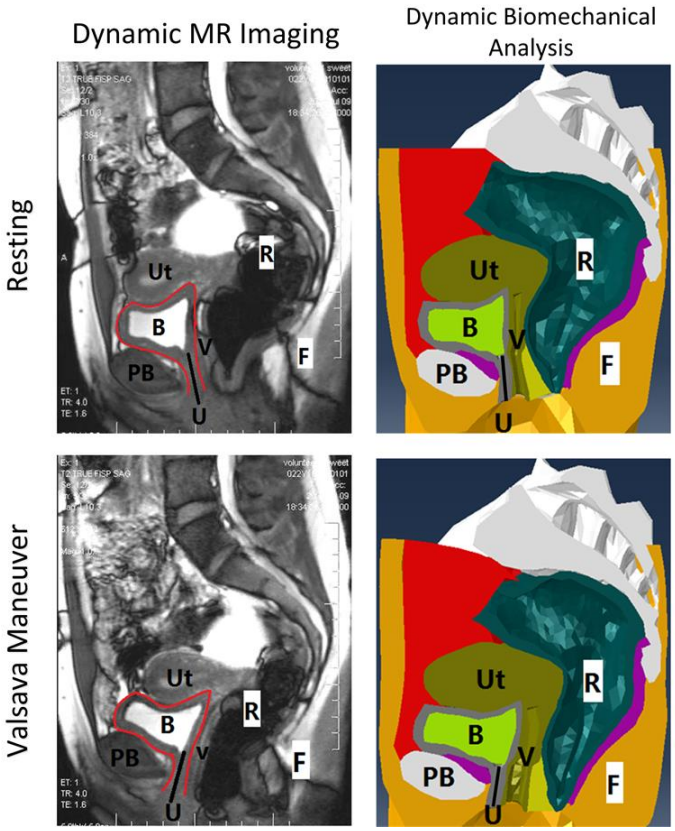

Figure 2.2 Comparison (dynamic MR imaging vs. biomechanical analysis) of the pelvic structures of the female subject in the sagittal plane, at resting stage and at Valsalva stage. Reproduced from Y. Peng, R. Khavari, et al. (2016), with permission of Springer.

The plan of simulation used in this study is listed in Table 2.1. The first two columns list the test numbers and weakened parts with their abbreviations in brackets. The impairment of each structure was simulated by reducing the stress-strain response by 90% (S. Brandao et al., 2015). Test00 serves as the asymptomatic control test based on the intact model in which no impairment was present. In each test from 01 to 07, a single USS component was weakened (hereafter referred to as single tests); in each test from 08 to 12, a specific group of USS components was weakened (hereafter referred to as group tests. Weakening the levator ani muscle was considered as a group test because the levator ani muscle group is composed of three individual muscle components. SUI is often associated with urethral hypermobility. Transperineal ultrasound reveals that the alpha-angle, defined as the angle between the vertical axis and the urethral axis (Sendag et al., 2003), was significantly different on straining ($P<0.05$) between the study (SUI)

and control groups. In this study, the alpha angle was monitored from the onset of the simulation to the final status, at which the IAP reached 100cmH_2O (Cobb et al., 2005). The urethral excursion angle, defined by the corresponding change in the α-angle ($\Delta\alpha$) and mathematically equal to the Q-tip excursion in clinical tests (Ghoniem et al., 2008), was also monitored as an alternative metric to examine the urethral support function in this study. Since the α-angle at rest showed no significant difference (P=0.650) between SUI and control groups (Sendag et al., 2003) and only the urethral support loss attributed to the weakness of specific anatomical structure(s) is considered in this computation study, the static morphologic variation in the α-angle between asymptomatic and SUI subjects was not accounted for.

Linear regression analyses were performed for all curves (urethral excursion angles vs. intra-abdominal pressure) in MATLAB R2014 (Mathworks Inc., Natick, MA) using a linear model ($\Delta\alpha \sim k * IAP$). The interception of the linear model was set to zero considering that the urethral excursion angle should be zero at the onset of simulation (IAP = 0cmH_2O). The $\Delta\alpha$ achieved in the intact test (noted as $\Delta\alpha_{Intact}$) indicates the inherent response to the applied IAP of an asymptomatic USS. A weakening effect index ($WEI = \Delta\alpha - \Delta\alpha_{Intact}$) was also employed to elicit the degree of mobility caused solely by the weakened structure in each weakening test.

2.4 Results

The α-angle at the onset of simulation (at rest) was 15.9° for all tests. Table 2.1 shows the α-angles achieved at the final status with the IAP of 100cmH_2O for all tests. The final α-angles ranged from 30.3° (intact test) to 50.7° (weakened levator ani muscle and vaginal wall). The corresponding urethral excursion angles ($\Delta\alpha$) were calculated based on the difference between the onset and final α-angles (Table 2.1). The $\Delta\alpha_{Intact}$ reached 14.4° for the particular participant in this study. The results further showed that, $\Delta\alpha$ values were below 20° when only single pelvic muscle was weakened (from 15.3° to 19.4°). The vaginal wall, the puborectalis muscle and the pubococcygeus muscle were found to be the top three most contributing structures. Weakening these parts generated the top three largest urethral excursion angles ($\Delta\alpha = 20.1°$, 19.4° and

18.8°, respectively), while weakening other muscles (the iliococcygeus, piriformis, coccygeus and obturator internus muscles) generated relatively smaller excursion angles ($\Delta\alpha < 17°$). Weakening the levator ani muscle alone (test09) or in combination with other pelvic muscles (test10-12) raised the $\Delta\alpha$ value above 30°. The fitted R-square values for the urethral excursion angle-IAP curves (see Figure 2.3) fall into the range between 0.95 and 0.99, indicating a strong linear relationship between the urethral excursion angle and increased IAP for all the tests.

A nonlinearly-additive pattern was found among the three levator ani muscle components in terms of weakening effect (WEI = $\Delta\alpha - \Delta\alpha_{Intact}$). A WEI of 12.0° was achieved when weakening the puborectalis and pubococcygeus muscles together (test08), which is larger than the sum of WEIs achieved by weakening these two muscles separately (WEI = 5.0° in test05 and WEI = 4.4° in test06). The same nonlinear additive pattern was more remarkable by comparing the WEI obtained from weakening the entire levator ani muscle (WEI = 18.5°, test09) with the sum of WEIs from tests in weakening the three components weakened separately (WEI = 1.4° in test02, WEI = 5.0° in test05 and WEI = 4.4° in test06). Such a pattern did not exist for combinations of the levator ani muscle with other muscle groups (test10, 11 and 12). This finding suggests that the levator ani muscle is a sophisticated structure which provides support to the urethra in a well-coordinated fashion.

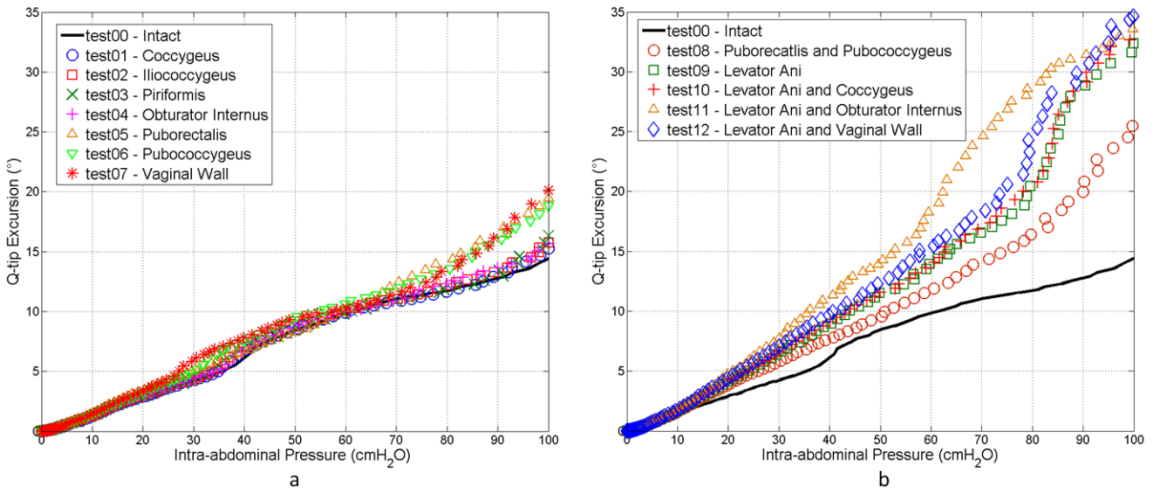

Figure 2.3 Plots of urethral excursion angle against intra-abdominal pressure for (a) single tests and (b) group tests. Reproduced from Y. Peng, R. Khavari, et al. (2016), with permission of Springer.

Table 2.1 Simulation Plan and Results

Test #	Weakened Part (Abbreviation)		α-angle (°) at IAP= 100cmH_2O	Q-tip Excursion $\Delta\alpha$ (°)	Weakening Effect Index WEI = $\Delta\alpha - \Delta\alpha_{intact}$ (°)
00	None		30.3	14.4 ($\Delta\alpha_{Intact}$)	0.0
Single Tests					
01	Coccygeus Muscle	(CM)	31.1	15.3	0.8
02	Iliococcygeus Muscle	(ICM)	31.6	15.8	1.4
03	Piriformis Muscle	(PM)	32.2	16.3	1.9
04	Obturator Internus Muscle	(OIM)	31.5	15.6	1.2
05	Puborectalis Muscle	(PRM)	35.3	19.4	5.0
06	Pubococcygeus Muscle	(PCM)	34.7	18.8	4.4
07	Vaginal Wall	(VW)	36.0	20.1	5.7
Group Tests					
08	PRM + PCM		42.2	26.4	12.0
09	PRM+PCM+ICM = Levator Ani Muscle (LAM)		48.8	32.9	18.5
10	LAM + CM		49.0	33.2	18.8
11	LAM + OIM		50.0	34.1	19.7
12	LAM + VW		50.7	34.9	20.4

α-angle = 15.9° at rest for all tests

Reproduced from Y. Peng, R. Khavari, et al. (2016), with permission of Springer.

Distinct deformation patterns were found in the pelvic floor responses under different weakening conditions (see Figure 2.4). When the vaginal tissues were weakened, an observation was made that the vaginal canal underwent severe compression and the vaginal wall became extremely thin, yielding more space for extra urethral motions, while the shape and position of the levator ani muscle did not show evident difference. However, when the levator ani muscle was weakened, a different pattern was observed: the vaginal wall remained at its normal thickness, while the levator ani muscle showed remarkable backward and downward yielding especially in the mid-portion, as the combinational effect of the front and top pressures applied on the bodyfill part on the entire pelvic floor is similar to a body force that is oriented in the inferoposterior direction and perpendicular to the levator plate. The urethral axis excursion in this case was attributed more to the insufficient support by the weakened levator ani muscle rather than the

collapsed vaginal canal. When the levator ani muscle and the vaginal wall were both weakened simultaneously, both syndromes could be identified.

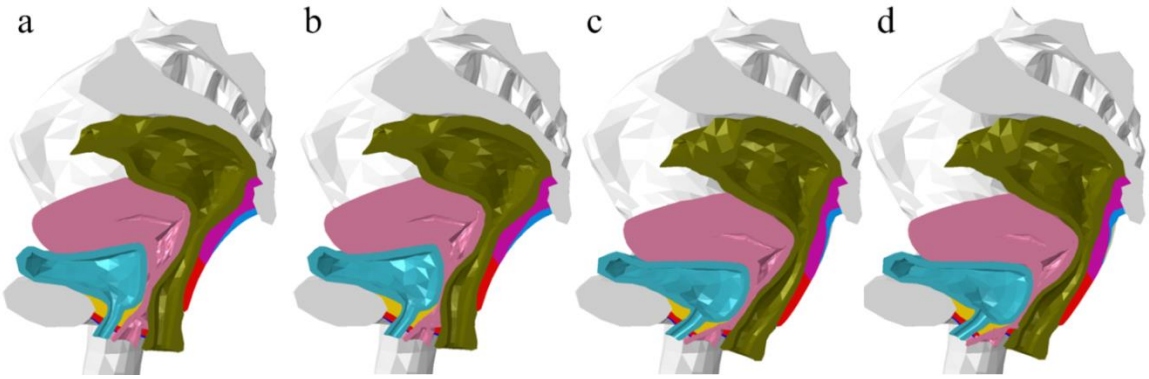

Figure 2.4 Deformation patterns of (a) intact test (b) weakened vaginal wall (c) weakened levator ani muscle and (d) weakened levator ani muscle together with vaginal wall. Reproduced from Y. Peng, R. Khavari, et al. (2016), with permission of Springer.

2.5 Discussion and Conclusions

Our female pelvic model consisting of 44 anatomical structures to mimic the dynamic response to pressure events represents, to the best of our knowledge, the most comprehensive and complete pelvic model in female SUI research. The validation study demonstrated consistency between the computer simulation results and the dynamic MR imaging observations along the sagittal plane of the pelvis of the same subject. A parametric study was designed and performed to investigate the relative importance of individual structures or their combination on urethral support in women. The α-angles from our computer simulations are in agreement with findings from transperineal ultrasound (Sendag et al., 2003).

The relationship between the IAP and the induced urethral hypermobility may vary widely across subjects due to differences in anatomy and the functional status of the urethral support system (F. T. Brandt et al., 2006). However, simultaneous examination of these two metrics may provide useful information for a standardized evaluation of the functional status of the female pelvis. A significant association ($p=0.012$) between the ratio of IAP over Q-tip angle (urethral mobility index) and the degree of cystourethrocele was reported in a study that involved with eighty-four incontinence women (Alafraa & Schick, 2008). The authors proposed this urethral

mobility index as a standardized index for crossing-subject comparison. Although it is often intuitively assumed that the extent of urethral hypermobility should be positively related to IAP, this is the first time that this relationship has shown to be linear. The linear relationship over the entire IAP range identified in this study provided a substantialized ground for the application of the urethral mobility index as this index could be obtained consistently at any IAP level with less vulnerability to IAP variations. Moreover, it could provide a comprehensive functional profile of the female pelvic floor to discern urethral mobility indices specific to each weakening condition. Any anatomical (such as mid-urethral sling surgery) or functional (e.g., enhanced pelvic muscle strength) change in the pelvis could also be simulated in the computational model to provide valuable references in pre-surgery planning, training, or other SUI treatment options.

In our model, the weakening effect is mild when only one single structure is weakened, consistent with Crystle et al. who found patients with good urethral support to have a rotation angle of less than 20° (Crystle et al., 1971). This finding reveals that the female USS is a stable system and could still provide sufficient support to the urethra under mild impairment. Considering the Q-tip excursion >30° as a criteria for urethral hypermobility (Crystle et al., 1971; Ghoniem et al., 2008), we find that weakening the entire levator ani muscle (comprised of the iliococcygeus, puborectalis and pubococcygeus muscles) caused more urethral mobility and could possibly result in urethral hypermobility ($\Delta\alpha = 32.9°$). This is consistent with the clinical observation that female SUI patients with urethral hypermobility are often associated with damages in the levator ani muscle (J. O. L. DeLancey, 2002).

Medical imaging techniques such as MRI or ultrasound have been widely used for diagnosis of SUI characterized by urethral hypermobility, but their application is limited to cases where morphologic defects of urethral support structures are main causes. However, the impairment is not always morphologically observable. Reduced stiffness in pelvic muscle (Verelst & Leivseth, 2007), ligament and vaginal wall tissues due to aging or trauma (Chantereau et al., 2014) could also be associated with insufficient support. The computational modeling and biomechanical approach provides a useful tool for those cases where there is no imaging evidence of morphologic abnormalities in the USS. Moreover, with the capability to reproduce the pelvic floor

deformation under different weakening scenarios and exporting dynamic or static landmarks of interest, our model could be employed to establish a subject-specific SUI profile that manifests the deformation pattern uniquely associated with each possible weakening scenario. The functional status of the urethral support structure could then be assessed by comparing the imaging finding with the established profile. The distinct deformation patterns under different weakening conditions provide valuable references for subject-specific SUI diagnosis, which would be difficult to obtain from other methods considering the particularly challenging requirement of the same patient to develop different weakening syndromes successively as well as the difficulty in capturing the extremely instantaneous dynamic deformation.

The computational modeling and biomechanical analysis approach presented in this study could also be employed to develop, design and optimize interventional treatment approaches/devices such as mid-urethral slings. The results under different weakening conditions provided in our model could be valuable in simulating worst case scenarios and determining the safety factor for sling products. Kociszewski et al. (2010) showed that the success and complication rates of the sling surgery were highly associated with the implant position. Our model could also be used as a pre-surgery planning tool to reduce potential postoperative complications and improve treatment success rate on a subject-specific basis.

Limitations of this study are discussed below. First, this study lacks statistical information as our model was built based on one subject-specific anatomy. The subject-specific modeling approach provides a tool for personalized diagnosis and treatment outcome prediction for a specific patient. Analyses will be performed in the future based on the results from a group of patients to provide statistical information. Second, the pelvic model currently relies on the high-resolution MR images, which remains a relatively expensive procedure (approximately $500/MRI scan). The modeling procedure also takes about 1-2 weeks for experienced engineers and radiologists. A possible solution to make this approach more accessible is to build a pelvic model template based on the features of the patient group and use subject-specific ultrasound images for model modification. Another limitation, commonly shared by many other pelvic models, is that the voluntary contraction of muscles is not realized in the pelvic model. To do so it would require

a non-trivial finite element implementation technique as well as critical physiological calibrations for different levels of voluntary pelvic floor muscle contractions. Very recently, an advanced voluntary pelvic model was proposed and provides a way to model voluntary muscle contractions (F. S. Brandao et al., 2016). Nevertheless, the parameters associated with the voluntary muscle model were not obtained from actual voluntary contraction experiments in this study. A specially designed transvaginal and a transrectal high-density surface EMG probe, along with the internal muscle activity imaging technique (Liu et al., 2014; Liu et al., 2015), were recently developed in our group. We are currently using high-density surface EMG measurements to quantitatively characterize voluntary contractions of muscles in the female pelvis to further improve our pelvic modeling approach.

In conclusion, a comprehensive computational model of the female pelvis was reconstructed. The vaginal wall, puborectalis muscle and pubococcygeus muscle were found as the top three most important urethral support structures. Some unique patterns of the female pelvic floor deformation were identified, which indicate that the computational modeling and dynamic biomechanical analysis approach presents a powerful tool for female SUI research and clinical diagnosis. It could be potentially employed for subject-specific SUI evaluation and pre-surgery planning.

We would like to thank Dr. John O. DeLancey from the University of Michigan for his valuable consultation and Mr. Thomas Potter for editing the manuscript.

CHAPTER 3 – The Single-Incision Sling to Treat Female Stress Urinary Incontinence

3.1 Abstract

Dynamic behaviors of the single incision sling to correct urethral hypermobility are investigated via dynamic biomechanical analysis using a computational model of the female pelvis, developed from a female subject's high-resolution MR images. The urethral hypermobility is simulated by weakening the levator ani muscle in the pelvic model. Four positions along the posterior urethra (proximal, mid-proximal, middle and mid-distal) were considered for sling implantation. The alpha-angle, urethral excursion angle and sling-urethra interaction force generated during Valsalva maneuver were quantitatively characterized to evaluate the effect of the sling implantation position on treatment outcomes and potential complications. Results show concern for over-correction with a sling implanted at the bladder neck, based on a relatively larger sling-urethra interaction force of 1.77N at the proximal implantation position (compared with 0.25N at mid-distal implantation position). A sling implanted at the mid-distal urethral location provided sufficient correction (urethral excursion angle of 23.8° after mid-distal sling implantation vs. 24.4° in the intact case) with minimal risk of over-tightening, and represents the optimal choice for sling surgery. This study represents the first effort utilizing a comprehensive pelvic model to investigate the performance of an implanted sling to correct urethral hypermobility. The computational modeling approach presented in the study can also be used to advance pre-surgery planning, sling product design and to enhance our understanding of various surgical risk factors which are difficult to obtain in clinical practice.

3.2 Introduction

Stress urinary incontinence (SUI), the involuntary urinary leakage associated with increases in intra-abdominal pressure (IAP), affects about 25%-50% women in the United States with an annual treatment cost exceeding $12 billion (Chong et al., 2011). The total number of women who will undergo SUI surgery will increase 47.2% from 210,700 in 2010 to 310,050 in 2050 (Wu et al.,

2011). In recent decades, mid-urethral sling has become the standard treatment for women with SUI when conservative treatments have failed. The typical outcome of a successful sling surgery corrects urethral hypermobility (Karateke, Haliloglu, Cam, & Sakalli, 2009), which is often associated with SUI patients due to insufficient pelvic floor support to the urethra and can be clinically assessed by the Q-tip test (Crystle et al., 1971). By providing additional support to the urethra, the implanted sling helps restore the continence mechanism. Most recently, the single-incision sling (SIS) (Molden & Lucente, 2008), with only one single incision of the anterior vaginal wall made for the sling passage, was touted with high expectation. However, the actual clinical performance has not been encouraging with many differing conclusions reported regarding its effectiveness and safety (Bernasconi et al., 2012; Cornu et al., 2012; Oliveira, Resende, Silva, Dinis, & Cruz, 2014; Revicky & Tincello, 2014). Urinary retention is a serious post-operative complication of failed sling surgeries and may attribute to excessive sling-urethra interaction force, which over-tightens the sling and obstructs the urethra blocking normal urethral opening required for voiding (E. Costantini, Lazzeri, & Porena, 2007). Post-operative pain may also be associated with excessive sling tension as too much force may cause implant shrinkage, which has been reported as a major cause of severe pain after pelvic floor repair surgeries (Feiner & Maher, 2010). Currently, there is no agreement regarding which type of sling is the best in terms of effective surgical outcome with the lowest complication rate. Many studies advocate that the mid-urethral sling technique should be put under more scrutiny with larger controlled clinical trials. A better understanding of the dynamic process required to stabilize the urethra under stress using the mid-urethral sling would be useful to advance sling design and proper placement. In spite of a large amount of existing clinical trial data, the outcomes are often subjective with no ability to objectively study the dynamic process that a sling-tissue interaction represents in a real world setting. Medical imaging techniques, such as perineal ultrasonography (Kociszewski et al., 2010) or magnetic resonance (MR) imaging (Boyadzhyan, Raman, & Raz, 2008) have been employed to study this topic. However, only two-dimensional images can be provided and more importantly, the critical biomechanical information such as interaction behaviors between the sling and surrounding tissues is still missing, which limits the quantitative analysis of some key aspects of

the sling performance. Computational models, based on realistic female pelvic anatomy, offer a useful tool for quantitative biomechanical analysis to female pelvic floor dysfunctions (Rostaminia & Abramowitch, 2015). Models have been employed to study pelvic organ prolapse (L. Chen, Ashton-Miller, & DeLancey, 2009; Z. W. Chen et al., 2015; Luo et al., 2015), childbirth-related trauma (D. Jing, J. A. Ashton-Miller, & J. O. L. DeLancey, 2012b; Parente, Jorge, Mascarenhas, Fernandes, & Martins, 2008) and ligament impairment (S. Brandao et al., 2015). However, these models often missed some necessary anatomical structures that maintain the integrity of the natural pelvic anatomy, and efforts have been rarely made to study the interventional treatments. In this study, a comprehensive pelvic model was developed with 44 anatomical structures in the female pelvis incorporated to study the mid-urethral sling performance on a subject-specific basis. A single-incision sling was incorporated in the pelvic model at four different locations along the posterior urethra and dynamic biomechanical analysis was performed. The interaction behaviors of the mid-urethral sling in the female pelvis were investigated by examining the dynamics of the bladder neck, urethra and sling under increased IAP. Analyses of biomechanical parameters (alpha-angle (Sendag et al., 2003), Q-tip excursion angle (Crystle et al., 1971) and sling-urethra interaction forces) obtained from computer simulation results were performed to investigate the effect of implant positions on the treatment outcome (urethral hypermobility) as well as potential risk factors (retention and pain). The computational modeling and dynamic biomechanical analyses provide insights into underlying mechanics for SUI treatments that are difficult to obtain from clinical trials or static imaging tools alone.

3.3 Materials and Methods

3.3.1 Female Pelvic Model

The computational model of the female pelvis and the mechanical properties of tissues involved in the pelvic model are adopted from a previous study based on subject-specific MR images of a 21-year-old asymptomatic female (nulliparous, non-smoker, BMI=22) (Y. Zhang, Sweet, et al., 2009) (Figure 3.1). Slight geometric modifications were made to accommodate the sling to the established model. Very briefly, axial MR images were acquired in the supine position

at rest using a 3.0T MR scanner (Trio Tim, Siemens, Germany) (slice thickness 3mm; matrix 320 × 160; field of view 430mm; pixel size 1.344mm). Segmentation was performed on axial MR images for each anatomical pelvic structure with the guidance of one urologist using Mimics 11.0 (Materialise Group, Leuven, Belgium). The closed surfaces were then imported into MAYA 8.5 (Autodesk, Inc., San Rafael, CA) and Rhinoceros 4.0 (McNeel North America, Seattle, WA) for artifact smoothing and intersecting surface correction and converted into solid geometries. All solid geometries were discretized into a finite element mesh with 126,378 tetrahedral elements using Abaqus 6.12 (SIMULIA, Providence, RI). The final 3D pelvic model contains 44 anatomical parts including pelvic muscles, ligaments, bones, fat, bladder, urethra, uterus, vagina, colon, rectum and anus. ABAQUS general contact function and tie constraints were employed to realize the interactions and connections between soft tissues.

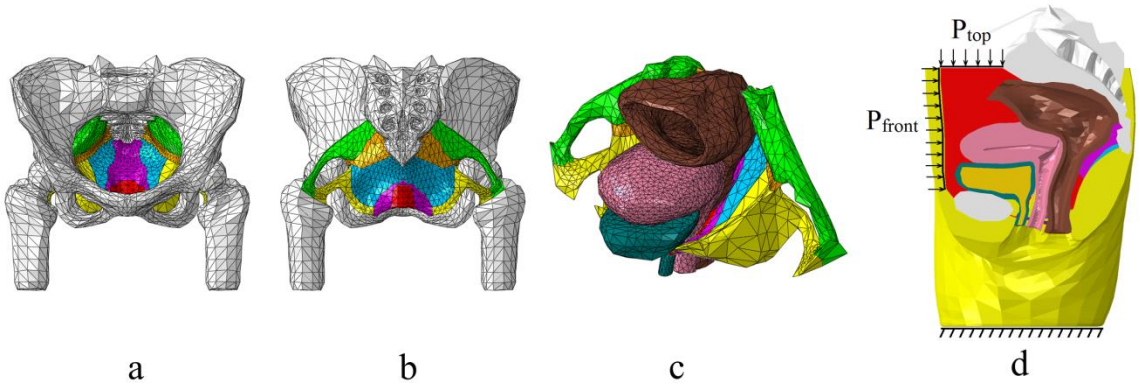

Figure 3.1 Illustration of subject-specific pelvic floor model. Reproduced from Y. Peng et al. (2015), with permission of the American Society of Mechanical Engineers

The general contact algorithm in ABAQUS was applied to mimic the natural interaction between parts that are in contact but anatomically independent (e.g., the interaction between the bladder and the uterus). Tie constraints that binds two shared surfaces were used to couple motions of parts which are biologically connected and to model the connecting effects of fasciae (e.g., the tendineous arch of levator ani muscle). Connector elements, with the ability to model connective tissues such as ligaments (Luo et al., 2015), were employed in this study to model the ligaments surrounding the urethra (e.g. the pubourethral ligament). Soft tissues involved in the pelvic model were modeled as linear elastic solids using material properties from Young's moduli

of the bladder, urethra, uterus, rectum, muscle, ligament and vaginal tissue (0.05, 0.03, 0.05, 0.1, 2.4, 1.2 and 7.4e-3 MPa) (Y. Zhang, Kim, et al., 2009). The bony pelvis was modeled as one rigid and fixed structure considering its negligible deformation under normal pelvic functions due to its much higher stiffness compared with soft tissues (Dalstra, Huiskes, Odgaard, & Van Erning, 1993). Two uniformly distributed pressures were applied on the front and top surface of the pelvic model to induce intra-abdominal pressure (Figure 3.1d). A specifically designed bodyfill part, which fills the abdominal cavity, was created for the pressure transmission (Figure 3.1d). The bottom of the model was constrained from all displacements. The IAP was calculated as the averaged contact pressure (Abaqus variable *CPRESS*) between the urine and inner bladder wall. Abaqus Explicit solver was used for the FEM implementation. The intra-abdominal pressure (IAP) was calculated as the averaged contact pressure between the inner bladder wall and the urine. The IAP achieved at maximal Valsalva was assumed as 100cmH_2O, which is within the physiological range as SUI patients exhibited an IAP at maximum straining of 99.3 ± 51.8 cmH_2O (7-193 cmH_2O) (Frederico Teixeira Brandt et al., 2006).

For the validation purpose, dynamic MR images were acquired in the mid-sagittal plane approximately every 1.5 seconds while the subject performed several Valsalva maneuvers. High consistency was achieved between the simulated pelvic floor deformation and the dynamic MR imaging observation.

3.3.2 Single-Incision Sling Model

The simulated single-incision sling (SIS) was modeled based on realistic specifications of MiniArcTM (American Medical Systems, Minnetonka, MN). The sling was modeled as a strip (length × width × thickness: 2.8 inch × 0.42 inch × 0.025 inch) as shown in Figure 3.2a. The sling was meshed into 4600 eight-node hexahedral elements, as shown in Figure 3.2b. The experimental uniaxial stress-strain data, provided by American Medical Systems, is shown in Figure 3.2(c). A 2nd-order polynomial hyperelastic model (Rivlin & Saunders, 1951) was used as the constitutive model of the sling. The test data was imported into the Abaqus hyperelastic material model and the least-square fit was performed automatically by the solver to obtain the optimal parameters (C_{10} = -0.160, C_{01} = 0.389, C_{20} = 6.014, C_{11} = -9.059 and C_{02} = 3.808). As the

sling was modeled with its ideal shape in the undeformed state, before the Valsalva simulation, a separate preparation simulation was performed to move it to the planned implantation positions in a shape that is conforming to the surfaces of posterior urethral wall and anterior vaginal wall (Figure 3.3). After the preparation simulation, the sling was deformed to the planned implantation position and shape and then imported to the Valsalva simulation model as the initial status. The sling motion was controlled by three reference points: one at the middle bottom position of the sling (mid-bottom point) and two at each end (end points), as shown in Figure 3.2b.

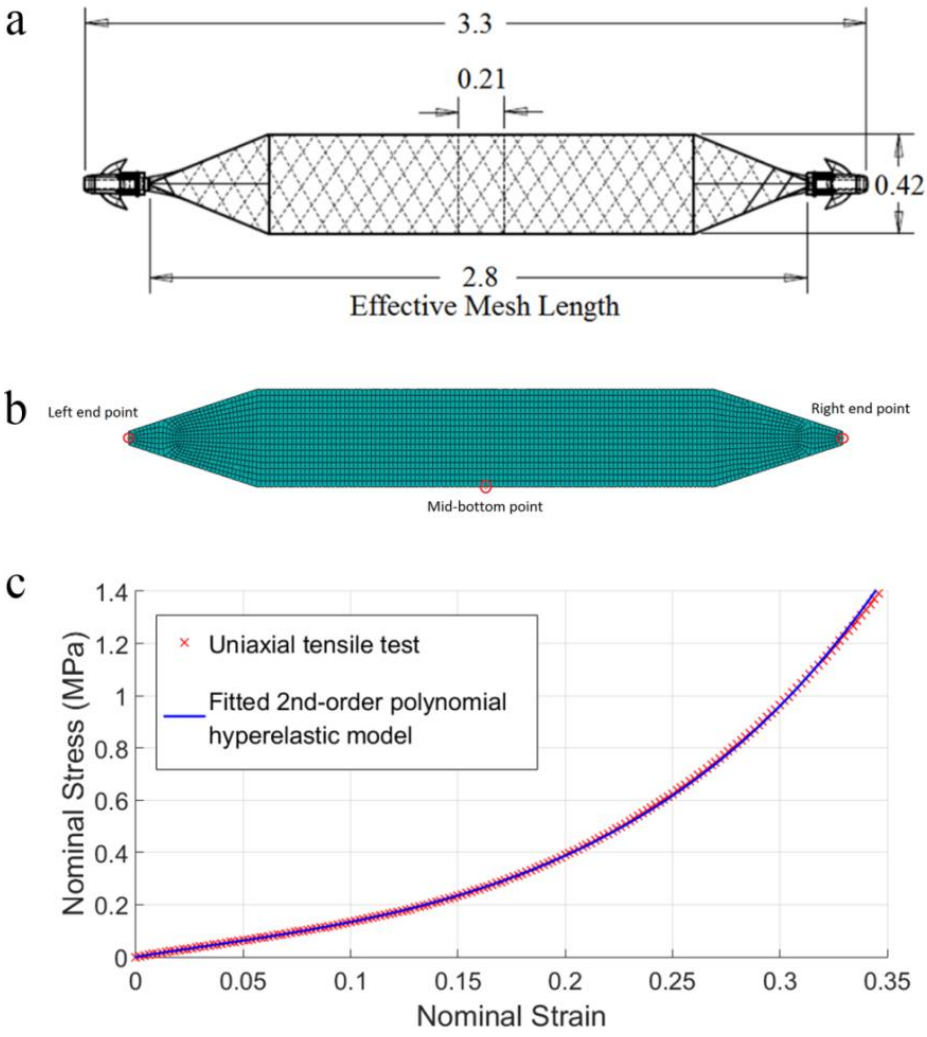

Figure 3.2 Design of the implanted single-incision sling. Reproduced from Y. Peng et al. (2015), with permission of the American Society of Mechanical Engineers.

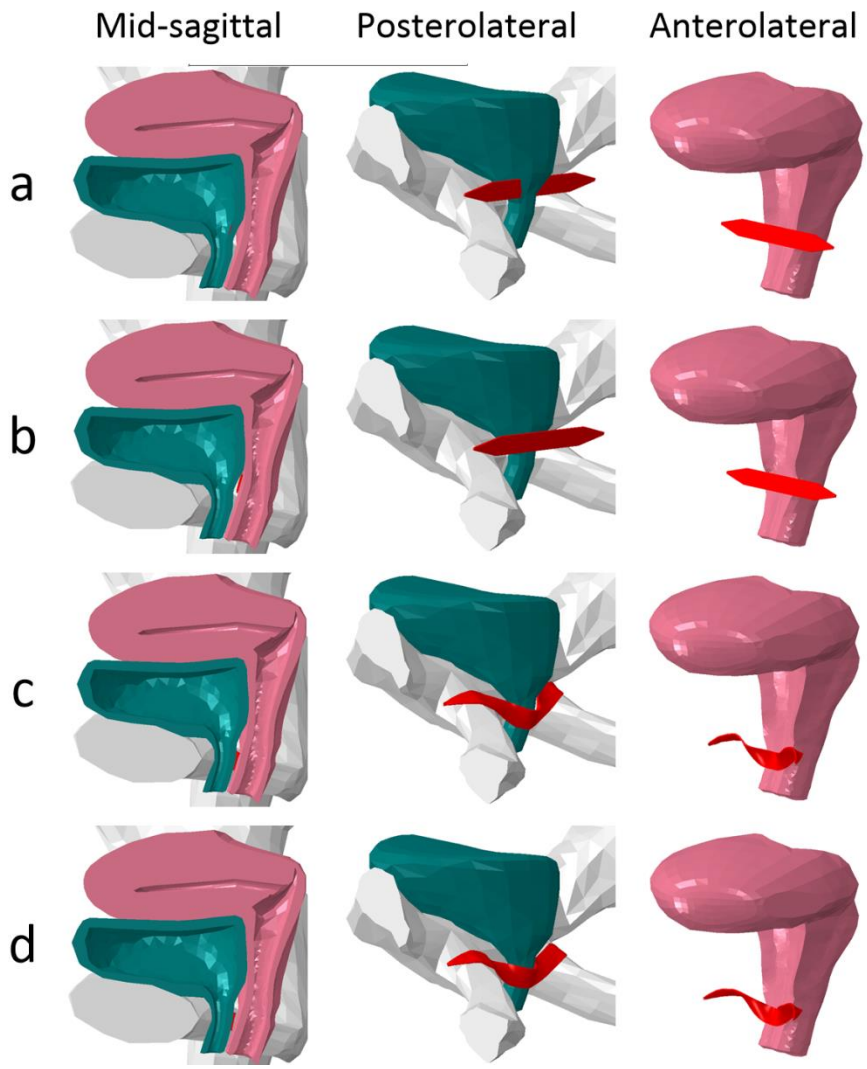

Figure 3.3 Illustration of the preparations of the sling for testA4. Three columns show the relative positions of the sling to pelvic organs in different views. Reproduced from Y. Peng et al. (2015), with permission of the American Society of Mechanical Engineers.

Step 1: The sling was first placed below the bladder neck (Figure 3.3a), between the anterior and posterior urethral walls without touching the anterior vaginal wall. All interactions with the sling were excluded except for the vaginal wall. A uniform posterior displacement boundary condition was assigned to the center nodes of the sling in order to move the sling off from posterior urethral wall and push the sling against the anterior vaginal wall. The sling surface adjusted to the anterior vaginal wall due to their interaction. At the end of this step, the sling was completely out from touch with the urethra and tightly pressed against the vagina (Figure 3.3b).

Step 2: The interaction of the sling with the urethral wall and the pelvic bones was activated in this step. A displacement boundary condition was assigned to the mid-bottom point to drag the entire sling down along the posterior urethra to the desired implantation position. The amount of displacement was directly calculated based on the vector distance from its initial position to the desired position on the posterior urethral wall. Another displacement boundary condition was assigned to each end point to advance the sling arms into the obturator foramen in each side. The displacements were obtained from several preliminary tests so that the sling was advanced into the obturator internus muscle and the obturator membrane below the inferior pubic ramus, while the maximum principal strain was kept under 10% for the entire sling except a few regions around the reference nodes. At the end of this step, the sling reached its desired position, but a certain amount of oscillations existed because of the motions in the previous steps (Figure 3.3c).

Step 3: The sling ends were then fixated in space and the sling was kept at rest to attenuate the oscillations. When the equilibrium state was achieved, the deformed sling was in its desired implantation state (Figure 3.3d) and exported as an orphan mesh (Abaqus (Systèmes, 2012) orphan mesh), which preserved the deformed shape and also released the tension caused during the previous boundary conditions as the sling should be implanted in a tension-free manner. The orphan mesh sling was then re-imported into the pelvic model for Valsalva maneuver simulation.

The friction coefficient of the sling with surrounding tissues (bladder, urethra, vagina and pelvic bones) was 0.2 as suggested by American Medical Systems. To simulate the fixating effect of the obturator internus muscle on the sling, the portion of the nodes on the sling arms that were in contact with the obturator internus muscles were constrained with ENCASTRE boundary conditions (Abaqus (Systèmes, 2012) ENCASTRE) which prohibited all translation and rotation displacements.

3.3.3 Plan of Simulation

Table 1 lists all six tests performed in this study. Test C0 serves as the intact control test in which no urethral support structures were weakened. Test C1 serves as the SUI control test in which the levator ani muscle, the most important urethral support structure, was weakened by reducing its stiffness by 95% to simulate the insufficient urethral support in SUI patient. In neither

control test was the sling implanted. Ideally, after implantation, a single-incision sling would be placed at the junction between the lower and middle urethra and present a flat to a gentle C shape at rest. Poorly placed slings may shift upwards or downwards along the posterior urethral wall. To compare the effect of different sling implantation positions on the treatment outcome, four tests were performed (tests 01-04, sling tests). In each test, the levator ani muscle was weakened and the sling was implanted at a different location along the posterior urethral wall using the method described previously. The center of the sling was placed at positions from the bladder neck by 10% (test A1, proximal), 30% (test A2, mid-proximal), 50% (test A3, middle) and 70% (test A4, mid-distal) relative to the urethral length (Figure 3.4).

3.3.4 Quantitative Analysis of Sling Performance

SUI is often characterized by urethral hypermobility. Transperineal ultrasound reveals that the alpha-angle, a measure of urethral mobility and defined as the angle between the vertical axis and the urethral axis, was significantly different on straining ($P<0.05$) between the study (SUI) and control groups (Sendag et al., 2003). In this study we employed the alpha-angle as a key biomechanical parameter to evaluate the sling surgery treatment outcome, as the successful sling surgery would significantly decrease the urethral hypermobility ($P<0.001$) (Karateke et al., 2009).

To measure the alpha-angle in Abaqus, two reference points along the posterior urethra were selected to define the urethral axis (Figure 3.4). The static alpha-angle was calculated using the initial coordinates of these two points. A history output request was set to monitor the displacements of these two points so the change of the alpha-angle during the simulation could be calculated. The urethral excursion angle, defined as the change of the alpha-angles at rest and at maximal Valsalva (denoted by $\Delta\alpha$), was used as an alternative measure to examine the urethral mobility, as $\Delta\alpha$ is mathematically equal to the Q-tip excursion angle that is frequently used in clinical Q-tip tests to assess urethral hypermobility (Crystle et al., 1971; Ghoniem et al., 2008). The sling-urethra interaction force was used to assess potential postoperative over-correction, considering that too much interaction force (over-tightened sling) might cause urethral retention, which is a common complication of failure sling surgery (E. Costantini et al., 2007). A history output request was set to monitor the total contact force for the sling-bladder interaction

pair. The history output requests were executed once every 1ms throughout the entire Valsalva simulation.

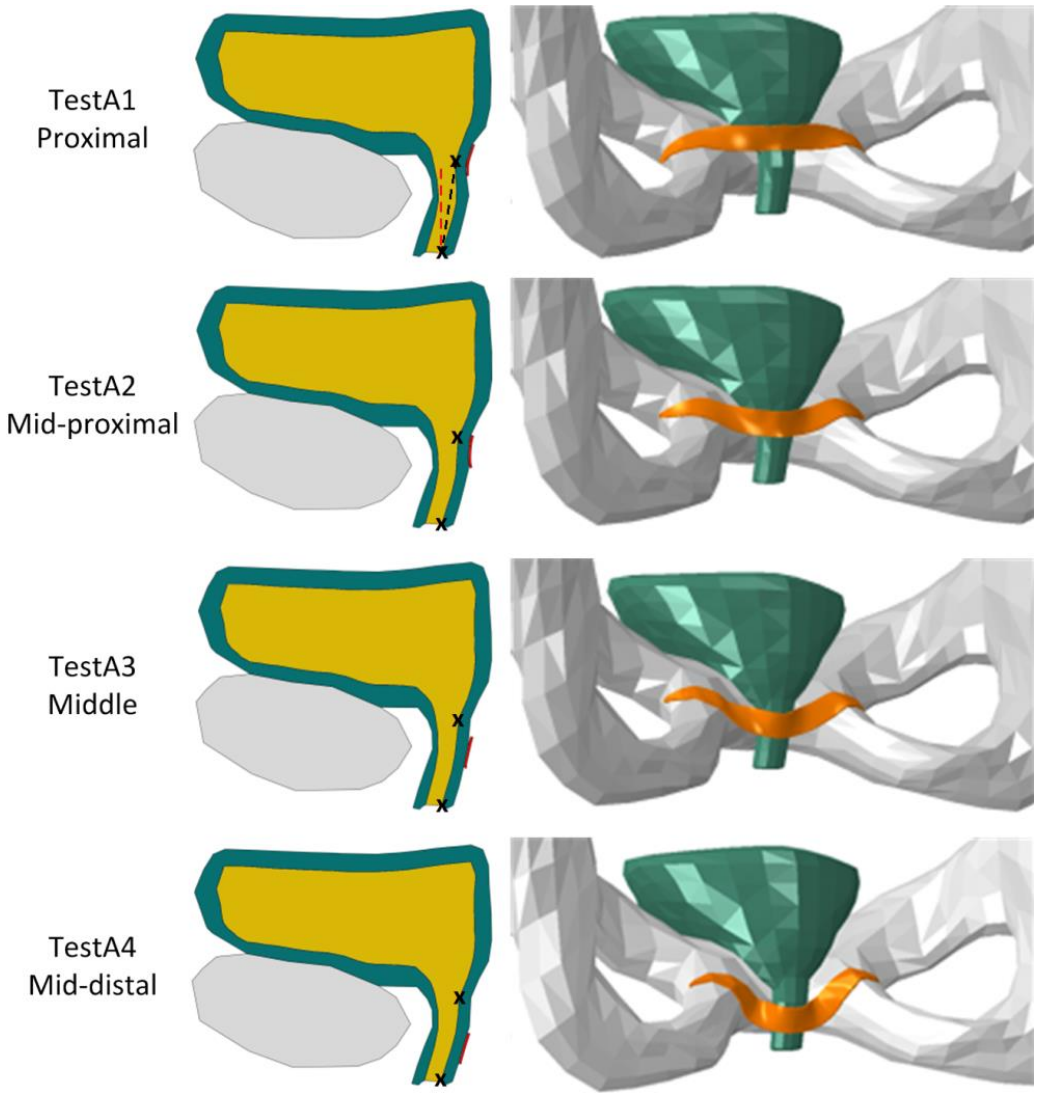

Figure 3.4 Sling implantation positions at rest status. Reproduced from Y. Peng et al. (2015), with permission of the American Society of Mechanical Engineers.

3.4 Results

Table 3.1 summarizes the simulation results obtained from all six tests. The α-angle at the rest state is 15.9° for all tests, as they shared the same geometric model of the pelvis. An α-angle of 40.3° was achieved in the intact control test and an α-angle of 52.5° was achieved in the SUI

control test at maximal Valsalva. α-angle of 39.7° (Mid-distal, test A4), 36.0° (Middle, test A3), 29.8° (Mid-proximal, test A2) and 26.5° (Proximal, test A1) were achieved in the 4 sling tests.

Table 3.1 Plan of simulations and results

Test #	Impaired Structure	Sling Implantation Position	α-angle (°)			Sling-Urethra Interaction Force F (N)
			Rest	Maximal Valsalva	Difference Δ α	
Control tests						
C1	None	No Sling	15.9	40.3	24.4	
C2	LAM	No Sling	15.9	52.5	36.6	
Sling tests						
A1	LAM	Proximal	15.9	26.5	10.6	1.77
A2	LAM	Mid-proximal	15.9	29.8	13.9	1.37
A3	LAM	Mid	15.9	36.0	20.1	0.96
A4	LAM	Mid-distal	15.9	39.7	23.8	0.25

LAM = Levator Ani Muscle

Reproduced from Y. Peng et al. (2015), with permission of the American Society of Mechanical Engineers.

The increase of IAP with the simulation time for all tests is presented in Figure 3.5a. The corresponding urethral excursion angles ($\Delta\alpha$) were calculated for each test and plotted against the IAPs in Figure 3.5b. A urethral excursion angle of 24.4° was achieved from the intact control test (test C0) and a urethral excursion angle of 36.6° was achieved from the SUI control test (test C1). Urethral excursion angles of 23.8° (Mid-distal, test A4), 20.1° (Middle, test A3), 13.9° (Mid-proximal, test A2) and 10.6° (Proximal, test A1) were achieved in sling tests respectively. The sling intervention demonstrated its efficiency in bringing down all large urethral excursion angles achieved in the sling tests to lower levels (reduced by 35.0% in test A4, 45.1% in test A3, 62.0% in test A2 and 71.0% in test A1).

Figure 3.4 shows that all implanted slings present a shape of a flat line in the mid-sagittal view at rest. Figure 3.6 shows the deformed bladder, urethra and sling at maximal Valsalva in both control tests and four sling tests. Please note that slings implanted at proximal and mid-proximal urethra locations resembled a “C”-shape due to the applied pressure, while slings implanted at middle and proximal urethra locations still maintained the shape of a flat line.

Figure 3.5c shows the development of the sling-urethra interaction forces over the increase of intra-abdominal pressures. It can be seen that the interaction force increases as the IAP increases in all the tests. Please also note that the magnitude of the interaction force increases as the implantation location of the sling approaches the urethrovesical junction. The interaction forces of 0.25N (Mid-distal, test A4), 0.96N (Middle, test A3), 1.37N (Mid-proximal, test A2) and 1.77N (Proximal, test A1) were achieved in the sling tests at maximal Valsalva respectively.

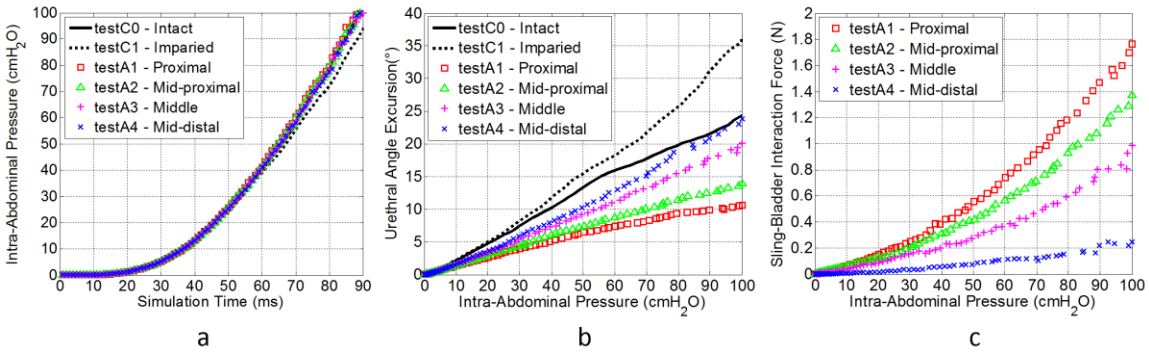

Figure 3.5 Plots of sling simulation results. Reproduced from Y. Peng et al. (2015), with permission of the American Society of Mechanical Engineers.

3.5 Discussion and Conclusions

Over the last two decades, numerous slings have been invented and made available for SUI surgery. The mechanical properties of these slings varied significantly (Afonso et al., 2008) but there is no unequivocal agreement regarding the best material (Mangera, Bullock, Chapple, & MacNeil, 2012). A number of poor quality slings have been implanted into women with SUI and caused severe complications in the past years. A reliable and convenient method to test the sling products is lacking. A computational model and dynamic biomechanical analysis approach will bridge this gap by providing 3-dimentional dynamic responses of the organs and tissues in the pelvis in response to sling implantation.

In this study, a computational model of the female pelvis, which consists of 44 anatomical structures of the female pelvis and represents the most comprehensive model of the female pelvis in SUI research, to the best of our knowledge, was developed and utilized to investigate the performance of mid-urethral sling surgery in correcting urethral hypermobility.

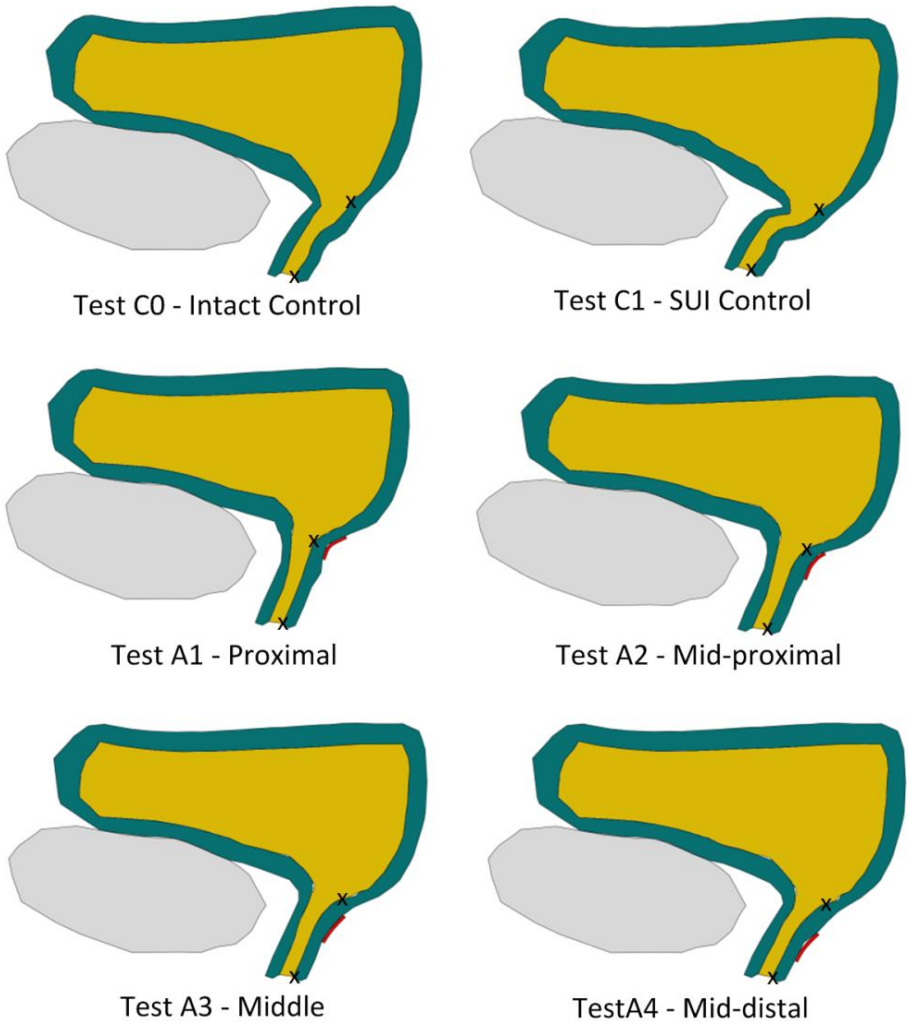

Figure 3.6 Shapes of sling in the mid-sagittal view at maximal Valsalva. Reproduced from Y. Peng et al. (2015), with permission of the American Society of Mechanical Engineers.

The pelvic floor deformation in response to increased IAP during the Valsalva maneuver was predicted by the computer simulation. Urethral mobility was quantitatively characterized by α-angles and urethral excursion angles (the change in α-angle from rest to maximal Valsalva) and compared across different scenarios (control tests and sling tests). In addition, the interaction behavior of the single-incision sling with urethra was studied. The potential complication of over-correction or muscle pain was assessed by comparing the sling-urethra interaction forces for four sling implantation locations.

The α-angles predicted by the computational model in the control tests are in agreement with perineal sonography findings (Sendag et al., 2003) (For intact subjects, 15.9° vs. 15.0° ± 6.7° at

rest and 40.3° vs. 31.3° ± 11.7° at maximal Valsalva; for SUI patients, 52.5° vs. 51.0° ± 14.0° at maximal Valsalva). The predicted α-angles in the sling tests are in agreement with post-sling surgery Q-tip tests (Karateke et al., 2009) (26.5° for test A1 with the proximal sling implanted, 29.8° for test A2 with the mid-proximal sling, 36.0° for test A3 with the middle sling and 39.7° for test A4 with the mid-distal sling vs. 30.19° ± 9.37° at maximal Valsalva). The urethral excursion angles characterized in the two control tests ($\Delta\alpha$=24.4° intact control; $\Delta\alpha$=36.6° SUI control) are qualitatively in agreement with reported Q-tip test using $\Delta\alpha$=30° as the criteria for urethral hypermobility (Ghoniem et al., 2008). After sling implantation, the urethral excursion angle was lowered down from 36.6° to 10.6° (test A1), 13.9° (test A2), 20.1° (test A3) and 23.8° (test A4). The simulated sling intervention showed successful corrections of urethral hypermobility.

Studies show that the single-incision sling with a shorter arm length causes less pain to patients in the short term than TOT or TVT slings (Duckett & Baranowski, 2013). Although urinary bladder nociceptors respond to the stimuli that cause pains, it remain unclear how they are distributed exactly. Nevertheless, our clinical experience shows that many patients got pain relief after removing a sling that was too tight. The sling-urethra interaction forces, indicating the force which the implanted sling exerts on the urethra during a pressure event, may properly characterize the tightness of the sling against the urethra and therefore was chose as a measure of potential pains. This study represents the first effort, to the best of our knowledge, to investigate the interaction forces during pressure events. Specifically, our computation results show that the interaction force was much higher (1.77N in test A1 compared with 0.25N in test A4) when the sling was placed in a more proximal position, which may indicate that a sling implanted at a more proximal position will more likely lead to pain and urine retention to SUI patients.

Impropriate sling implantation positions may lead to over-tightened slings and cause severe complications such as retention and postoperative pain. The maximal sling-urethra interaction force developed postoperatively in response to increased IAP can be used to better understand and predict those complications. Unfortunately, the sling-urethra interaction force information is difficult to obtain in practice due to the lack of appropriate measurement tools. Based on the

force-IAP relationship observed from this study, the maximal sling-urethra interaction force can be estimated from IAP measurements using the computational modeling and biomechanical analysis approach. This provides a way to predict the surgery outcome (through the correction of urethral hypermobility) and the potential risks the patient may be exposed to (through the sling-urethral interaction forces at maximal Valsalva).

Biomechanical analysis results indicate that the proximal urethra sling may provide the best performance in correcting the urethral hypermobility, as the $\Delta\alpha$ (10.8°, test A1) was the lowest among all four sling tests. The appearance of the proximal urethra sling in the mid-sagittal view (Figure 6, test A1, flat line at rest and "C"-shaped at maximal Valsalva) also fell into the group that may represent the best outcome reported in (Kociszewski et al., 2010). However, this $\Delta\alpha$ value was even less than the intact $\Delta\alpha$ (24.4°, test C1), indicating an over-tightened sling that might obstruct the urethra. This was also demonstrated by the largest sling-urethra interaction force (Table 1). Our results also showed, on the other hand, that a sling implanted at the mid-distal position generated a $\Delta\alpha$ value of 23.8° (testA4) which is closest to the intact $\Delta\alpha$. The interaction force in this case was also the lowest. As such, a sling implanted in the mid-urethral location will provide sufficient correction with minimal risk of over-tightening and represent the optimal choice for sling surgery. This finding is in consistency with the optimal outcome achieved when the sling is placed at the junction of the middle and distal thirds (Kociszewski et al., 2010).

The simulations results showed consistency with clinical findings and suggested that the computational model would help us gain a thorough understanding of mechanics of various physiological phenomena inside the female pelvis. Preoperative surgery planning could also be optimized based on the computational model.

In conclusion, a computational model of the female pelvis with an implanted single-incision sling was developed in this study to examine the effect of different implantation positions on the treatment outcome and potential complication factors. Four different locations along the posterior urethral wall were examined. Dynamic biomechanical analysis results showed that the mid-distal position for sling implantation offered the best overall performance for restoring urethral support while keeping the sling-urethral interaction force low. This study represents the first effort in

utilizing a comprehensive pelvic model to investigate the performance of mid-urethral surgery in correcting urethral hypermobility. The computational modeling and biomechanical analysis approach presented in the study can also be used to advance pre-surgery planning, sling product design and our understanding of various pathophysiological phenomena which are difficult to obtain with currently available technology.

We would like to thank the American Medical Systems for providing specifications for the MiniArc^{TM} sling. We would also like to thank Dr. John O. DeLancey from the University of Michigan for his valuable consultation.

CHAPTER 4 – Pelvic Floor Dynamics during High-Impact Athletic Activities

4.1 Abstract

Background - Stress urinary incontinence is a significant problem in young female athletes, but the pathophysiology remains unclear because of the limited knowledge of the pelvic floor support function and limited capability of currently available assessment tools. The aim of our study is to develop an advanced computer modeling tool to better understand the dynamics of the internal pelvic floor during highly transient athletic activities.

Methods – A pelvic model was developed based on high-resolution MRI scans of a healthy nulliparous young female. A jump-landing process was simulated using realistic boundary conditions captured from jumping experiments. Hypothesized alterations of the function of pelvic floor muscles were simulated by weakening or strengthening the levator ani muscle stiffness at different levels. Intra-abdominal pressures and corresponding deformations of pelvic floor structures were monitored at different levels of weakness or enhancement.

Findings - Results show that pelvic floor deformations generated during a jump-landing process differed greatly from those seen in a Valsalva maneuver which is commonly used for diagnosis in clinic. The urethral mobility was only slightly influenced by the alterations of the levator ani muscle stiffness. Implications for risk factors and treatment strategies were also discussed.

Interpretation - Results suggest that clinical diagnosis should make allowances for observed differences in pelvic floor deformations between a Valsalva maneuver and a jump-landing process to ensure accuracy. Urethral hypermobility may be a less contributing factor than the intrinsic sphincteric closure system to the incontinence of young female athletes.

4.2 Introduction

Stress urinary incontinence (SUI), the involuntary leakage of urine under increased intra-abdominal pressure (IAP), has an observed prevalence of between 4% and 35% (Luber, 2004). Though SUI is a common problem for elderly and parous women, recent studies showed that SUI

is a non-negligible problem in nulliparous female athletes, with the prevalence varying from 12.5% to as high as 80% (Almousa, Moser, & Kitsoulis, 2015). SUI in young athletes often goes unreported for fear of embarrassment (Hägglund & Wadensten, 2007). It can result in the athlete's modifying her technique, or even completely abandoning the sport and becoming physical inactivity (Salvatore et al., 2009).

In the "hammock hypothesis" theory, the levator ani muscle (LAM) plays a significant role in maintaining urinary continence (DeLancey, 1994). During an IAP increase, the LAM, a stiff posterior supportive structure, helps the urethral closure by allowing the urethra and other pelvic organs to be tightly compressed against it. Clinical observations found that LAM injuries can lead to a reduced urethral support (urethral hypermobility) (J. O. DeLancey, 2002), which is often associated with SUI. However, significant differences exist between the physiological conditions and environments of young female athletes and those of women in the general population. What these factors contribute to the pathophysiology of SUI remains unclear and warrants further investigation.

First, young female athletes often experience significantly greater and more sudden IAP increases, especially during high-impact activities such as running and jumping (Goldstick & Constantini, 2014). However, existing techniques for SUI diagnosis, including magnetic resonance (MR) imaging (Da Roza et al., 2015), perineometry (da Silva Borin, Nunes, & de Oliveira Guirro, 2013), and electromyography (H. Luginbuehl et al., 2016), are unable to non-invasively characterize the highly transient internal mechanics of the pelvic floor during these activities. Instead, diagnosis is often made on the basis of observations from Valsalva maneuvers (Kruger, Dietz, & Murphy, 2007). Differences in results obtained with this alternative approach require investigation, in order to ensure the correctness of the corresponding diagnosis.

Second, our knowledge of the pelvic floor muscles (PFMs) of young female athletes is limited. Two existing hypotheses regarding their PFMs are totally opposite: one suggests that female athletes have strong PFMs because of the training stimulus from the co-activation of the abdominal muscle, while the other theory postulates that repeated increases in IAP can cause fatigue and weaken the pelvic floor (Bø, 2015). To date, no equivocal evidence has been

presented to support either one. The effect of neither of these hypothesized alterations in PFM functions on the urethral integrity during the sudden IAP increase could be properly tested.

Computer modeling and simulation provide a potential solution to these challenges in testing. Recent advances in medical imaging allowed the reconstruction of computer models based on high-resolution subject-specific MR images (Y. Peng, R. Khavari, et al., 2016; Y. Peng et al., 2015), maximally preserving anatomical integrity and correctness. Computer simulation provides a reliable tool for characterizing dynamic biological processes that are otherwise difficult to observe through traditional techniques (S. Brandao et al., 2015; Z. W. Chen et al., 2015; Dai et al., 2014; Luo et al., 2015; Mayeur et al., 2016; S. Wang et al., 2014; H. Zhang, Nussbaum, & Agnew, 2015, 2016; Y. Zhang, Kim, et al., 2009; Y. Zhang, Sweet, et al., 2009). Several computer models have been developed to study SUI (S. Brandao et al., 2015) and pelvic organ prolapse (Z. W. Chen et al., 2015; Luo et al., 2015), but limited efforts have been made to apply this approach to explore the pathophysiology of SUI in young female athletes (Da Roza et al., 2015; Y. Zhang, Kim, et al., 2009).

In this study, we presented a complete pelvic model obtained from high-resolution subject-specific MR images of a young healthy female. The dynamic pelvic floor deformation during a jump-landing process was characterized and compared with the results of a Valsalva maneuver. The effect of the hypothesized alterations in the PFM function on urethral mobility was tested.

4.3 Materials and Methods

4.3.1 3D Female Pelvic Modeling

The 3D computational model of the female pelvis used in this study was adopted from previous modeling works (Y. Peng, R. Khavari, et al., 2016; Y. Peng et al., 2015). Briefly, T2 weighted MR images of the pelvis of a healthy female (21-year-old, white, Caucasian, nulliparous, nonsmoker, non-athletic, body mass index=22) were obtained axially with a 3T MR imaging scanner (Trio Tim, Siemens, Germany), with a slice thickness of 3mm, matrix of 320 x 160, field of view of 430mm and pixel size of 1.344mm. The images were manually segmented in Mimics (Materialise Group, Leuven, Belgium). Closed-surface 3D geometries were calculated from the

segmentation results for each pelvic floor component and then smoothed in MAYA 8.5 (Autodesk, Inc., San Rafael, CA, USA) and Rhinoceros 4.0 (McNeel North America, Seattle, WA, USA) for artifact and intersections removal. The smoothed geometries were then imported into ABAQUS 6.12 (SIMULIA, Providence, RI, USA) for tetrahedral element discretization. Segmentation and smoothing were performed under the guidance of an experienced urologist to minimize errors between the reconstructed model and original MR images. The final model consisted of 44 parts in 61,867 elements, as shown in Figure 4.1. Essential pelvic floor components including the pelvic floor muscles, bladder, vagina, uterus, rectum, ligaments, etc. were included to maximally maintain the integrity of the female pelvic anatomy. A specially-designed bodyfill part was used to represent the intra-abdominal contents and to allow the transmission of IAP during athletic activities. This modeling approach has been validated using dynamic MR imaging in our previous study (Y. Peng, R. Khavari, et al., 2016).

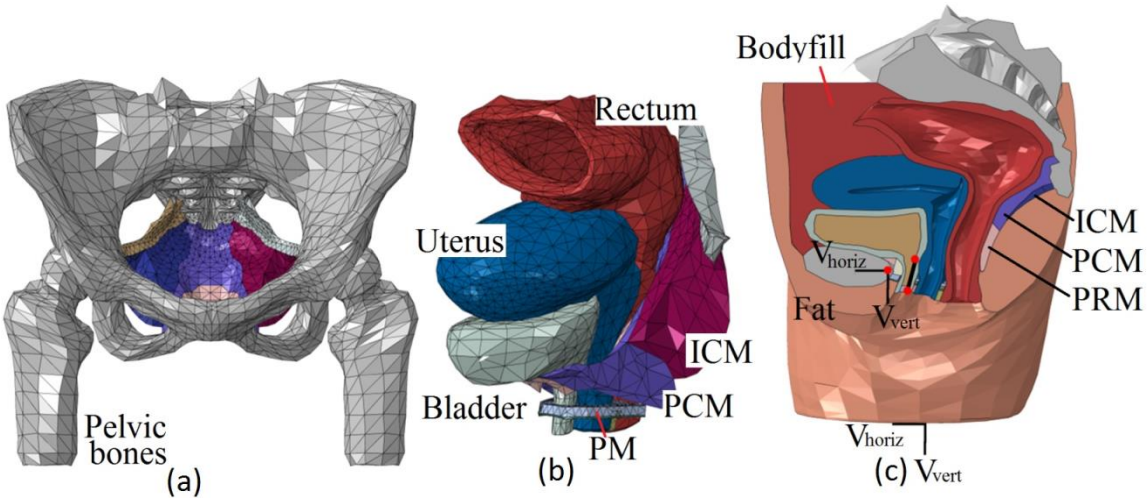

Figure 4.1 Illustration of the pelvic floor model in different views. Reproduced from Dias, Peng, Khavari, et al. (2016), with permission of Elsevier.

4.3.2 Contacts, Interactions and Boundary Conditions

Anatomical connections between soft tissues were imposed using the ABAQUS ‘‘surface-to-surface’’ tie constraint option, which couples the motion of nodes from two parts that are anatomically bound. Interactions between tissues that are not anatomically connected were defined using the ABAQUS “general contact” algorithm, which allows parts to interact with each

other with a defined interaction behavior and resist unrealistic surface intersections. Pelvic ligaments (cardinal, uterosacral and pubourethral ligaments) were modeled using connector elements with an axial elastic behavior (Luo et al., 2015). A vertical jump was simulated in this study to induce the high-impact effect, as previous studies found a higher prevalence of SUI in young female athletes whose activities involve jumping (Jácome, Oliveira, Marques, & Sá-Couto, 2011). Realistic boundary conditions were set using velocity recordings from accelerometer (Crossbow Technology, Inc., San Jose, CA). In the jump experiment, the subject jumped from a 30 cm box and landed on a hardwood floor. This height can fairly reflect the typical vertical jumping heights of collegiate female ball game players (Dalrymple, Davis, Dwyer, & Moir, 2010). The accelerometer sensor was placed on the skin directly above the iliac crest, as data captured above the approximate location of the iliac crest on the left and right lower back proved to be the most reliable (H Luginbuehl et al., 2013). During the jump process, the entire body first falls freely in the air, accelerating all body tissues uniformly because of gravity. No relative motions exist during this phase. Upon the initiation of landing (when both feet touch the ground), the bony pelvis starts to decelerate gradually because of the combined effect of inertia and the buffering effect from lower limbs. The sensor placed on the iliac crest most accurately records the motions of the bony pelvis during this process. Meanwhile, soft tissues interact with pelvic bones because of the difference in velocities and pelvic floor contents start to show deformation because of this interaction. Thus, the landing phase provides the most critical information to characterize the deformations of pelvic floor structures. The velocity recorded during the landing phase, as shown in Figure 4.2, was assigned as boundary conditions to the reference point that controlled the motion of the pelvic bones and to the bottom surface of the model, as shown in Figure 4.1c. The initial velocity upon the initiation of landing was set to move in vertical direction at 2.81 m/s and in the horizontal direction at 0.29 m/s according to the accelerometer readings.

4.3.3 Material Properties

Although biological soft tissues demonstrate viscoelastic properties (Dai et al., 2014; Q. Wang et al., 2014; J. Zhang, Koo, Subramanian, Liu, & Chattopadhyay, 2015; Zhou et al., 2014), previous studies have found a quasi-linear material property of urological soft tissues when the

stress level is under 70% of the maximal stress value (Y. Zhang, Sweet, et al., 2009). Consequently, elastic material properties were used to represent mechanical behaviors of soft tissues. Most soft tissues were modeled as linear elastic materials (Y. Peng, R. Khavari, et al., 2016; Y. Peng et al., 2015), as it has been found that linear elasticity produces a displacement field similar to that produced using nonlinear elasticity, while benefiting the computation efficiency (Mayeur et al., 2016). However, to better characterize the behaviors of the bladder and LAM, hyperelastic models were adopted (Z. W. Chen et al., 2015; Krcmar et al., 2015). The pelvic bone was modeled as a rigid body because of its much greater stiffness than soft tissues (S. Brandao et al., 2015). Table 1 summarizes the constitutive models used for soft tissues within this study.

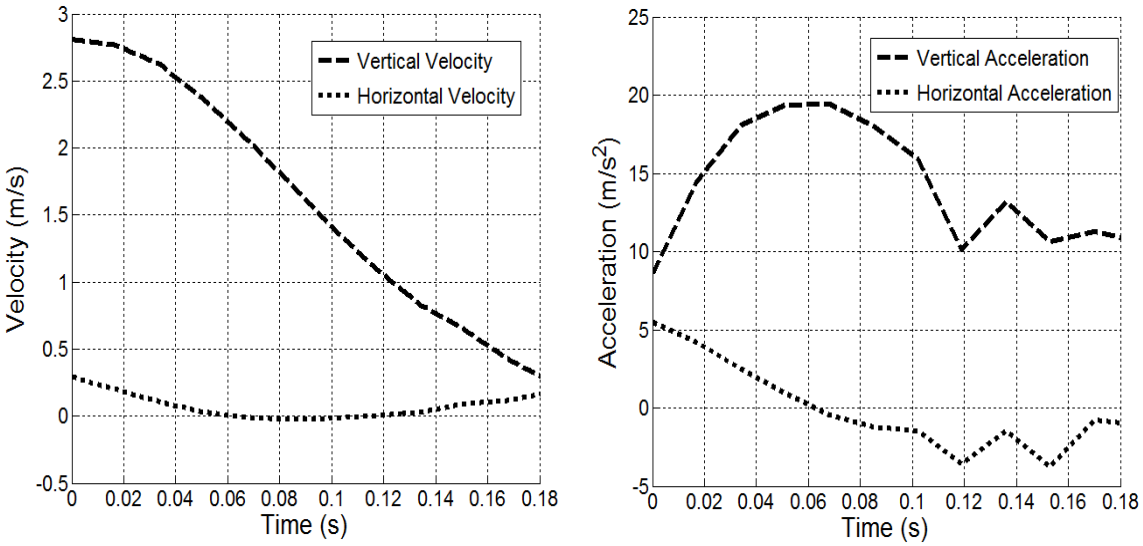

Figure 4.2 Left - horizontal and vertical velocity boundary conditions recorded from jump experiment and right - corresponding acceleration history. Reproduced from Dias, Peng, Khavari, et al. (2016), with permission of Elsevier.

Published literature postulates that PFM in athletes could be either strengthened or weakened (Bø, 2015). Our model simulated the hypothesized weakness or enhancement of pelvic floor muscles by multiplying the uniaxial stress-strain data of the LAM with a scaling coefficient (S. Brandao et al., 2015). The resulting stress-strain data was then used as the altered mechanical properties of the LAM, as shown in Figure 4.3.

Table 4.1 Material properties for the soft tissues included in the model

Structures	Material Constants		Constitutive Models	Sources
Linear elastic structures	*Young's modulus* (MPa)	*Poisson's ratio*		
Vagina and uterus	0.005	0.49	Hooke	(Haridas, Hong, Minoguchi, Owens, and Osborn (2006); Yamada and Evans (1970))
Rectum	0.1	0.49		
Fat	0.05	0.49		
Bodyfill	0.05	0.49		
Muscles (excluding LAM)	2.4	0.49		
Urine	1.0e-3	0.49		Y. Peng, R. Khavari, et al. (2016)
Hyperelastic structures				
Levator ani muscle	μ_1 = 0.0082 MPa μ_2 = 0.0216 MPa	α_1 = 0.1803 α_2 = 15.112	Ogden (N = 2)	Krcmar et al. (2015)
Bladder and urethra	C_{10} = 0.071 MPa C_{20} = 0.202 MPa C_{30} = 0.048 MPa		Yeoh	Z. W. Chen et al. (2015)
Others				
Pelvic ligaments	Axial elasticity = 0.15 N/mm *		Hooke	(Luo et al., 2015)
Pelvic bones	Rigid		Rigid body	(S. Brandao et al., 2015)
**linearized*				

Reproduced from Dias, Peng, Khavari, et al. (2016), with permission of Elsevier.

4.3.4 Design of Simulations

A total of nine tests were performed. Table 4.2 summarizes the plan of simulations conducted in this study. In the control test, there was no enhancement or impairment of the LAM. In the weakening tests, impairments of 25%, 50%, 75% and 95% were simulated using a scaling coefficient of 0.75, 0.5, 0.25, and 0.05, respectively. In the strengthening tests, enhancements of 25%, 50%, 75% and 100% were simulated using a scaling coefficient of 1.25, 1.50, 1.75 and 2.00.

Table 4.2. Plan of simulations and results

Test #	Change in Material Properties	Scaling Coef.	First Peak IAP (cmH_2O)	Second peak IAP (cmH_2O)	Maximum Bladder neck displacement (mm)	Maximum urethral excursion angle (°)
Control						
C0	0	1.00	191.5	109.6	12.1	22.9
Weakened						
1	25	0.75	193.5 (+2.0)*	112.3 (+2.7)	12.2 (+0.1)	22.9 (+0.0)
2	50	0.50	193.2 (+1.7)	112.9 (+3.3)	12.6 (+0.5)	23.3 (+0.4)
3	75	0.25	193.5 (+2.0)	112.4 (+2.8)	13.1 (+1.0)	24.0 (+1.1)
4	95	0.05	193.7 (+2.2)	112.3 (+2.7)	13.7 (+1.6)	24.9 (+2.0)
Strengthened						
1	25	1.25	194.6 (+3.1)	113.2 (+3.6)	11.9 (−0.2)	22.3 (−0.6)
2	50	1.50	193.8 (+2.3)	112.7 (+3.1)	11.6 (−0.5)	21.9 (−1.0)
3	75	1.75	193.3 (+1.8)	112.7 (+3.1)	11.2 (−0.9)	21.1 (−1.8)
4	100	2.00	192.8 (+1.3)	112.9 (+3.3)	11.1 (−1.0)	20.1 (−2.8)

* *Number in bracket represents the amount of change from the control test, applies to all*

Reproduced from Dias, Peng, Khavari, et al. (2016), with permission of Elsevier.

In each test, the bladder neck displacement in the sagittal plane and the urethral excursion angle (clinically equivalent with Q-tip rotational angle) were used as metrics to assess the urethral hypermobility (Y. Peng, R. Khavari, et al., 2016; Y. Peng et al., 2015). Definitions of these two metrics are shown in Figure 4.1. The IAP, calculated as the contact pressure between the inner bladder wall and the urine, was also reported. All of these metrics were monitored dynamically throughout the simulation time using ABAQUS history and field output request functions. The computation was conducted in parallel processing with an AMD Cluster (Maxwell, 8 cores on 2 CPUs: 16 nodes total, 2GB RAM) in the Center for Advanced Computing and Data Systems at the University of Houston. On average, it took about 5 hours for the Maxwell cluster to complete 1 computation task.

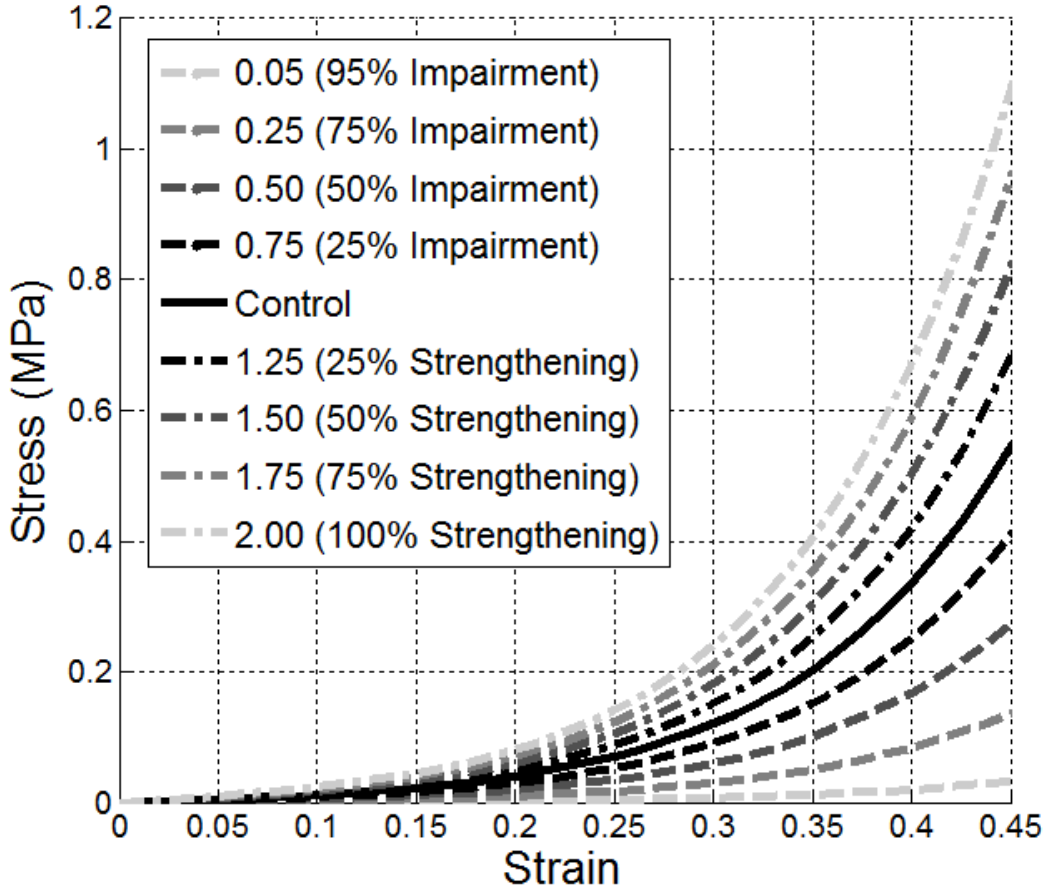

Figure 4.3 Stress-strain curves of the intact, impaired and strengthened levator ani muscle. Reproduced from Dias, Peng, Khavari, et al. (2016), with permission of Elsevier.

4.4 Results

The simulation results showed that the pelvic floor deformation during a jump landing process demonstrated two stages (Figure 4.4). During stage one, the pelvic floor showed a “leaning forward compression”. Compared with the resting state configuration (Figure 4.4a), the bladder was compressed against the decelerating pubic bone and stretched anteroposteriorly (Figure 4.4b). The frontal bladder leaned forward partly because of the compression and partly because of the initial horizontal velocity. At the end of stage one, the bladder was maximally compressed against the front bodyfill part with all of its kinetic energy converted to the elastic potential energy. During stage two, the bladder started to “bounce back” because of the release of the stored elastic potential energy and to develop posterior deformations further differing from the resting

state, as shown in Figure 4.4c. Supports were provided by the posterior compartments (vaginal wall and LAM) to counterbalance the excessive posterior motions (hypermobility).

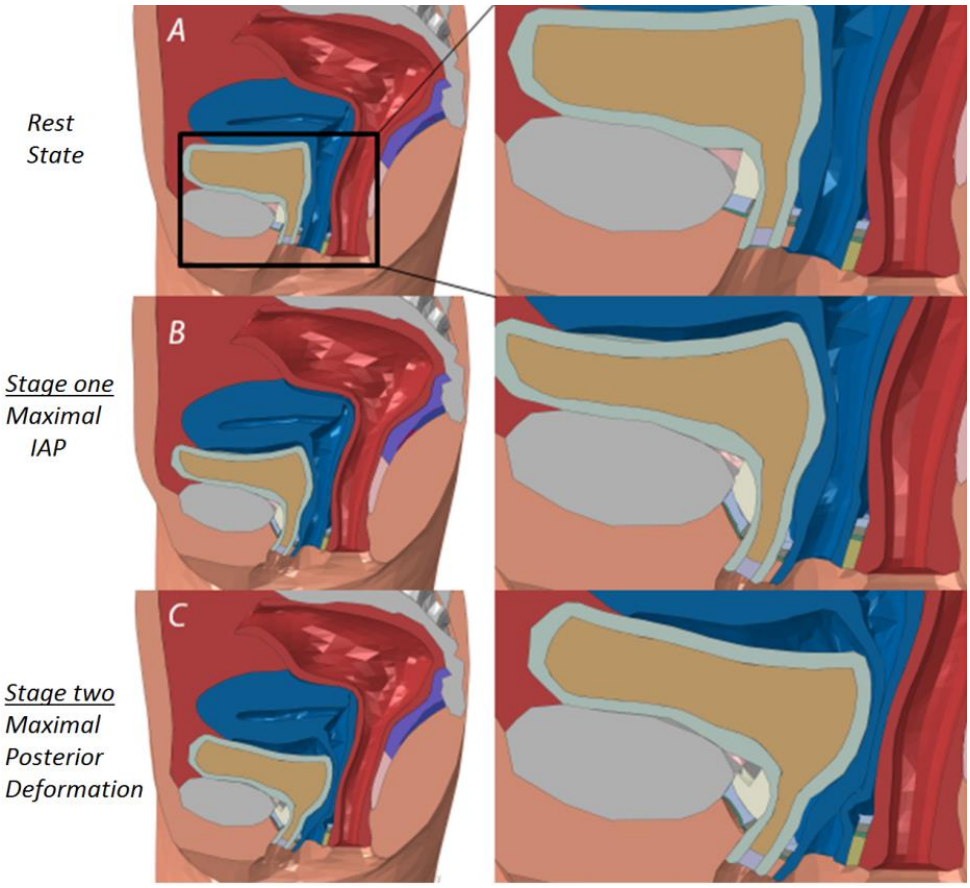

Figure 4.4 Pelvic floor configurations at the (a) rest state, (b) maximal IAP and (c) maximal posterior deformation. Reproduced from Dias, Peng, Khavari, et al. (2016), with permission of Elsevier.

For the control test, the IAP reached a first peak of 194.6 cmH_2O at 0.064 seconds. A second peak of 114.1 cmH_2O was found at 0.136 seconds. A maximum bladder neck displacement of 12.1 mm and a maximum urethral excursion angle of 22.9° were found in the control test, both occurring at a time instance close to the second IAP peak. Table 2 summarizes the results for all tests. Altering the LAM stiffness caused only slight differences in the two peak IAPs (all less than 4%). The differences in the maximum bladder neck displacement ranged from −0.2 mm to +1.6 mm and in the maximum urethra excursion angles from −2.8° to 2.0°.

4.5 Discussion and Conclusions

In this study, we developed a whole-pelvic model from a healthy nulliparous female subject and used it to describe the deformations of pelvic floor structures during the jump-landing process and test the effects of altered LAM stiffness on the urethral mobility metrics.

4.5.1 Comparison with the Valsalva Maneuver

A separate Valsalva simulation was performed using the method described in a previous simulation study (Y. Peng, R. Khavari, et al., 2016; Y. Peng et al., 2015). Our simulation showed that the deformations of pelvic floor structures during the jump-landing process differed greatly from that produced in the Valsalva maneuver. The obtained IAP history and the deformation of pelvic floor structures at the maximal IAP were compared. First, at the maximal IAP, the deformation pattern in jump-landing was both anterior and posterior because of the compression against the pelvic bone (Figure 4.4b and 4.5a), while in the Valsalva maneuver, the deformations were presented more in an inferoposterior direction (Figure 4.5b). This is consistent with our preliminary simulation observations (Peng, Khavari, Stewart, Boone, & Zhang, 2015), and can be explained by the directions of the efforts applied. In jump-landing, the deformation was largely due to the vertical compression of the organs against the pelvic bone, while in straining activities, the effort was oriented at 45 degrees with respect to horizontal axis, from anterior to posterior direction (Mayeur et al., 2016). Second, there was a distinct difference in the history of the IAP development, as seen in Figure 4.5c. Unlike the Valsalva maneuver, which only produced one single IAP increase (Y. Peng, R. Khavari, et al., 2016), the jump-landing process produced two IAP peaks (Figure 4.6a). The first peak can be explained by the intensifying compression between the free falling soft tissues and the decelerating pubic bone during the falling stage, and was evidenced by the simultaneous occurrence of the maximum IAP (Figure 4.6a) and the maximum deceleration (Figure 4.2b) around 0.07 seconds. The second peak can be explained by the “bouncing back” motion of the bladder during stage two. The bladder was compressed horizontally against the vaginal wall and the LAM and thus caused the contact pressure between the inner bladder wall and the urine to increase. This was evidenced by the simultaneous occurrence of the maximal urethral mobility with the second IAP peak around 0.14 seconds.

Third, in terms of the IAP magnitude, the maximal IAP observed in the jump landing simulation (194.5 cmH_2O) was much higher than Valsalva simulation results (Figure 4.5c) or clinical recordings (Cobb et al., 2005). This IAP value was consistent with pressure readings obtained from previous tests using a transurethral bladder catheter (232 ± 66 cmH_2O) (Cobb et al., 2005).

Because of the challenging nature of performing internal imaging tasks during high-impact athletic activities, Valsalva maneuvers are often used alternatively to assess the pelvic floor dynamics of young female athletes (Kruger et al., 2007). Our simulation results showed that differences exist in terms of IAP development, IAP peak values and pelvic floor deformation patterns. Clinical diagnosis should make allowances for these differences to ensure accuracy.

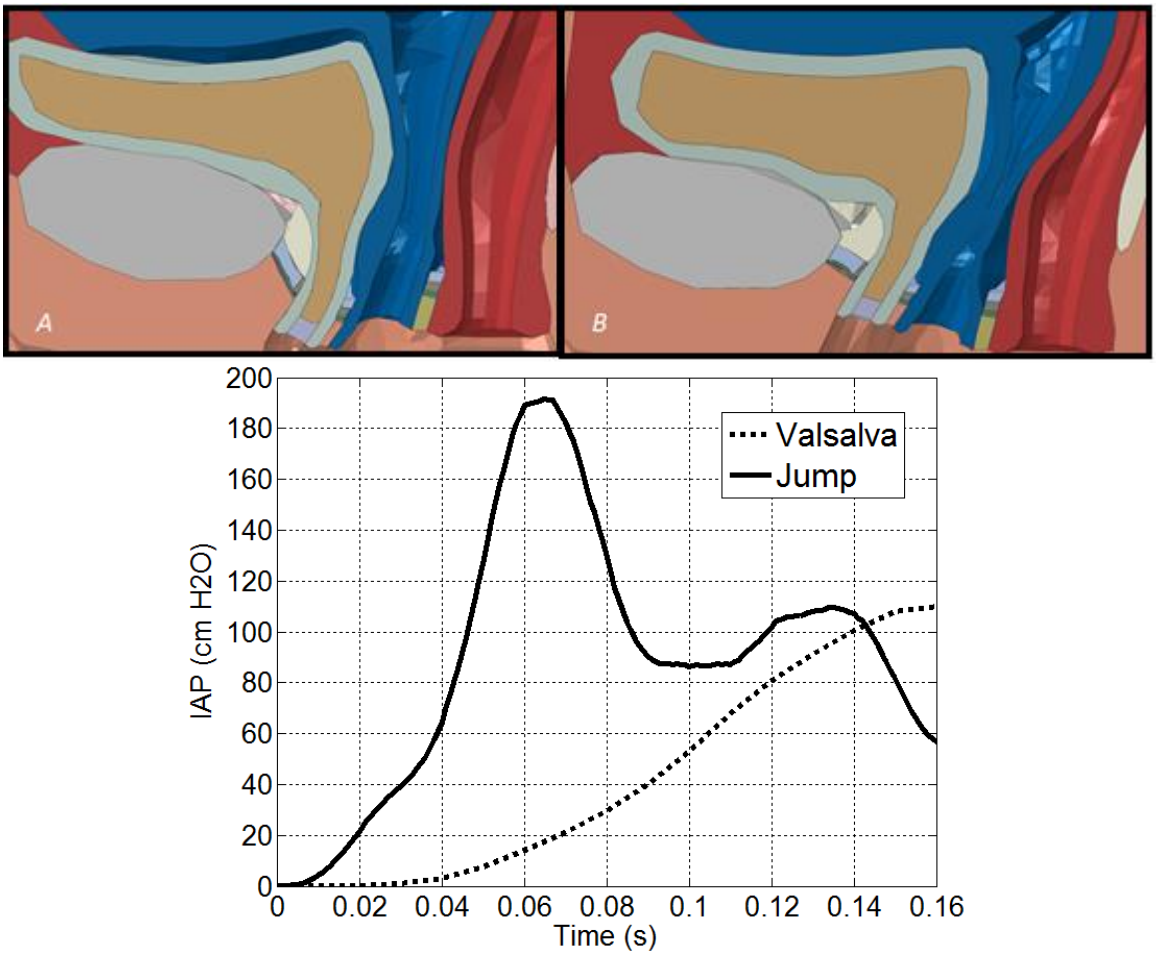

Figure 4.5 The comparison of the pelvic floor deformations between (a) jumping and (b) Valsalva at maximal IAP. (c) The comparison of the IAP history plots of jumping and Valsalva. Reproduced from Dias, Peng, Khavari, et al. (2016), with permission of Elsevier.

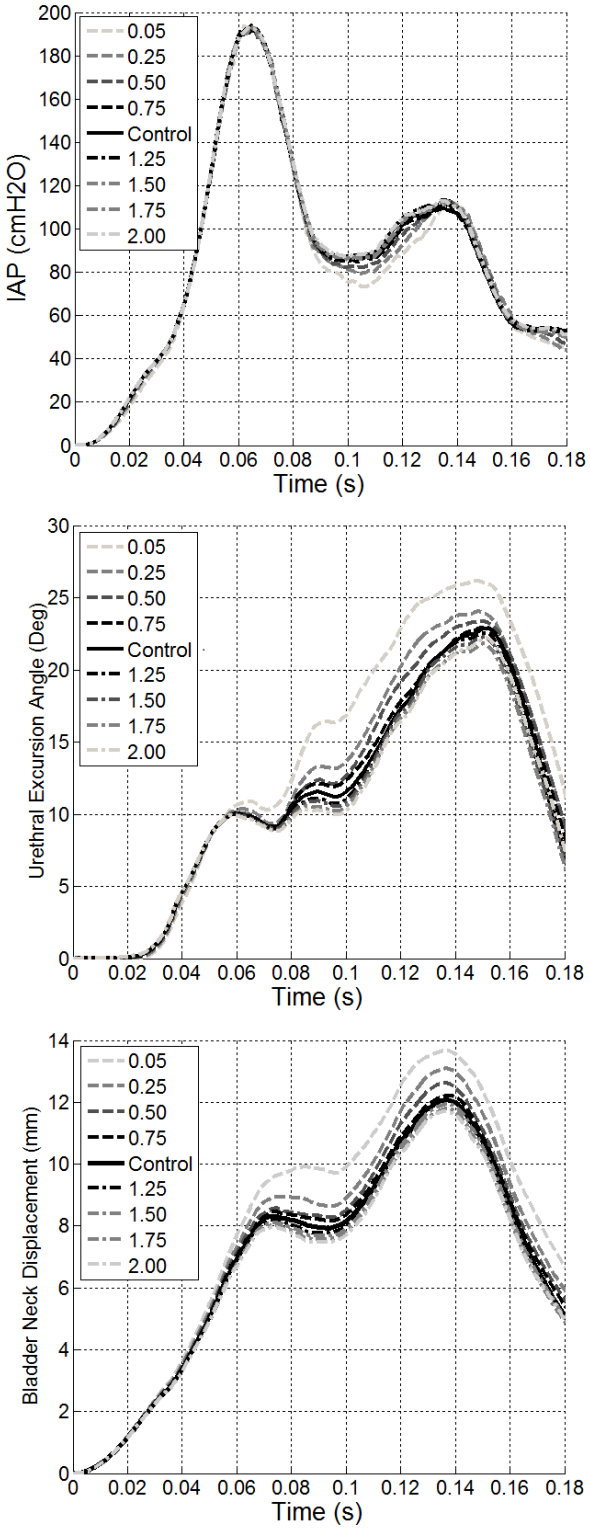

Figure 4.6 Plots of the evolutions of the (a) Intra-abdominal pressure, (b) urethral excursion angle and (c) bladder neck displacement. Reproduced from Dias, Peng, Khavari, et al. (2016), with permission of Elsevier.

4.5.2 Relation to the Risk Factors for SUI

We found that the effect of weakened LAM stiffness on the proposed urethral hypermobility metrics was minor. The displacement and urethral rotation were increased by only 1.6 mm (13%) and 2° (9%). They differed from common clinical observations: Kruger el. al found that athletes showed greater bladder neck descent on maximal Valsalva maneuver when compared with the control group (Kruger et al., 2007). Previous simulation results showed that LAM impairment highly impacts the urethral excursion angle on Valsalva maneuver (Y. Peng, R. Khavari, et al., 2016). A possible explanation for this difference is that the previous studies focused on the Valsalva maneuver, while our model examines the urethral excursion during a jump landing. These activities are quite different in nature - Valsalva produces a slow and steady increase in intra-abdominal pressure, while a jump landing results in an intra-abdominal pressure that is strong but transient. The directions of pressure loads in these two activities on pelvic organs are also distinct, as described in Section 4.1. Combined together, these factors made urethral hypermobility a noticeable observation in Valsalva but less obvious during landing a jump. These differences suggested that, during jump-landing, the female pelvic floor reacts to the sudden IAP increase quite differently from the way commonly seen in daily pressure activities. This finding downplayed the role of the weakened LAM stiffness as an etiological factor of the weakened urethral closure functions in young female athletes.

What remains unanswered is what puts the young female athlete at risk for developing SUI. Ashton-Miller and DeLancey explained the urinary continence mechanism through two systems: the intrinsic sphincteric closure system, formed by the urethral sphincteric muscles, and the urethral support system, formed by pelvic floor muscles and connective tissues (ASHTON-MILLER & DeLANCEY, 2007). Although the pelvic floor can effectively balance the sharp IAP increase during athletic activities to avoid urethral hypermobility, this increases may exceed the capability of the intrinsic closure system. The intrinsic sphincteric closure system seems to contribute more to the maintenance of continence. This may explain why many athletes reported leakage only during athletic activities but not in daily life.

To further explore the risk factors for weakened urethral closure functions in young female athletes, attention should be focused on the characterization of the strength of the urinary sphincteric closure system and, for severe cases, on the neurogenic impairment of urinary sphincter muscles. Preventative actions should also be directed towards enhancing the urethral closure functions.

4.5.3 Relation to the Pelvic Floor Muscle Training

Pelvic floor muscle training has been shown to be effective at treating SUI for the general population (Bø, 2012). A recent study also evidenced the effect of pelvic floor muscle training on incontinence of young nulliparous female athletes (N=7) (Da Roza et al., 2012). As one hypothesis was that athletes have strong pelvic floor muscles because of training stimulus, we tested the effect of enhanced LAM stiffness on urethral mobility. The results showed that the effect of enhanced LAM stiffness on urethral mobility metrics was not remarkable: the maximum bladder neck displacement was lowered by 1 mm (8%) and the urethral excursion angle by 2.8° (12%). These results suggested that the enhanced stiffness of LAM does not reduce the urethral mobility. A possible explanation for weakened urethral closure function in athletes is the repeated stretching of the pudendal nerve in response to repeated instances of substantially increased intra-abdominal pressure. Previous studies have correlated a state of chronic increased intra-abdominal pressure in obese patients with a weak urethra and urinary incontinence (Noblett, Jensen, & Ostergard, 1997). Considering the broad benefits of pelvic floor muscle training, we should not be discouraged by the findings presented in this paper. On one hand, in addition to increased muscle stiffness, pelvic floor muscle training also means a conscious pre-contraction of PFM during physical stress and a muscle volume increase (Bø, 2004; Brækken, Majida, Engh, & Bø, 2010). These changes are found to benefit the maintenance of continence and provide opportunities for future computer simulation work. On the other hand, the observed limited impact of LAM stiffness on the reduction in urethral mobility would otherwise help redirect the focus of physical therapists towards more efficient biometrics in assessing the urethral integrity in young female athletes.

4.5.4 Limitations and Future Research

One limitation is that we only studied the effects of altered LAM stiffness. Athletes may also demonstrate increased muscle thickness and diameter, and elevated bladder and rectum (Brækken et al., 2010; Kruger et al., 2007). These anatomical changes should also be considered to ensure the complete characterization of the pelvic floor structures of young female athletes. With the convenience in MR imaging and computer modeling, these morphological factors can be included in future studies. Another limitation of this study is the lack of statistical power, as the results reported in the study are achieved based on one single pelvic model constructed from one particular subject's MRI data. Efforts will be taken in the future to perform this study based on multiple subjects' pelvic models to take into account the effects of the pelvic anatomy variations on simulation results.

4.5.5 Conclusions

The computational modeling and simulation approach is a useful tool for studying the highly-transient pelvic floor dynamics. We found that pelvic floor deformed distinctly during jump-landing and Valsalva. Clinical diagnosis should make allowances for differences between the pelvic floor deformations in a Valsalva maneuver and those in a jump-landing process to ensure accuracy. We also found that altered LAM stiffness caused only slight changes in urethral mobility, suggesting that urethral hypermobility may be less dominant than expected as a factor causing weakened urethral functions and SUI in young female athletes. Future studies are encouraged to investigate the function of the intrinsic urethral closure system.

CHAPTER 5 – Development of a Subject-Specific Electrophysiological Pelvic Model

5.1 Abstract

Introduction and Hypothesis: Knowledge of the innervation of pelvic floor and sphincter muscles is of great importance to understanding the pathophysiology of female pelvic floor dysfunctions. This study aims to present our high-density intravaginal and intrarectal electromyography (EMG) probes and a comprehensive innervation zone (IZ) imaging technique based on high-density EMG readings to characterize the IZ distribution. *Methods*: Both intravaginal and intrarectal probes are covered with a high-density surface electromyography electrode grid (8 X 8). Surface EMG signals were acquired in 10 healthy female subjects during maximum voluntary contractions of their pelvic floor. EMG decomposition was performed to separate the motor unit action potentials (MUAPs) and then localize their IZs. *Results:* High-density surface EMG signals were successfully acquired over the vaginal and rectal surfaces. The propagation patterns of muscle activity were clearly visualized for multiple muscle groups of the pelvic floor and anal sphincter. Up to 218 repetitions of vaginal motor units and 456 repetitions of rectal motor units were detected during each contraction. MUAPs were separated with their IZs identified at various orientations and depths. *Conclusions:* The proposed probes are capable of providing a comprehensive mapping of the innervation zones of the pelvic floor and sphincter muscles. They can be employed as diagnostic and preventative tools in clinical practices.

5.2 Introduction

Pelvic floor muscles (PFMs) are intimately involved in normal pelvic floor functions. Neuromuscular injury to PFMs may cause pelvic floor dysfunctions such as incontinence or prolapse. Electromyography (EMG) has been widely used to assess the neuromuscular function of PFMs in clinical and research environments (Enck & Vodusek, 2006). Needle EMG is known for its high selectivity and has been used to investigate the neuronal control of the external anal sphincter (EAS) in patients with incontinence (Enck, Hinninghofen, Wietek, & Becker, 2004).

However, this technique is not only invasive but also lacks the ability to provide global information of the muscle activation. Perineal EMG, in which the electrode is attached to the perineal skin surface, is not selective because of high risk of crosstalk (Keshwani & McLean, 2015). Consequently, efforts have been made to develop intravaginal probes and intrarectal probes with mounted electrodes as a minimally-invasive alternative (Enck & Vodusek, 2006; Keshwani & McLean, 2015).

In order to provide a comprehensive functional map of PFMs through EMG, an ideal EMG probe should have two characteristics: 1) sufficient electrodes longitudinally to detect and differentiate superficial and deep muscles (Voorham-van der Zalm et al., 2013), and 2) sufficient electrodes circumferentially aligned parallel to the muscle fiber to perform motor unit action potential (MUAP) detection and to study the muscle innervation (Enck, Franz, et al., 2004; R. Merletti et al., 2004). These two characteristics require that an ideal probe has high-density electrodes in both longitudinal and circumferential dimensions. A recent state-of-art review showed that current commercially available intravaginal probes are limited by their probe geometry, large detection surfaces and inappropriate electrode configurations (Keshwani & McLean, 2015). The lack of a sufficient number of channels also prevented them from being used for MUAP detection. Recently, a high-density anal EMG probe (three circumferential arrays with 48 electrodes) has shed new light on the investigation of the innervation of EAS muscles (Cescon et al., 2014; Enck, Franz, et al., 2004; R. Merletti et al., 2004). However, its application is limited in assessing deep PFMs, such as the pubococcygeus muscle because of insufficient longitudinal electrodes. In another recently reported study, a multiple-electrode probe (with a measurement range of 50mm longitudinally) demonstrated the capability of differentiating deep and superficial muscles (Voorham-van der Zalm et al., 2013), but the low spatial circumferential resolution made it inappropriate for MUAP detections. A recent study showed the possibility of mounting EMG electrodes on a urethral catheter surface to measure the activity of urethral sphincter muscles (Stafford, Sapsford, Ashton-Miller, & Hodges, 2010). However, compared with the urethra, the vaginal and rectal spaces have greater volumes and are more distensible. These characteristics challenge the intravaginal or intrarectal catheter probe designs because high-density electrodes

require accommodation on highly-stretchable probe surfaces. Although a few attempts have been made to design compressible electrodes (Boyd, Gregson, & Herbert, 2015; Sim et al., 2015), published results are scarce in the existing literature.

In this study, we present our newly developed high-density, two-dimensional intravaginal and intrarectal surface EMG probes to feature the desired characteristics (Peng, He, Khavari, Boone, & Zhang, 2015). The probes are equipped with an 8X8 high-density electrode grid which allows the MUAP detection and innervation zone (IZ) mapping from the entire vaginal and anorectal canal surface. It is expected that our new probes will provide a comprehensive functional mapping of the female PFM/EAS and meet the imperative need for neurogenic PFM/EAS disorder characterization (Whitehead et al., 2015).

5.3 Materials and Methods

5.3.1 Subjects

Ten healthy young female subjects (age [mean ± S.D.]: 29.1 ± 7.1 years) participated in the study. Enrollment was limited to normal, healthy female volunteers with no history of pelvic injuries or neuromuscular diseases. The EMG studies were carried out at the Houston Methodist Hospital with the protocol approved by both the University of Houston and Houston Methodist Hospital Institutional Review Boards. All participants gave informed consents.

5.3.2 Probe Design

The intravaginal and intrarectal probes were designed at the University of Houston and manufactured by the Twente Medical Systems International (Enschede, The Netherlands). Both probes are cylindrical in shape with a total length of 175 mm. A high-density electrode grid (8 X 8) is coated on the surface of each probe (see Figure 5.1a). The intravaginal probe is 22.7 mm in diameter. The electrode surface is circular with a diameter of 4.0 mm. The inter-electrode spacing (center to center) is 8.8 mm both longitudinally and circumferentially. The intrarectal probe is 14.4 mm in diameter. The electrode surface is rectangular with a length of 4.0 mm and a width of 2.4 mm. The inter-electrode spacing (center to center) is 8.0 mm longitudinally and 5.7 mm circumferentially. The top of both probes is spherical. The application of a proper amount of gel is

advised for ease of insertion. Compared with existing probes (Cescon et al., 2014; Enck, Franz, et al., 2004; R. Merletti et al., 2004), our probes have more channels that are in favor of advanced EMG analysis techniques and a better longitudinal coverage that enables the access to deep PFMs. Our intravaginal probe is the first high-density intravaginal probe.

For a convenient reference to the electrode locations on the probe surface, we adopted a row and column numbering convention (see Figure 5.1a). Hereinafter, the circumferential rows are numbered from 1 (superficial) to 8 (deep). The longitudinal columns are numbered in a counter-clockwise way in the caudal view and divided into four quadrants: ventral (8, 1), right (2, 3), dorsal (4, 5) and left (6, 7).

5.3.3 Experimental Protocol

All tests were performed at the Houston Methodist Hospital guided by an experienced urologist (R.K). All subjects were instructed by the urologist to contract their pelvic floor muscles prior to the insertion of the probes. The individuals were re-examined for appropriate pelvic floor contractions following the insertion of the probes. The subjects were tested in the lithotomy position leaning their backs on a tilted exam table (about 30° from horizontal). The probes were inserted with the help of the urologist to maintain the correct orientation and depth, as shown in Figure 5.1b. A correct insertion was described as having the trademarks faced dorsally and the edge of the electrode grid aligned with the urogenital orifices. After probe placement, a few trial PFM contractions were attempted while the signals were visually inspected in real time for quality check.

Subjects were involved in two test sessions. Ten short contractions were performed in session one to give as hard as possible contraction forces, and ten sustained long contractions were performed in session two. The subjects were allowed sufficient resting time between two continuous contractions and rested fully to relax their PFMs between two sessions. The ground electrode was placed at the wrist of the subject connecting to a fully-soaked wristband in accordance to the manufacturer’s recommendation. The wrist area was slightly abraded and cleaned using alcohol patches to lower the surface impedance.

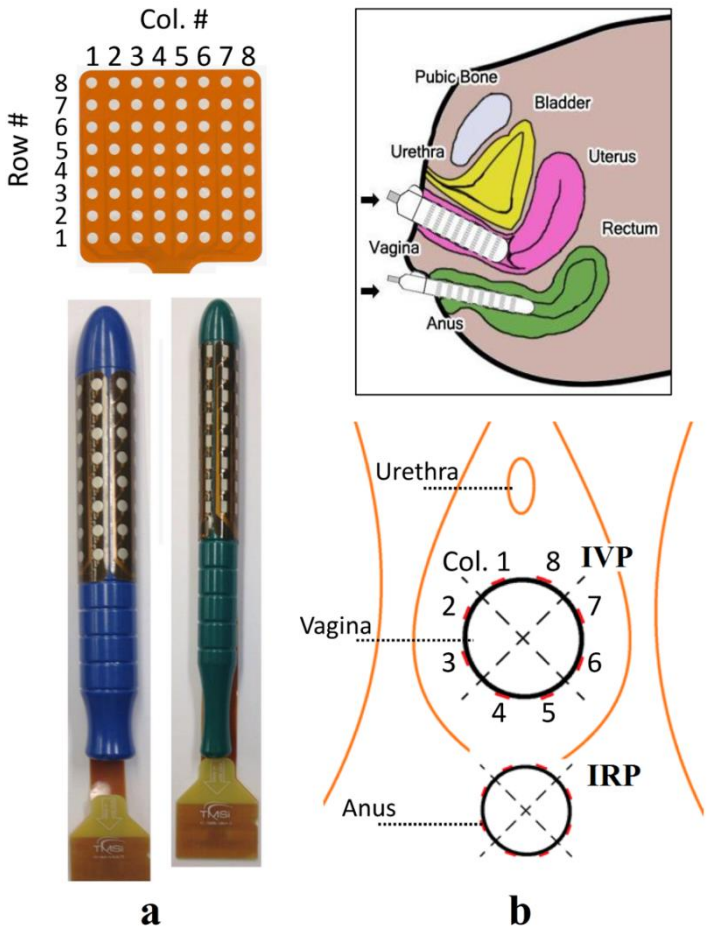

Figure 5.1 Illustration of intravaginal and intrarectal probes, the description of the channel numbering convention and insertion positions. Reproduced from Peng, He, Khavari, Boone, and Zhang (2016), with permission of Springer.

5.3.4 Data Collection and Processing

Myoelectric signals were acquired with a 136 channel Refa amplifier (Twente Medical Systems International, The Netherlands) at a sample rate of 2048 Hz and stored in a personal computer. During offline process, the signals were digitally filtered in MATLAB R2015 (Mathworks Inc., Natick, MA) with a 4th-order band-pass Butterworth filter (15-400 Hz band) without phase distortions. The root mean squares of the EMG recordings from a window of 0.1s (205 samples) were calculated for three muscles (the external anal sphincter, the puborectalis muscle and the pubococcygeus muscle) from the rectal recordings for each contraction of each subject, following the method used in (Voorham-van der Zalm et al., 2013). To test the reliability of the probes, the intraclass correlations between two sessions (ICCs) for these three muscles were calculated to

determine different sources of EMG measurement variation (between subjects and within subject) following the method previously used in assessing an intravaginal probe (Grape, Dedering, & Jonasson, 2009).

EMG decomposition based on the convolution kernel compensation (CKC) has been shown to be an effective tool for identifying the single MUAP from interferential surface EMG signals (A. Holobar & D. Zazula, 2007). This technique has been validated extensively with both simulated and experimental signals (A. Holobar & D. Zazula, 2007; X. Li et al., 2015). Our newly developed K-means clustering and convolution kernel compensation (KmCKC) approach was utilized to decompose the high-density rectal and vaginal EMG signals into their constituent MUAP trains (Liu et al., 2015; Ning, Zhu, Zhu, & Zhang, 2015). Briefly, the K-mean clustering method was first adopted to cluster firing times of the same motor unit (MU). The initial innervation pulse train can be estimated during this process by choosing an appropriate number of clustered groups and time instants so that the time instants fired by a single MU can be gathered into one group as completely as possible. Then an improved multi-step iterative CKC method was employed to update the estimated innervation pulse trains to improve the decomposition accuracy in a noisy environment.

The IZ is the region of a MU including the neuromuscular junction where the MUAPs are generated and propagate in two opposing directions along the muscle fibers (Enck, Franz, et al., 2004). The EMG signals propagating in opposite directions appear with opposite phases in the bipolar MUAP maps (Liu et al., 2015). Therefore, the position of the IZ of a particular MU can be localized from the bipolar map of the decomposed high-density MUAPs by checking the phases of the propagating signals.

5.4 Results

Ten healthy female subjects (age<40) were enrolled in this study. EMG recordings from two of them (1009 and 1010) were excluded because of large movement artifacts during contractions and bad electrode-mucosa contacts. The ICCs between two sessions were calculated (EAS 0.95,

puborectalis 0.88 and pubococcygeus 0.90), demonstrating a good (0.80<ICC<0.89) to high (ICC>0.90) reliability (Grape et al., 2009). Figure 5.2 shows an example of acquired EMG signals.

MUAPs were detected at different depths of the EMG grid. Figure 5.3 shows an example of MUAP propagation patterns obtained from circumferential electrodes. EMG decomposition was successfully performed. IZs were visually inspected for each MUAP of each subject. The propagations of each MUAP were estimated from the high-density surface EMG signals. Figure 5.4 shows an example of the identified IZs at different depths of the rectal probe. Up to 10 (5 ± 3) vaginal motor units with 107 ± 80 repetitions of the MUAPs and up to 15 (9 ± 3) rectal motor units with 263 ± 111 repetitions of MUAPs were detected during each contraction. Figure 5.5 shows an example of the IZ distributions obtained from the vaginal and rectal readings.

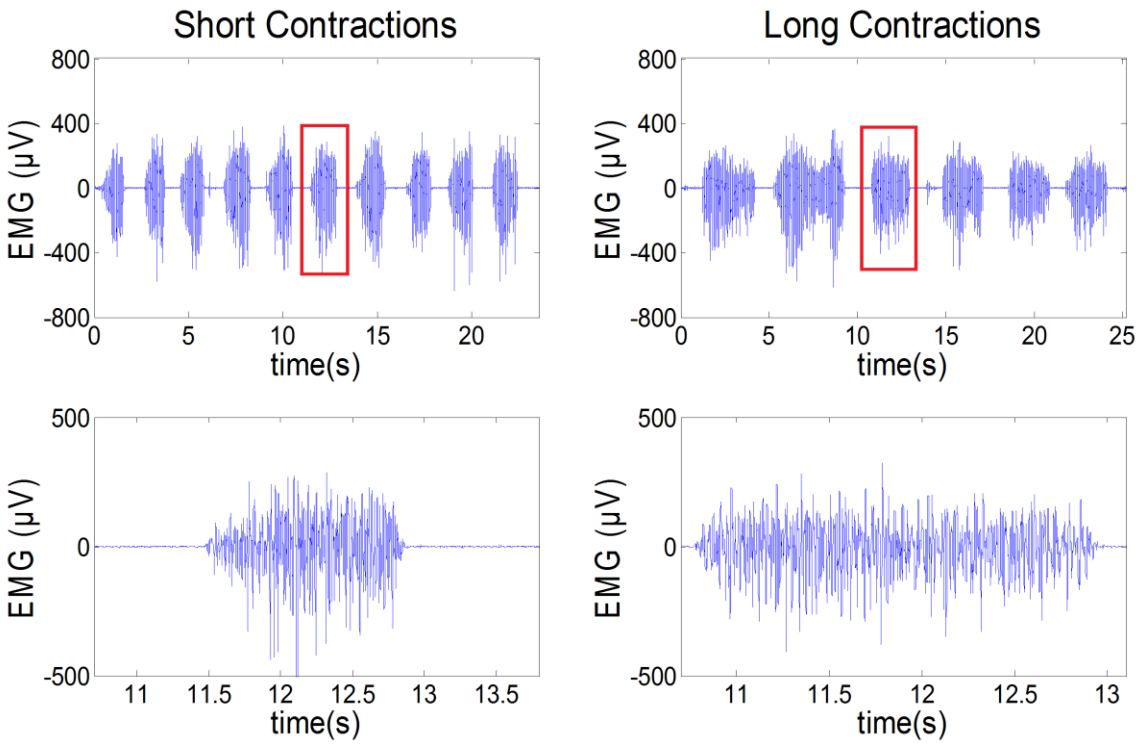

Figure 5.2 Examples consecutive short contractions and sustained contractions. Reproduced from Y. Peng, J. He, R. Khavari, et al. (2016), with permission of Springer.

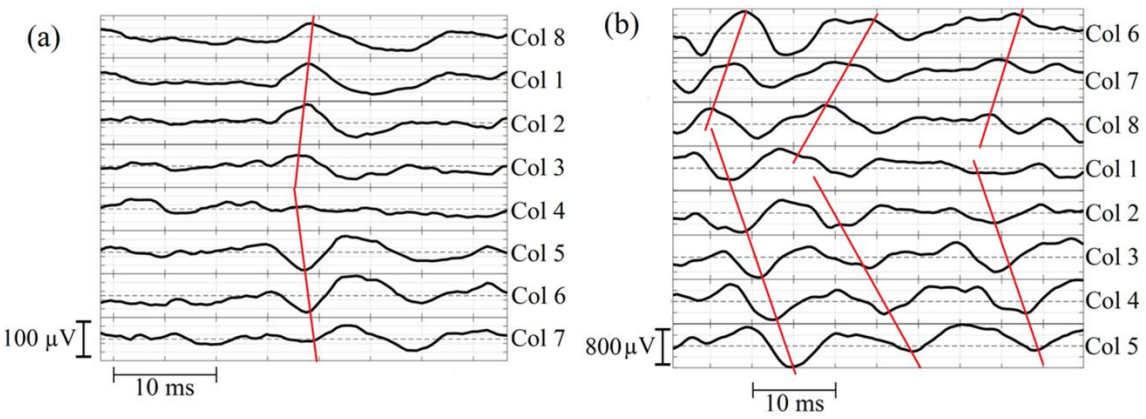

Figure 5.3 Example of MUAP propagation patterns. Reproduced from Y. Peng, J. He, R. Khavari, et al. (2016), with permission of Springer.

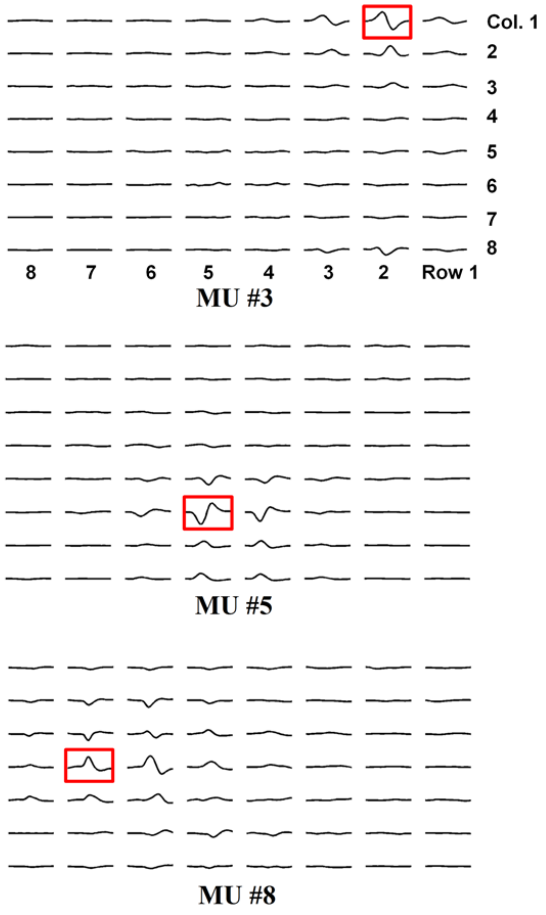

Figure 5.4 Examples of the MUAP distributions among the entire grid surface of three MUs at the (a) superficial, (b) intermediate and (c) deep levels of the rectal probe. Reproduced from Y. Peng, J. He, R. Khavari, et al. (2016), with permission of Springer.

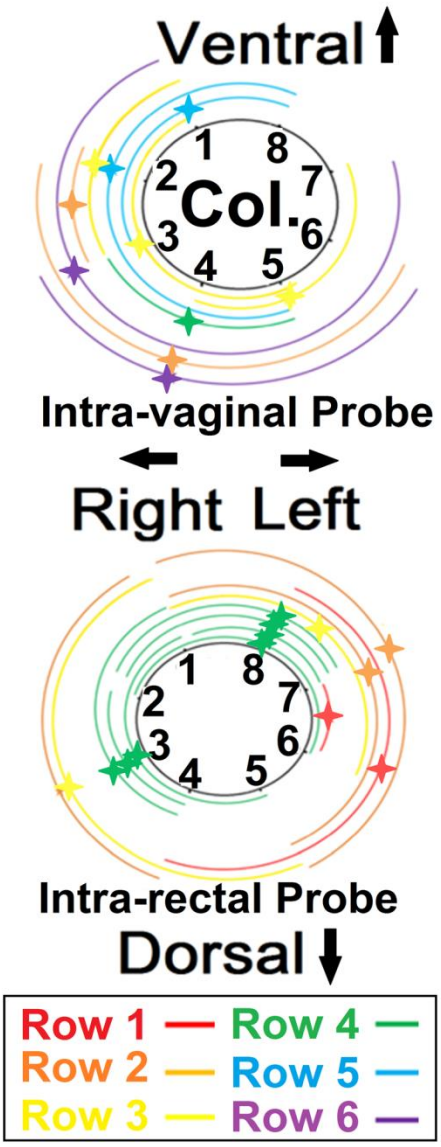

Figure 5.5 An example of the mapped IZ distributions and MUAP propagations of one subject. Reproduced from Y. Peng, J. He, R. Khavari, et al. (2016), with permission of Springer.

5.5 Discussion and Conclusions

In this study, we report development and testing of minimally-invasive intravaginal and intrarectal probes for simultaneous EMG acquisition of the PFM/EAS in women. EMG decomposition was performed using the KmCKC algorithm. MUAPs from different MUs separated and their IZs identified. A global IZ distribution map was provided for each probe of each subject.

For the vaginal signals, an average number of 5.1 ± 3.3 IZs were identified. To the best of our knowledge, this is the first effort made to perform MUAP detection using EMG readings recorded with an intravaginal probe. This may have important implications for prolapse studies. Cystocele and uterine prolapse have been found to be associated with levator avulsion injuries, in which the levator ani muscle may be disconnected from the side of the vaginal wall (H. P. Dietz & Simpson, 2008). The MUAP and IZ information revealed from vaginal recordings may provide useful information in assessing the vaginal wall support from the lateral levator ani muscle attachment if the disrupted attachment creates a denervation-based injury. For the rectal signals, an average number of 9.3 ± 2.8 IZs were identified. This was qualitatively in agreement with number of IZs in reported studies (Cescon, Bottin, Fernandez Fraga, Azpiroz, & Merletti, 2008; Cescon et al., 2014). We found that the IZ distributions obtained from both probes were not strictly left-right symmetric (Figure 5.5). This may be due to the unique innervation that each side of each PFM/EAS receives and this asymmetric innervation may exist in healthy females (Enck, Hinninghofen, et al., 2004; Enck & Vodusek, 2006). These results provide valuable information towards a better understanding of the synergistic activation of the PFM/EAS musculature. Though synergistic activations are found between the abdominal muscles and PFMs in women (Madill & McLean, 2008), it has never been investigated between muscles within the pelvic girdle musculature. Such information, available through concurrently monitoring EMG activity of different muscles with the developed EMG probes, would provide insights into the physiology of continence maintenance and compensation mechanism with functional defects.

We also found that the anorectal MUAPs encircled the lumen more extensively compared with vaginal MUAPs. This may be due to the fact that the vaginal canal is only bilaterally attached to the PFM, while the anorectum is more fully surrounded by the PFM/EAS musculature. This finding may provide valuable information for clinical practice and pelvic floor physiotherapy. For example, mediolateral episiotomy is often preferred over midline episiotomy due to lower rates of obstetric injuries when episiotomy is deemed necessary, however, the selection of the incision angle and side, which should aim to minimize potential trauma, was often subjectively (Cescon et al., 2014). The map of the IZ distribution and muscle fiber extensions may help surgeons

objectively determine the incision location in order to minimize the obstetric trauma and the likelihood of postpartum pelvic floor disorders.

Our probes could be employed to estimate the EMG signal crosstalk, defined as undesirable EMG signals from other muscles arising from volume-propagation (De Luca, Kuznetsov, Gilmore, & Roy, 2012). Crosstalk has been a persistent problem in the community and can severely misdirect the interpretation of results (Bo & Sherburn, 2005). The complexity of the female pelvic floor musculature is a confounding factor. The MUAP propagation mapped on the high-density electrode grid surface, as shown in Figure 5.4, showed the possibility of quantifying the volume-propagation of one MU's activity. The superficial muscle MU (Figure 5.4a, potentially from the EAS) and intermediate muscle MU (Figure 5.4b, likely from the puborectalis muscle) caused crosstalk only to the neighboring two rows, with about half of the original strength; however, the deep muscle MU (Figure 5.4c, likely from the pubococcygeus muscle) caused a more severe crosstalk, evidenced by the MUAPs seen in two rows away from the row in which the IZ was located with less attenuated magnitudes. Localizations and quantifications of these surface interference patterns would provide references for the crosstalk estimation and signal restoration.

The EMG probes may help advance pelvic biomechanical modeling and muscle imaging research (Y. Peng, R. Khavari, et al., 2016). Many computational pelvic floor models have been developed recently to investigate the biomechanics of incontinence and prolapse (Chanda, Unnikrishnan, Roy, & Richter, 2015). Unfortunately, voluntary contraction of PFM/EAS has not been objectively considered in previously reported pelvic models because of the lack of appropriate techniques which can be used to quantitatively characterize pelvic muscle contractions. As a consequence, the performance of current pelvic modeling and biomechanical analysis approaches is limited. Incorporating the EMG measurements of different PFMs with the proposed probes in this study makes it possible to objectively quantify pelvic muscle contractions. This in turn will allow a more realistic characterization of the dynamic deformation of the female pelvic floor.

One difficulty in this study was establishing the electrode-mucosa contact, a common challenge in such studies (Cescon et al., 2014; Enck & Vodusek, 2006; Keshwani & McLean,

2015). The signal quality was affected by the subject's cooperation with the task and by the operator's experience and ability to use a proper amount of gel, relieve the subject's anxiety through communication and maintain correct probe placement. From these preliminary studies, we are gaining more experience and preparing for future tests in patients with incontinence. Another limitation is related to the MUAP detection technique. This technique provides information on only a representative MU pool because of factors such as the decomposition algorithm used and MU recruitment (R. Merletti, Holobar, & Farina, 2008). Alternatively, the complete quantification of MUs can be achieved by characterizing the number of functioning motor units (Gooch et al., 2014), which suggests another direction for future research.

In this study, we describe and discuss minimally invasive intravaginal and intrarectal probes that were successfully developed and applied in MUAP detection and analysis. Preliminary results of a study of ten healthy female subjects are reported. The main findings of this study are that the muscle activity from different muscle groups can be simultaneously captured and that the distributions of the innervation zones of the pelvic floor muscle and extremal anal sphincters can be mapped with the high-density intravaginal and intrarectal surface EMG probes. The innervation zone distribution information obtained using our probes will be valuable in helping physicians better diagnose neuromuscular injuries that lead to alterations of the innervation zone distributions in PFM and EAS.

CHAPTER 6 – Surface EMG Decomposition Based Motor Unit Number Estimation

6.1 Abstract

Objective: To advance the motor unit number estimation (MUNE) technique using high density surface electromyography (EMG) decomposition.

Methods: The K-means clustering convolution kernel compensation algorithm was employed to detect the single motor unit potentials (SMUPs) from high-density surface EMG recordings of the biceps brachii muscles in eight healthy subjects. Contraction forces were controlled at 10%, 20% and 30% of the maximal voluntary contraction (MVC). Achieved MUNE results and the representativeness of the SMUP pools were evaluated using a high-density weighted-average method.

Results: Mean numbers of motor units were estimated as 288 ± 132, 155 ± 87, 107 ± 99 and 132 ± 61 by using the developed new MUNE at 10%, 20%, 30% and 10-30% MVCs, respectively. Over 20 SMUPs were obtained at each contraction level, and the mean residual variances were lower than 10%.

Conclusions: The new MUNE method allows a convenient and non-invasive collection of a large size of SMUP pool with great representativeness. It provides a useful tool for estimating the motor unit number of proximal muscles.

Significance: The present new MUNE method successfully avoids the use of intramuscular electrodes or multiple electrical stimuli which is required in currently available MUNE techniques; as such the new MUNE method can minimize patient discomfort for MUNE tests.

6.2 Introduction

Motor unit number estimation (MUNE) techniques are clinically useful by estimating the number of functioning motor units in a muscle, which can serve as a biomarker for the progression of motor neuron diseases or neuromuscular disorders. Various MUNE methods have been developed since the incremental counting technique was introduced in 1971

(McComas, Fawcett, Campbell, & Sica, 1971). The main limitation with the incremental counting technique is the problem known as “alternation”, which leads to an erroneous overestimation of the MUNE. This problem attributes to the procedure that all stimuli are applied at a single site of the nerve, which results in possible alternative activations of two or more motor neurons at an incremental stimulus and complicates the separation of single motor neurons.

The multiple-point stimulation (MPS) method was then developed to solve this problem by activating different single axons at different sites along nerves (Doherty & Brown, 1993; Kadrie, Yates, Milner-Brown, & Brown, 1976). However, the MPS MUNE is not applicable to proximal muscles, as it is difficult to stimulate a proximal nerve at enough sites to obtain a sufficient amount of single motor unit potentials (SMUPs) (Gooch et al., 2014). This limitation also challenges the statistical method (Gooch et al., 2014), possibly because of the difficulty in steadily sustaining a large number of stimuli at several levels of intensity at proximal nerves that are often with a poor accessibility. Alternatively, the spike-triggered average (STA) method and its variation, the decomposition enhanced spike-triggered average (DE-STA) method, were developed to overcome this limitation (Boe, Stashuk, Brown, & Doherty, 2005; Boe, Stashuk, & Doherty, 2004; Doherty & Stashuk, 2003). The STA and DE-STA methods can be performed on both distal and proximal muscles, as SMUPs are obtained from voluntary contractions rather than multiple-points stimulation along nerve courses. However, the need of using intramuscular needle electromyography (EMG) electrodes to obtain the triggers for the construction of the SMUP pool in the STA or DE-STA methods makes them an invasive approach and demands much patient tolerance. A more advanced MUNE technique that is non-invasive and not limited to distal muscles will greatly help extend the applicability of current MUNE methods.

High density (HD) surface EMG techniques have become a powerful tool for clinical neurophysiology (X. Li et al., 2015; Roberto Merletti, Botter, Troiano, Merlo, & Minetto, 2009; Van Dijk Johannes, 2012; Yao et al., 2015). Non-invasive HD surface EMG recordings can be decomposed into constituent motor unit action potential trains which can be further employed to extract SMUPs in a non-invasive manner for MUNE studies. Many surface EMG decomposition algorithms have been developed over the last decade (M. Chen & Zhou, 2016; Aleš Holobar &

Damjan Zazula, 2007; A. Holobar & D. Zazula, 2007; Kleine, van Dijk, Lapatki, Zwarts, & Stegeman, 2007; Ning et al., 2015) and undergone extensive investigations and validations (Almousa et al., 2015; Holobar, Minetto, Botter, Negro, & Farina, 2010; Liu et al., 2015; Marateb et al., 2011) in human. However, these algorithms have yet been applied to MUNE for the extraction of SMUP samples. Van Dijk and coworkers recently pioneered the application of the HD surface EMG in MUNE (J. Van Dijk et al., 2010; J. P. van Dijk et al., 2008; J. P. van Dijk et al., 2010). This method offered a comprehensive way to calculate MUNE and evaluate the representativeness of SMUP samples based on the HD information. However, this HD MUNE was essentially based on the multiple-points stimulation and therefore the applicability to proximal muscles remains unmet.

In this study, we present a new MUNE method that combines our earlier experience in HD surface EMG decomposition (Liu et al., 2015; Ning et al., 2015) and advantages offered by existing HD MUNE methods (J. P. van Dijk et al., 2008). This new method is non-invasive in nature and not limited by the locations of muscle.

6.3 Materials and Methods

6.3.1 Subjects

A total of 8 healthy and physically active male subjects (mean age: 29 ± 4) participated in this study, and none of them has a history of peripheral nerve disease. The research protocol was approved by the local ethic committee and all subjects were fully informed of the purpose and goal of the study and gave informed consents. The biceps brachii muscles of the dominant hand were investigated.

6.3.2 Stimulating and Recording Systems

The musculocutaneous nerve was stimulated using the DS7 current stimulator (Digitimer Ltd, Welwyn Garden City, United Kingdom) with a bipolar stimulating electrode by an experienced physician (S.L.). High-density surface EMG signals of the biceps brachii muscles were recorded using two 2 flexible 8 × 8 arrays (TMSi, Enschede, The Netherlands) with an electrode diameter of 4.5 mm, and a center-to-center electrode distance of 8.5 mm, as shown in Figure 6.1a. This

HD EMG grid showed great competency in our previous EMG analysis including EMG decomposition (Liu et al., 2015). The EMG signals were acquired by a 136 channel Refa amplifier (TMSi, Enschede, The Netherlands) at a sampling rate of 2048 Hz per channel and stored in a personal laptop for offline analysis.

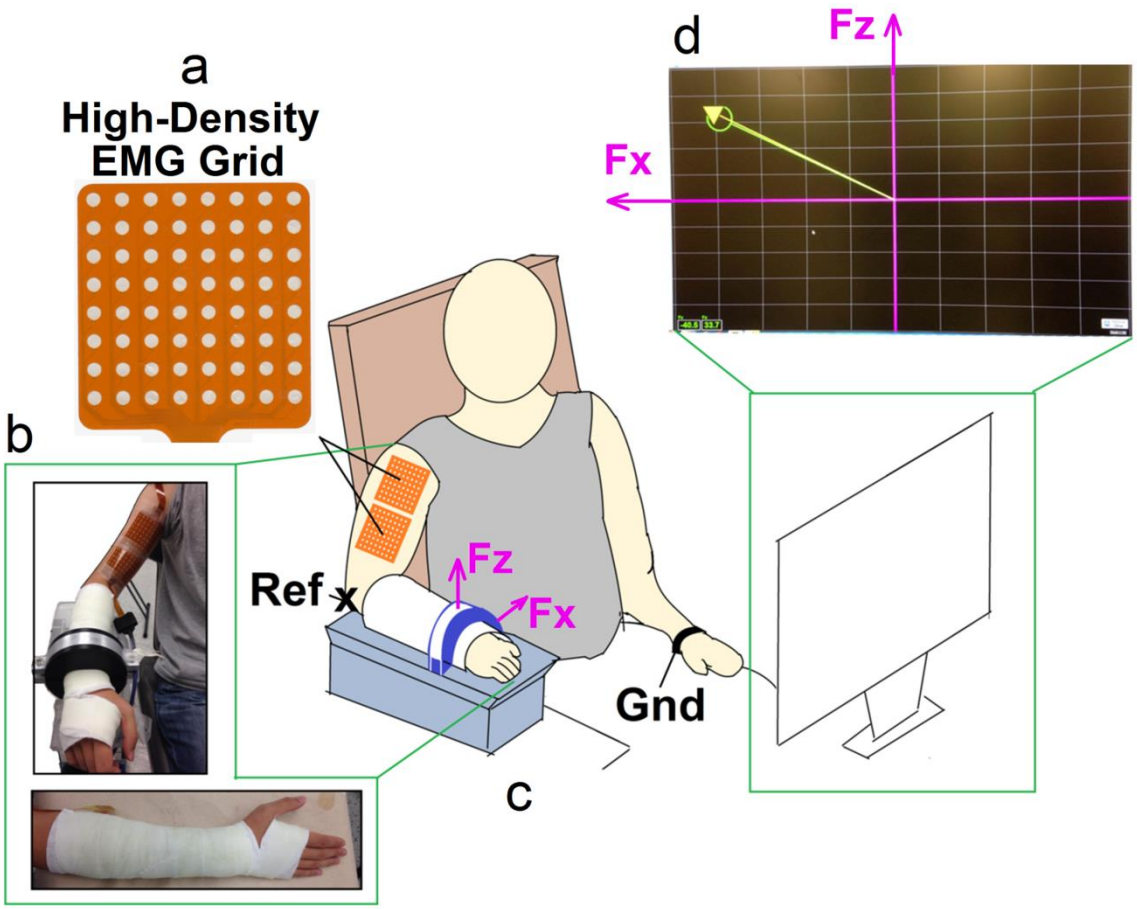

Figure 6.1 Illustration of the experimental setup. Reproduced from Y. Peng, J. He, B. Yao, et al. (2016), with permission of Elsevier.

6.3.3 Experimental Protocol

An earlier study demonstrated that the force level is an important factor to consider when utilizing voluntary contractions to provide SMUPs (Boe et al., 2005). Therefore, contraction force levels were rigorously controlled in our study. Each subject was seated upright in a mobile Biodex chair (Biodex, Shirley, NY) with a standard 6 degrees-of-freedom load cell (ATI Inc, Apex, NC) setup used to accurately record the isometric contraction force of the biceps brachii during

flexion. The forearm and wrist were mounted on a plastic platform inside a fiberglass cast (Figure 6.1b). A ring-mount interface was used to strap the wrist in a partial pronation position. This standard position served to minimize spurious force contributions from unrecorded muscles. The skin above the biceps brachii muscle was slightly abraded and cleaned. Two EMG grids were placed adjacently over the muscle belly and longitudinally along the muscle fiber direction. Double-sided tapes with electrode-matched holes were used to stick the grid surface to the skin to enhance the electrode-tissue contact with the help of conductive gels. The reference electrode was placed on the skin above the elbow of the arm on the same side of the EMG grids. A strap ground electrode was wrapped around the wrist on the contrary side. Monopolar surface EMG signals were obtained at each channel relative to the reference electrode.

The protocol to obtain the compound muscle action potential (CMAP) was adopted from our previous study (S. Li, Liu, Bhadane, Zhou, & Rymer, 2014). Briefly, trial electrical stimulation was first performed in an attempt to determine the optimal stimulation position that produced the maximal evoked CMAP. After the optimal stimulation position was localized and fixed, a series of stimuli was delivered with the stimulus strength increasing manually from 5 mA (in increments of 5 mA) to the strength when a supramaximal response was reached. Each stimulus was a rectangular pulse with a width of 200μs. The supramaximal stimulation was repeated for three times and the largest one was chosen as the source for the CMAP signal. After the stimulation, participants were asked to perform maximal voluntary contractions (MVC) for three times with the contraction force vector in the *x* and *z* direction measured, as shown in Figure 6.1. The averaged force vector was taken as the effective MVC. Subsequently, the participants were asked to perform a series of voluntary contractions at different percentage levels of MVC with visual feedback displayed on the computer screen controlled by a load cell (Figure 6.1d). For each subject, voluntary contractions were performed at three levels (10%, 20% and 30% MVC) and repeated for 3 times at each level. Each repetition lasted approximately 8 seconds. Subjects were given sufficient recovery time between any two consecutive contractions to minimize fatigue. The order of the contraction levels were randomized by the operator prior to each session (Boe, Stashuk, & Doherty, 2006).

6.3.4 Data Analysis

All data analysis was performed offline using Matlab (The Mathworks, Natick, MA). The surface EMG recordings were digitally bandpass filtered (10–500 Hz). Channels with poor signal qualities due to bad contacts were visually identified and removed from analysis.

A number of signal decomposition methods such as the wavelet-based decomposition and blind source decomposition can be employed to decompose the surface EMG signals into their constituent motor unit action potential trains. The wavelet-based algorithms are challenged by the high superimposition of the motor unit action potentials (Gazzoni, Farina, & Merletti, 2004), which are frequently encountered in EMG signals at moderate contraction levels.

Our recently developed K-mean clustering convolution kernel compensation (KmCKC) algorithm provides a suitable candidate for this purpose and was employed in this study to decompose the high-density surface EMG signals into SMUPs (Ning et al., 2015).

In the first step, the correlation matrix between the interferential measurements of all channels was calculated (Aleš Holobar & Damjan Zazula, 2007; A. Holobar & D. Zazula, 2007; Ning et al., 2015). This correlation matrix implicitly describes the firing patterns of all motor units (global pulse train) and can be further decomposed to extract the initial pulse trains (or trigger points) of different motor units through an appropriate selection of time instants to estimate the activity index of the global pulse train.

The K-means clustering technique was then employed to cluster the firing instants of individual motor units via evaluating a distance function (Ning et al., 2015). During this process, the initial pulse train can be estimated by choosing an appropriate number of clustered groups and time instants so that the firing instants of a single motor unit can be gathered into one group as completely as possible.

Then an improved multi-step iterative convolution kernel compensation method was employed to update the estimated initial pulse train to improve the decomposition accuracy. The final results of the decomposition method provide the intelligent trigger points of each identified motor unit and their waveforms can be constructed using the spike-triggered averaging (STA) method. It should be noted that our method is essentially different from STA or DE-STA MUNE methods, as the

spatiotemporal information from high-density EMG recordings was utilized to obtain intelligent triggers, avoiding the need of an invasive intramuscular needle electrode as used in DE-STA methods.

Each decomposed SMUP was stored as an array with a window size of 205 samples (~ 0.1 seconds) at each of the 128 channels. For simplicity, we use $SMUP_i(k; t)$ to represent the signals of the k-th channel of the i-th SMUP as a function of time sample t, where $1 \le k \le 128$, $1 \le t \le 205$.

First, all SMUPs obtained from the same repetition were compared by checking their firing sequences and waveforms. SMUPs with close firing sequences (difference < 1ms) or with similar waveforms were considered to originate from the same motor unit. This step was performed by the operator right after the decomposition results from each repetition were obtained. Then the entire SMUP pool, containing SMUPs from all repetitions of all MVCs, was systematically checked by calculating a modified channel-weighted correlation coefficient between any pair of SMUPs, as defined in Eq.(6.1):

$$M_{i,j} = \sum_{k=1}^{128} \left[W_{i,j}(k) \times Corr_{i,j}(k) \times Amp_{i,j}(k) \right], \qquad \text{Eq.(6.1)}$$

where $W_{i,j}(k)$ is the weight assigned to the k-th channel (k = 1,2,…,128), $Corr_{i,j}(k)$ and $Amp_{i,j}(k)$ measure the similarity in the waveform and amplitude between the k-th channels of the i-th SMUP and the j-th SMUP, respectively. Their definitions are provided in Eq. (6.2-6.4):

$$W_{i,j}(k) = A_i(k) \times A_j(k) / \sum_{m=1}^{128} A_i(m) \times A_j(m), \qquad \text{Eq.(6.2)}$$

where $A_i(k)$ is the negative peak amplitude of k-th channel of the i-th SMUP and m is the dummy index used to calculate the sum of the negative peak amplitude product over all channels,

$$Corr_{i,j}(k) = corrcoef \left[SMUP_i(k;t), \quad SMUP_j(k;t) \right], \qquad \text{Eq.(6.3)}$$

where *corrcoef* calculates the correlation coefficient between these two channels. Before the calculation, the two SMUPs were aligned by their onset time, defined as the time of instants of the largest negative peak among all channels, and

$$Amp_{i,j}(k) = 1 - \left|A_i(k) - A_j(k)\right| / 100\mu V,\ if\ \left|A_i(k) - A_j(k)\right| < 100\mu V. \quad \text{Eq.(6.4-a)}$$

$$Amp_{i,j}(k) = 0, else. \quad \text{Eq.(6.4-b)}$$

The introduction of this modified correlation coefficient was inspired by the work of J. P. van Dijk et al. (2008), who proposed the weighted-average method for the calculation of MUNE from high-density surface EMG signals. In addition to using correlation as a means to check multiples, we also introduced the criteria based on the SMUP size, which is defined as the largest negative peak amplitude among all channels throughout this study, given that correlation alone does not tell the differences in amplitudes.

SMUPs obtained from higher MVC levels may have high correlations but differ greatly in SMUP sizes. In our study, we employed an empirical value of 100μV to design the criteria in Eq.(6.4). The preliminary results suggested that two SMUPs are likely the same if the modified correlation coefficient is over 0.9 and less likely if it is less than 0.8. All SMUPs with a modified correlation coefficient larger than 0.8 were visually judged by the operator by comparing their waveforms and residuals (J. P. van Dijk et al., 2008).

The MUNE and residual variance (RV) were calculated following a similar approach introduced in (J. P. van Dijk et al., 2008). First, all SMUPs in the pool were aligned by their onset instants. The mean SMUP was then obtained by averaging all SMUPs, yielding a high-density mean SMUP that is representative for the entire SMUP pool. This mean SMUP was later aligned with the CMAP at their onset instants. The calculation of the MUNE was described in Eq. (6.5):

$$MUNE = \sum_{k=1}^{128} w_{meanSMUP}(k) A_{CMAP}(k) / A_{meanSMUP}(k), \quad \text{Eq.(6.5)}$$

where $A_{CMAP}(k)$ and $A_{meanSMUP}(k)$ are the negative peak amplitudes of *k*-th channels of the CMAP signal and the mean SMUP signal, respectively; the weight function $w(k)$ for calculating the MUNE, as described in Eq. (6.6), can be interpreted as the particular case of Eq. (6.2), when the *i*-th and *j*-th SMUPs are both replaced by the mean SMUP:

$$w_{meanSMUP}(k) = A^2_{meanSMUP}(k) / \sum_{m=1}^{128} A^2_{meanSMUP}(m). \quad \text{Eq.(6.6)}$$

To evaluate the representativeness, the RV was calculated using Eq. (6.7):

$$RV = \sum_{m=1}^{128} [A_{CMAP}(m) - MUNE \times A_{meanSMUP}(m)]^2 / \sum_{m=1}^{128} A^2_{CMAP}(m). \quad \text{Eq.(6.7)}$$

MUNE and RV were calculated separately at each MVC level as well as all MVCs. The CMAP was kept the same for all MUNE calculations.

6.4 Results

Main results achieved in this study are summarized in Table 6.1. The average CMAP across the eight subjects was 17.5 ± 3.3 mV. Initially, 1338 SMUPs were obtained from EMG decomposition results using the KmCKC algorithm, and 557 non-repeated SMUPs were kept after removing multiples for further analysis.

For all eight subjects, at 10%, 20% and 30% MVCs, the mean number of SMUPs obtained from three repetitions was 23 ± 5, 23 ± 6 and 26 ± 7, with a mean SMUP size (measured as the amplitude of the largest negative peak among all channels) of 91.3 ± 42.6 μV, 192.5 ± 96.0 μV and 350.8 ± 208.6 μV, respectively. Figure 6.2 shows the distribution of the SMUP sizes after removing multiples from all MVC levels of all eight subjects. Figure 6.3 shows the overlapping plot of the SMUPs obtained from three contraction levels for one exemplary subject.

The mean MUNE values obtained at three contraction levels for all subjects were 288 ± 132, 155 ± 87 and 107 ± 99, respectively. When SMUPs from all MVC levels were used, the mean SMUP size and MUNE were 214.0 ± 124.2 μV and 132 ± 61.

The mean RVs of 9.3% ± 5.9%, 10.1% ± 7.0% and 9.1% ± 5.8% were achieved at 10%, 20% and 30% MVCs, respectively, with an accumulative mean RV of 9.6% ± 6.0% for all MVC levels. Figure 6.4 shows the overlapping plot of the mean SMUP and the CMAP for exemplary subjects.

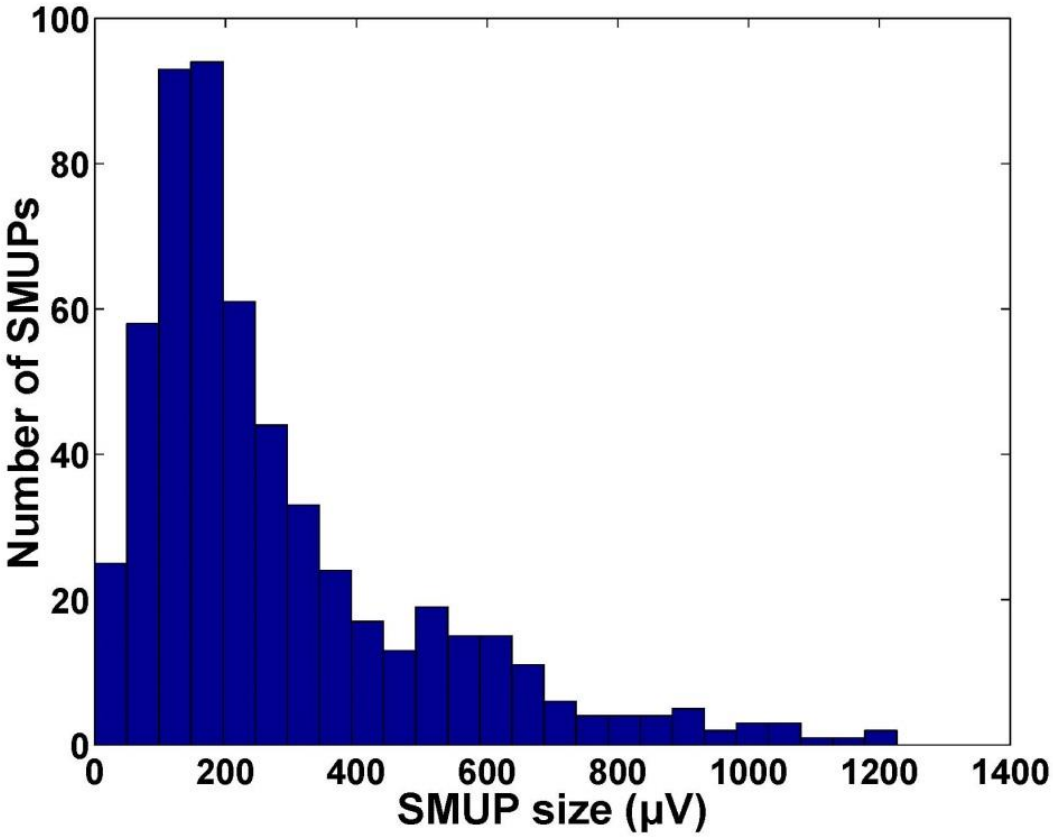

Figure 6.2 Histogram of all SMUP sizes for all eight subjects. The SMUP size was represented by the largest negative peak amplitude among all channels. Reproduced from Y. Peng, J. He, B. Yao, et al. (2016), with permission of Elsevier.

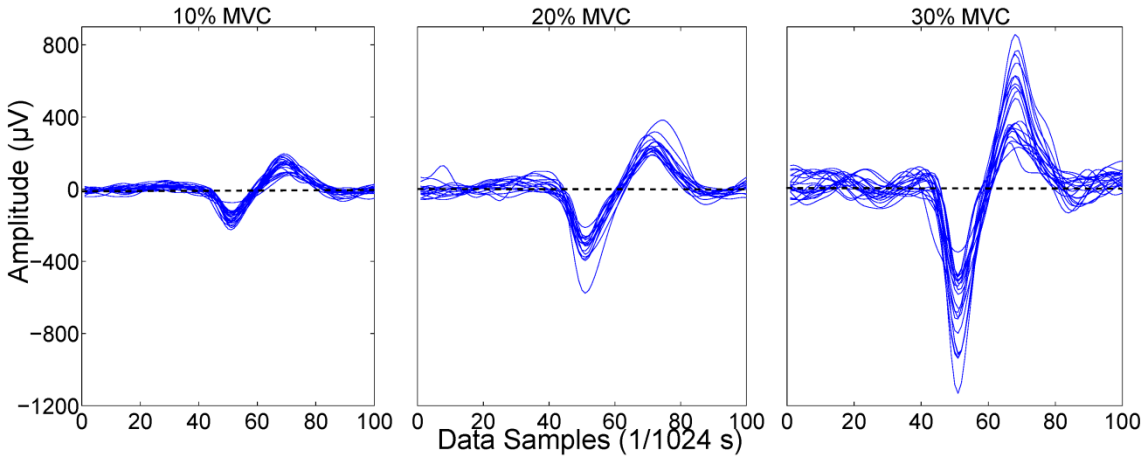

Figure 6.3 Overlapping plot of SMUPs obtained at three contraction levels for subject 6 (with multiples removed) in one channel. Reproduced from Y. Peng, J. He, B. Yao, et al. (2016), with permission of Elsevier.

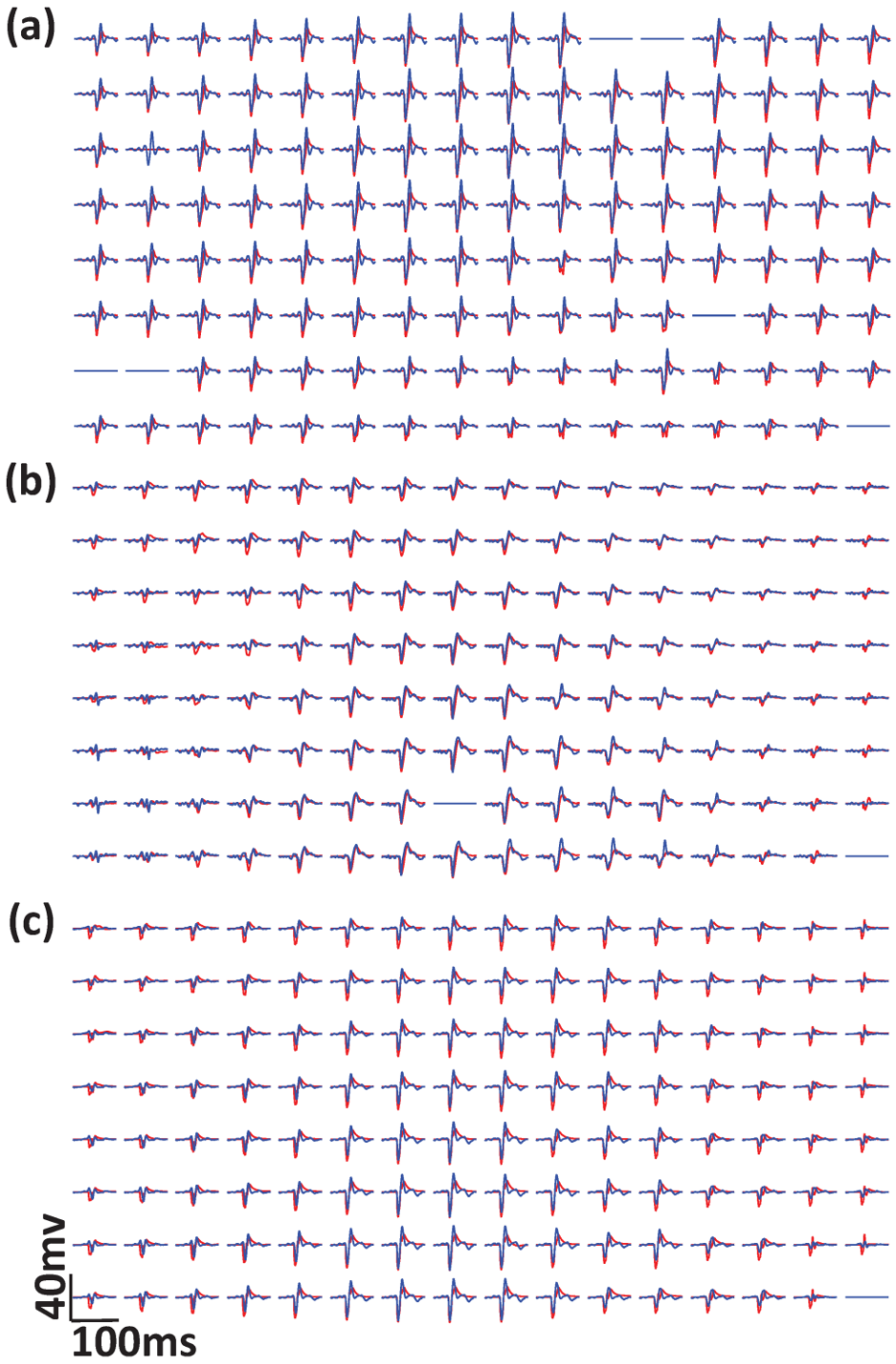

Figure 6.4 Spatiotemporal profiles of the mean SMUP (blue) and CMAP (red) for three subjects. Reproduced from Y. Peng, J. He, B. Yao, et al. (2016), with permission of Elsevier.

Table 6.1. CMAP, SMUP sizes, RV, MUNE at 10%, 20%, 30% and all levels for the biceps brachii

ID	CMAP	10% MVC			20% MVC			30% MVC			All MVCs (10% - 30%)		
		SMUP (No.)	RV (%)	MUNE	SMUP (No.)	RV (%)	MUNE	SMUP (No.)	RV (%)	MUNE	SMUP (No.)	RV (%)	MUNE
1	20.0	65.4 (19)	2	358	115.6 (20)	6	230	131.2 (21)	3	194	104.1 (60)	4	246
2	16.3	88.5 (28)	14	178	189.6 (30)	24	106	443.1 (34)	22	45	251.0 (92)	23	78
3	19.9	52.7 (18)	18	442	116.9 (30)	13	177	196.8 (35)	14	112	135.3 (83)	14	159
4	10.7	30.8 (20)	16	522	83.7 (13)	12	194	148.5 (25)	9	90	90.2 (58)	11	153
5	15.3	89.3 (35)	11	227	181.3 (25)	15	124	193.2 (12)	6	100	111.6 (47)	8	177
6	17.9	145.7 (22)	5	168	275.6 (16)	6	90	556.7 (21)	7	45	327.0 (59)	6	76
7	17.6	166.8 (22)	6	129	400.0 (29)	7	56	748.2 (31)	7	31	469.1 (82)	7	49
8	22.0	91.0 (22)	2	279	177.5 (24)	2	137	388.7 (29)	6	77	226.9 (75)	4	120
Ave	17.5	91.3 (23)	9.3	288	192.5 (23)	10.1	155	350.8 (26)	9.1	107	214.0 (70)	9.6	132
SD	3.3	42.6 (5)	5.9	132	96.0 (6)	7.0	87	208.6 (7)	5.8	99	124.2 (15)	6.0	61

* CMAP in mV, SMUP in μV
* CMAP and SMUP sizes are represented by the largest negative peak among all channels
Reproduced from Y. Peng, J. He, B. Yao, et al. (2016), with permission of Elsevier.

6.5 Discussion and Conclusions

In this study, we developed a novel MUNE method based on non-invasive high-density surface EMG decomposition and evaluated its performance on the biceps brachii muscles in eight healthy subjects.

6.5.1 Decomposition and Representativeness

A large pool of SMUPs (mean number > 20) was collected at each MVC level, with a high representativeness (mean RV < 10%). The uniformly low RV values in all MVC levels suggest that a representative SMUP pool can be well constructed under a fixed MVC below 30%, as long as a sufficiently large SMUP pool size is feasible. When all MVC levels were considered, more than 60 non-repeating SMUPs were available to provide a reliable estimation of the mean SMUP. This is reflected in the overlapping plot of the CMAP and the scaled mean SMUP using SMUPs from all MVCs, as shown in Figure 6.4, where great matches in waveforms are observed. The distribution of SMUP sizes across all subjects, as shown in Figure 6.2, is in accordance with

previously reported studies (Galea, Fehlings, Kirsch, & McComas, 2001; J. P. van Dijk et al., 2008).

It should be noted that the SMUP detection with the KmCKC algorithm is not exhaustive. This is actually a common challenge to all surface EMG decomposition methods (M. Chen & Zhou, 2016; Aleš Holobar & Damjan Zazula, 2007; A. Holobar & D. Zazula, 2007; X. Li et al., 2015; Ning et al., 2015). We found that in our decomposition results, SMUPs detected at higher contraction levels were larger in amplitude than those detected at lower contraction levels, as shown in Figure 6.3. This is consistent with the findings in previous studies that undetected motor unit action potential usually comes from smaller motor units (Holobar et al., 2010).

6.5.2 MUNE

As the actual number of motor units in human biceps brachii muscles remains unavailable because of the difficulty in performing non-invasive anatomical count, we compared our results with previous MUNE studies on the same muscle. At the 10% MVC level, our MUNE is similar with the results reported in the literature (288 ± 132 vs. 272 ± 124) (Boe et al., 2006), in which the DE-STA MUNE was employed at the same MVC level. The MUNE value achieved in this study when all MVC levels are considered is close to the report of Galea et al. (2001) (132.3 ± 60.5 vs. 135.5 ± 64.6), in which an incremental stimulation method was employed. This similarity suggests that the SMUP pool obtained from an incremental stimulation may resemble the one constructed using SMUPs from voluntary contractions up to 30% MVC. By separating the SMUPs from different MVC levels, our results may explain the existing variations among reports employing different MUNE approaches when the same muscle group was studied (Gooch et al., 2014).

A decreasing trend of MUNEs against MVC levels was found, which is similar with the report of Boe et al. (2005), although a quantitative comparison was not available because different muscles were studied. We also find that the CMAP sizes established in our study (negative peak amplitude: 17.5 ± 3.3 mV) are much greater than reports of Boe et al. (2006) (negative peak amplitude: 11.9 ± 2.4 mV) and Calder, Hall, Lester, Inglis, and Gabriel (2005) (peak to peak amplitude: 13.5 ± 4.1 mV). However, we tend to believe that this increase was more reliable

because of the employment of the high-density surface EMG grid, which allowed the recording site with the largest evoked response to be detected. The small electrode size, which helped reduce the effect of action potential averaging over the skin surface (J. Van Dijk, Lowery, Lapatki, & Stegeman, 2009), is also believed to be a factor leading to a higher amplitude. Besides, cross-subject variations and sample size might play a role in causing this difference.

6.5.3 Significance

Although decomposition-based MUNE has been reported previously in DE-STA MUNEs (Boe et al., 2005; Boe et al., 2004; Doherty & Stashuk, 2003; Ives & Doherty, 2014), one distinguishing feature of our new MUNE approach is that it avoids using invasive intramuscular needle electrodes to obtain the triggers of SMUPs (Gooch et al., 2014). The SMUPs are rather obtained from the spatiotemporal information provided by non-invasive HD surface EMG recordings using the KmCKC algorithm (Ning et al., 2015). Previous high-density MUNE methods (J. P. van Dijk et al., 2008; J. P. van Dijk et al., 2010) are inherently based on the multiple-points stimulation technique. This technique is limited to distal muscles, as the stimulation needs to be performed at multiple points along the course of the nerve, allowing the collection of multiple SMUPs and reducing the problem of “alternation” (Gooch et al., 2014). For proximal muscles, a very limited portion of the nerve is accessible for electrical stimulation, making multiple site stimulation unavailable and results susceptible to “alternation”. Our method extends the application of the high-density MUNE method to proximal muscles, as the collection of SMUPs does not rely on multiple point stimulation along the course of the nerve, but rather on the high-density surface EMG signals during voluntary contractions. The MUNE can be estimated for both the distal and the proximal muscles, as the high-density surface electrode grid can be placed flexibly on both muscles.

It is worth mentioning that the motor unit number index (MUNIX) approach has gained increasing popularity for its convenience in implementation (Nandedkar, Barkhaus, & StÅlberg, 2010; Neuwirth, Nandedkar, StåLberg, & Weber, 2010) and its good reliability (Neuwirth et al., 2011). However, its performance is limited when a muscle has server atrophy, as it cannot properly determine whether the decrease in MUNIX is accompanied with a reduction of the motor

unit action potential amplitude (loss of muscle fibers) or an actual loss of motor units (X. Li, Nandedkar, & Zhou, 2016; X. Y. Li, Rymer, & Zhou, 2012). Compared with MUNIX, MUNE approaches have the advantage that the MUNE results reflect the actual motor unit size and number, but they are less convenient in implementation. The HD-MUNE method proposed in our study can greatly improve the efficiency of MUNE implementation. Compared with traditional MUNE approaches, e.g., the MPS MUNE in which multiple-points stimulations are required or the DE-STA MUNE in which multiple needle insertions are needed, the proposed HD-MUNE method only requires a few voluntary contractions each of which lasts less than 10 seconds while still maintaining a high yield of SMUPs. The duration of the entire procedure could be further significantly reduced if contractions are only performed at one fixed MVC level, as long as the fixed MVC level is kept the same for the purpose of consistently tracking of the disease progression. In addition, with promising decomposition results achieved (Yun Peng, Jinbao He, et al., 2015; Y. Peng, J. He, R. Khavari, et al., 2016), we expect to apply this new MUNE method on pelvic floor muscles, the motor unit number of which plays an important role in the pathophysiology of pelvic floor disorders but has never been estimated.

6.5.4 Limitations

One limitation of this study is the lack of an assessment of the test-retest reliability. On one hand, it remains our next step to assess the reproducibility of this new approach for its further applications in clinical practices. On the other hand, the fact that the surface EMG decomposition algorithm has been extensively validated (Holobar et al., 2010; Marateb et al., 2011; Martinez-Valdes, Laine, Falla, Mayer, & Farina, 2016; Ning et al., 2015) provides a solid basis to the accuracy and reliability of this new MUNE method. A remaining question is at which force level the MUNE should be performed. Answer to this question would be of great clinical significance, as it allows the selection of the optimal force level that makes the MUNE results most sensitive to the disease progression. Nevertheless, the large variation in the MUNE with force levels revealed in this study provides insights into the physiology of MUNE, and thus we recommend MUNE to be performed in a consistent testing condition.

6.5.5 Conclusions

In conclusion, we presented a new MUNE method based on the high-density surface EMG decomposition that can non-invasively assess both distal and proximal muscles with a high yield of representative SMUPs. It is expected to extend the applicability of MUNE methods to more challenging clinical applications.

CHAPTER 7 – Conclusions and Suggestions for Future Research

7.1 Summary of this Dissertation

In summary, specific aims stated in Section 1.4 have been successfully achieved.

Specific Aim # 1: to develop a subject-specific biomechanical pelvic model

- First, a subject-specific biomechanical pelvic model has been successfully developed based on high-resolution MR images.

- Next, this model was utilized to study and compare the relative importance of multiple pelvic floor structures to the urethral supporting function. Our results showed that the vaginal wall, the puborectalis muscle and the pubococcygeus muscle are the most important structures.

- Next, this model was utilized to study the dynamic biomechanics of an implanted suburethral sling at different implantation locations. The simulation results suggested that the mid-distal location represented the optimal location as it best restored the urethral support with a minimal cost of interactional force.

- Last, this model was utilized to study the situation for female athletic SUI, which occurs to young female athletes. By assigning proper boundary conditions, the model can accurately reflect the dynamics during a jump landing process. Our results suggested that urethral hypermobility may not be the major concern for urine leakage, compared with the elevated intravesical pressure.

Specific Aim # 2: to develop a subject-specific electrophysiological pelvic model

- First, a subject-specific electrophysiological pelvic model has been successfully developed based on our novel intra-vaginal and intra-rectal high-density surface EMG probes.

- Next, EMG signals were acquired from ten healthy subjects from both probes. Our advanced KmCKC decomposition algorithm was used to separate the single MUs from the raw EMG signals, with the IZ distribution described in a subject-specific manner.

- Additionally, we have successfully developed a novel motor unit number estimation algorithm. This MUNE method is based on the KmCKC decomposition and therefore is non-invasive and patient-friendly. Pilot results were reported based on EMG signals of the bicep brachii muscles of eight healthy subjects. This method is directly applicable to pelvic floor muscles when used in combination with our novel EMG probes.

7.2 Suggestions for Future Research

A number of new research areas can be explored based on the preliminary results summarized in this dissertation.

First, the biomechanical models can be improved by properly describing the active contraction component of the muscle. Doing so will allow us to investigate not only passive pressure activities such as coughing, but also active process such as lifting the pelvic floor muscle to preserve continence.

Second, as the urine is the current model is simplified as elastic solids, its fluid behavior can be realized in future efforts. Through the fluid-structure interaction analysis, the true urodynamics inside the bladder can be better characterized. Besides, the modeling method can also be applied to study male incontinence which is considered as one main complication after radical prostatectomy (Dias, Peng, Miles, et al., 2016).

Third, based on the electrophysiological model findings, more physiological factors can be included such as aging or childbirth. These factors are believed to affect the peripheral and/or central nerve systems that may alter the motor functions of pelvic floor muscles. It would be meaningful to look into these aspects in new studies with a larger population size.

Finally, the subject-specific biomechanical and electrophysiological modeling approaches can be applied to the new research area of fecal incontinence, which shared a lot in common with urinary incontinence (Neshatian et al., 2016; Peng, Neshatian, Khavari, Boone, & Zhang, 2016; Peng, Neshatian, Quigley, & Zhang, 2016). The biomechanics and electrophysiology of the external anal sphincter muscle as well levator ani muscle can be characterized with our modeling approaches. These would provide new insights into the mechanism of fecal continence and may provide useful objective measures for better clinical application.

REFERENCES

Abrams, P., Cardozo, L., Fall, M., Griffiths, D., Rosier, P., Ulmsten, U., van Kerrebroeck, P., Victor, A., & Wein, A. (2002). The standardisation of terminology of lower urinary tract function: report from the Standardisation Sub-committee of the International Continence Society. *American journal of obstetrics and gynecology, 187*(1), 116-126.

Afonso, J., Martins, P., Girao, M., Jorge, R. N., Ferreira, A., Mascarenhas, T., Fernandes, A., Bernardes, J., Baracat, E., & de Lima, G. R. (2008). Mechanical properties of polypropylene mesh used in pelvic floor repair. *International Urogynecology Journal, 19*(3), 375-380.

Alafraa, T., & Schick, E. (2008). Relation between Intra-abdominal pressure variation and urethral hypermobility : the urethral mobility index. *Poster Abstract at International Continence Society*.

Almousa, S., Moser, H., & Kitsoulis, G. (2015). The Prevalence of Urine Incontinence in Nulliparous Female Athletes: A Systematic Review. *International Urogynecology Journal, 26*, S65-S65.

ASHTON-MILLER, J. A., & DeLANCEY, J. (2007). Functional anatomy of the female pelvic floor. *Annals of the New York Academy of Sciences, 1101*(1), 266-296.

Bernasconi, F., Napolitano, V., Natale, F., Leone, V., Lijoi, D., & Cervigni, M. (2012). TVT SECUR™ System: Final results of a prospective, observational, multicentric study. *International Urogynecology Journal, 23*(1), 93-98.

Bø, K. (2004). Pelvic floor muscle training is effective in treatment of female stress urinary incontinence, but how does it work? *International Urogynecology Journal, 15*(2), 76-84.

Bø, K. (2012). Pelvic floor muscle training in treatment of female stress urinary incontinence, pelvic organ prolapse and sexual dysfunction. *World journal of urology, 30*(4), 437-443.

Bø, K. (2015). Exercise and Pelvic Floor Dysfunction in Female Elite Athletes. *Handbook of Sports Medicine and Science: The Female Athlete*, 76-85.

Bo, K., & Sherburn, M. (2005). Evaluation of female pelvic-floor muscle function and strength. *Phys Ther, 85*(3), 269-282.

Boe, S. G., Stashuk, D. W., Brown, W. F., & Doherty, T. J. (2005). Decomposition-based quantitative electromyography: Effect of force on motor unit potentials and motor unit number estimates. *Muscle Nerve, 31*(3), 365-373.

Boe, S. G., Stashuk, D. W., & Doherty, T. J. (2004). Motor unit number estimation by decomposition-enhanced spike-triggered averaging: Control data, test–retest reliability, and contractile level effects. *Muscle Nerve, 29*(5), 693-699.

Boe, S. G., Stashuk, D. W., & Doherty, T. J. (2006). Within-subject reliability of motor unit number estimates and quantitative motor unit analysis in a distal and proximal upper limb muscle. *Clin Neurophysiol, 117*(3), 596-603.

Bonney, V. (1923). On Diurnal Incontinence of Urine in Women. *BJOG: An International Journal of Obstetrics & Gynaecology, 30*(3), 358-365.

Boyadzhyan, L., Raman, S. S., & Raz, S. (2008). Role of Static and Dynamic MR Imaging in Surgical Pelvic Floor Dysfunction 1. *Radiographics, 28*(4), 949-967.

Boyd, G. P., Gregson, I., & Herbert, J. H. (2015). COMPRESSIBLE ELECTRODES: US Patent 20,150,148,881.

Brækken, I. H., Majida, M., Engh, M. E., & Bø, K. (2010). Morphological changes after pelvic floor muscle training measured by 3-dimensional ultrasonography: a randomized controlled trial. *Obstetrics & Gynecology, 115*(2, Part 1), 317-324.

Brandao, F. S., Parente, M. P., Rocha, P. A., Saraiva, M. T., Ramos, I. M., & Natal Jorge, R. M. (2016). Modeling the contraction of the pelvic floor muscles. *Comput Methods Biomech Biomed Engin, 19*(4), 347-356. doi: 10.1080/10255842.2015.1028031

Brandao, S., Parente, M., Mascarenhas, T., da Silva, A. R., Ramos, I., & Jorge, R. N. (2015). Biomechanical study on the bladder neck and urethral positions: simulation of impairment of the pelvic ligaments. *J Biomech, 48*(2), 217-223. doi: 10.1016/j.jbiomech.2014.11.045

Brandt, F. T., Lorenzato, F. R., Nobrega, L. V., Albuquerque, C. D., Falcao, R., & Araujo Junior, A. A. (2006). Intra-abdominal pressure measurement during ultrasound assessment of women with stress urinary incontinence: a novel model. *Acta Cir Bras, 21*(4), 237-241.

Brandt, F. T., Lorenzato, F. R. B., Nóbrega, L. V., Albuquerque, C. D. C., Falcão, R., & Araújo Júnior, A. A. d. (2006). Intra-abdominal pressure measurement during ultrasound assessment of women with stress urinary incontinence: a novel model. *Acta Cirúrgica Brasileira, 21*(4), 237-241.

Calder, K. M., Hall, L.-A., Lester, S. M., Inglis, J. G., & Gabriel, D. A. (2005). Reliability of the biceps brachii M-wave. *J Neuroeng Rehabil, 2*, 33-33. doi: 10.1186/1743-0003-2-33

Cescon, C., Bottin, A., Fernandez Fraga, X. L., Azpiroz, F., & Merletti, R. (2008). Detection of individual motor units of the puborectalis muscle by non-invasive EMG electrode arrays. *J Electromyogr Kinesiol, 18*(3), 382-389. doi: 10.1016/j.jelekin.2006.11.007

Cescon, C., Riva, D., Zacesta, V., Drusany-Staric, K., Martsidis, K., Protsepko, O., Baessler, K., & Merletti, R. (2014). Effect of vaginal delivery on the external anal sphincter muscle innervation pattern evaluated by multichannel surface EMG: results of the multicentre study TASI-2. *Int Urogynecol J, 25*(11), 1491-1499. doi: 10.1007/s00192-014-2375-0

Chanda, A., Unnikrishnan, V., Roy, S., & Richter, H. E. (2015). Computational Modeling of the Female Pelvic Support Structures and Organs to Understand the Mechanism of Pelvic Organ Prolapse: A Review. *Applied Mechanics Reviews, 67*(4), 040801. doi: Artn 040801 10.1115/1.4030967

Chantereau, P., Brieu, M., Kammal, M., Farthmann, J., Gabriel, B., & Cosson, M. (2014). Mechanical properties of pelvic soft tissue of young women and impact of aging. *Int Urogynecol J, 25*(11), 1547-1553. doi: 10.1007/s00192-014-2439-1

Chen, L., Ashton-Miller, J. A., & DeLancey, J. O. L. (2009). A 3D finite element model of anterior vaginal wall support to evaluate mechanisms underlying cystocele formation. *Journal of biomechanics, 42*(10), 1371-1377. doi: http://dx.doi.org/10.1016/j.jbiomech.2009.04.043

Chen, M., & Zhou, P. (2016). A Novel Framework Based on FastICA for High Density Surface EMG Decomposition. *IEEE Trans Neural Syst Rehabil Eng, 24*(1), 117-127. doi: 10.1109/TNSRE.2015.2412038

Chen, Z. W., Joli, P., Feng, Z. Q., Rahim, M., Pirro, N., & Bellemare, M. E. (2015). Female patient-specific finite element modeling of pelvic organ prolapse (POP). *J Biomech, 48*(2), 238-245. doi: 10.1016/j.jbiomech.2014.11.039

Chong, E. C., Khan, A. A., & Anger, J. T. (2011). The financial burden of stress urinary incontinence among women in the United States. *Current urology reports, 12*(5), 358-362.

Cobb, W. S., Burns, J. M., Kercher, K. W., Matthews, B. D., Norton, H. J., & Heniford, B. T. (2005). Normal intraabdominal pressure in healthy adults. *Journal of Surgical Research, 129*(2), 231-235.

Cornu, J.-N., Lizée, D., Sèbe, P., Peyrat, L., Ciofu, C., Cussenot, O., & Haab, F. (2012). TVT SECUR single-incision sling after 5 years of follow-up: the promises made and the promises broken. *European urology, 62*(4), 737-738.

Costantini, E., Lazzeri, M., & Porena, M. (2007). Managing Complications after Midurethral Sling for Stress Urinary Incontinence. *EAU-EBU Update Series, 5*(6), 232-240. doi: http://dx.doi.org/10.1016/j.eeus.2007.07.004

Costantini, S., Nadalini, C., Esposito, F., Valenzano, M. M., Risso, D., Lantieri, P., & Mistrangelo, E. (2005). Perineal ultrasound evaluation of the urethrovesical junction angle and urethral mobility in nulliparous women and women following vaginal delivery. *International Urogynecology Journal, 16*(6), 455-459.

Crystle, C. D., Charme, L. S., & Copeland, W. E. (1971). Q-TIP TEST IN STRESS URINARY INCONTINENCE. *Obstetrics and Gynecology, 38*(2), 313-&.

Da Roza, T., Brandão, S., Oliveira, D., Mascarenhas, T., Parente, M., Duarte, J. A., & Jorge, R. N. (2015). Football practice and urinary incontinence: relation between morphology, function and biomechanics. *Journal of biomechanics*.

Da Roza, T., de Araujo, M. P., Viana, R., Viana, S., Jorge, R. N., Bø, K., & Mascarenhas, T. (2012). Pelvic floor muscle training to improve urinary incontinence in young, nulliparous sport students: a pilot study. *International Urogynecology Journal, 23*(8), 1069-1073.

da Silva Borin, L. C. M., Nunes, F. R., & de Oliveira Guirro, E. C. (2013). Assessment of pelvic floor muscle pressure in female athletes. *Pm&r, 5*(3), 189-193.

Dai, Z., Peng, Y., Mansy, H. A., Sandler, R. H., & Royston, T. J. (2014). Comparison of Poroviscoelastic Models for Sound and Vibration in the Lungs. *J Vib Acoust, 136*(5), 0510121-5101211. doi: 10.1115/1.4026436

Dalrymple, K. J., Davis, S. E., Dwyer, G. B., & Moir, G. L. (2010). Effect of static and dynamic stretching on vertical jump performance in collegiate women volleyball players. *The Journal of Strength & Conditioning Research, 24*(1), 149-155.

Dalstra, M., Huiskes, R., Odgaard, A., & Van Erning, L. (1993). Mechanical and textural properties of pelvic trabecular bone. *Journal of biomechanics, 26*(4), 523-535.

Daneshgari, F., & Moore, C. (2006). Advancing the understanding of pathophysiological rationale for the treatment of stress urinary incontinence in women: the 'trampoline theory'. *BJU international, 98*(s1), 8-14.

De Luca, C. J., Kuznetsov, M., Gilmore, L. D., & Roy, S. H. (2012). Inter-electrode spacing of surface EMG sensors: reduction of crosstalk contamination during voluntary contractions. *J Biomech, 45*(3), 555-561. doi: 10.1016/j.jbiomech.2011.11.010

Del Vescovo, R., Piccolo, C. L., Della Vecchia, N., Giurazza, F., Cazzato, R. L., Grasso, R. F., & Zobel, B. B. (2014). MRI role in morphological and functional assessment of the levator ani muscle: Use in patients affected by stress urinary incontinence (SUI) before and after pelvic floor rehabilitation. *European journal of radiology, 83*(3), 479-486.

DeLancey, J. O. (1994). Structural support of the urethra as it relates to stress urinary incontinence: the hammock hypothesis. *American journal of obstetrics and gynecology, 170*(5), 1713-1723.

DeLancey, J. O. (2002). Fascial and muscular abnormalities in women with urethral hypermobility and anterior vaginal wall prolapse. *American journal of obstetrics and gynecology, 187*(1), 93-98.

DeLancey, J. O. (2010). Why do women have stress urinary incontinence? *Neurourology and urodynamics, 29*(S1), S13-S17.

DeLancey, J. O. L. (2002). Fascial and muscular abnormalities in women with urethral hypermobility and anterior vaginal wall prolapse. *American journal of obstetrics and gynecology, 187*(1), 93-98. doi: http://dx.doi.org/10.1067/mob.2002.125733

Derpapas, A., Digesu, G. A., Fernando, R., & Khullar, V. (2011). Imaging in urogynaecology. *International Urogynecology Journal, 22*(11), 1345-1356.

Dias, N., Peng, Y., Khavari, R., Nakib, N. A., Sweet, R. M., Timm, G. W., Erdman, A. G., Boone, T. B., & Zhang, Y. (2016). Pelvic floor dynamics during high-impact athletic activities: A computational modeling study. *Clinical Biomechanics*. doi: 10.1016/j.clinbiomech.2016.11.003

Dias, N., Peng, Y., Miles, B., Khavari, R., MacDonnell, V., Boone, T., & Zhang, Y. (2016). PD49-07 URETHRAL MOBILITY STUDY WITH A COMPUTATIONAL MODEL OF THE MALE PELVIS. *The Journal of urology, 195*(4), e1182-e1183.

Dietz, H. P. (2010). Pelvic floor ultrasound: a review. *American journal of obstetrics and gynecology, 202*(4), 321-334.

Dietz, H. P., & Simpson, J. M. (2008). Levator trauma is associated with pelvic organ prolapse. *Bjog, 115*(8), 979-984. doi: 10.1111/j.1471-0528.2008.01751.x

Doherty, T. J., & Brown, W. F. (1993). The estimated numbers and relative sizes of thenar motor units as selected by multiple point stimulation in young and older adults. *Muscle Nerve, 16*(4), 355-366.

Doherty, T. J., & Stashuk, D. W. (2003). Decomposition-based quantitative electromyography: Methods and initial normative data in five muscles. *Muscle Nerve, 28*(2), 204-211.

Dooley, Y., Kenton, K., Cao, G., Luke, A., Durazo-Arvizu, R., Kramer, H., & Brubaker, L. (2008). Urinary incontinence prevalence: results from the National Health and Nutrition Examination Survey. *The Journal of urology, 179*(2), 656-661.

Duckett, J., & Baranowski, A. (2013). Pain after suburethral sling insertion for urinary stress incontinence. *International Urogynecology Journal, 24*(2), 195-201.

Enck, P., Franz, H., Azpiroz, F., Fernandez-Fraga, X., Hinninghofen, H., Kaske-Bretag, K., Bottin, A., Martina, S., & Merletti, R. (2004). Innervation zones of the external anal sphincter in healthy male and female subjects. Preliminary results. *Digestion, 69*(2), 123-130. doi: 10.1159/000077878

Enck, P., Hinninghofen, H., Wietek, B., & Becker, H. D. (2004). Functional asymmetry of pelvic floor innervation and its role in the pathogenesis of fecal incontinence. *Digestion, 69*(2), 102-111. doi: 10.1159/000077876

Enck, P., & Vodusek, D. B. (2006). Electromyography of pelvic floor muscles. *J Electromyogr Kinesiol, 16*(6), 568-577. doi: 10.1016/j.jelekin.2006.08.007

Enhorning, G. (1961). Simultaneous recording of intravesical and intra-urethral pressure. A study on urethral closure in normal and stress incontinent women. *Acta chirurgica Scandinavica. Supplementum*, 1.

Feiner, B., & Maher, C. (2010). Vaginal mesh contraction: definition, clinical presentation, and management. *Obstetrics & Gynecology, 115*(2, Part 1), 325-330.

Galea, V., Fehlings, D., Kirsch, S., & McComas, A. (2001). Depletion and sizes of motor units in spinal muscular atrophy. *Muscle Nerve, 24*(9), 1168-1172.

Garely, A. D., & Noor, N. (2014). Diagnosis and surgical treatment of stress urinary incontinence. *Obstetrics & Gynecology, 124*(5), 1011-1027.

Gazzoni, M., Farina, D., & Merletti, R. (2004). A new method for the extraction and classification of single motor unit action potentials from surface EMG signals. *J Neurosci Methods, 136*(2), 165-177. doi: 10.1016/j.jneumeth.2004.01.002

Ghoniem, G., Stanford, E., Kenton, K., Achtari, C., Goldberg, R., Mascarenhas, T., Parekh, M., Tamussino, K., Tosson, S., & Lose, G. (2008). Evaluation and outcome measures in the

treatment of female urinary stress incontinence: International Urogynecological Association (IUGA) guidelines for research and clinical practice. *International Urogynecology Journal, 19*(1), 5-33.

Goldstick, O., & Constantini, N. (2014). Urinary incontinence in physically active women and female athletes. *Br J Sports Med, 48*(4), 296-298. doi: 10.1136/bjsports-2012-091880

Gooch, C. L., Doherty, T. J., Chan, K. M., Bromberg, M. B., Lewis, R. A., Stashuk, D. W., Berger, M. J., Andary, M. T., & Daube, J. R. (2014). Motor unit number estimation: a technology and literature review. *Muscle Nerve, 50*(6), 884-893. doi: 10.1002/mus.24442

Grape, H. H., Dedering, A., & Jonasson, A. F. (2009). Retest reliability of surface electromyography on the pelvic floor muscles. *Neurourol Urodyn, 28*(5), 395-399. doi: 10.1002/nau.20648

Hägglund, D., & Wadensten, B. (2007). Fear of humiliation inhibits women's care-seeking behaviour for long-term urinary incontinence. *Scandinavian journal of caring sciences, 21*(3), 305-312.

Haridas, B., Hong, H., Minoguchi, R., Owens, S., & Osborn, T. (2006). PelvicSim—A computational-experimental system for biomechanical evaluation of female pelvic floor organ disorders and associated minimally invasive interventions. *Stud. Health Technol. Inf, 119*, 182-187.

Heilbrun, M. E., Nygaard, I. E., Lockhart, M. E., Richter, H. E., Brown, M. B., Kenton, K. S., Rahn, D. D., Thomas, J. V., Weidner, A. C., & Nager, C. W. (2010). Correlation between levator ani muscle injuries on magnetic resonance imaging and fecal incontinence, pelvic organ prolapse, and urinary incontinence in primiparous women. *American journal of obstetrics and gynecology, 202*(5), 488. e481-488. e486.

Holobar, A., Minetto, M. A., Botter, A., Negro, F., & Farina, D. (2010). Experimental analysis of accuracy in the identification of motor unit spike trains from high-density surface EMG. *IEEE Trans Neural Syst Rehabil Eng, 18*(3), 221-229.

Holobar, A., & Zazula, D. (2007). Gradient convolution kernel compensation applied to surface electromyograms *ICA 2007* (pp. 617-624): Springer.

Holobar, A., & Zazula, D. (2007). Multichannel Blind Source Separation Using Convolution Kernel Compensation. *Signal Processing, IEEE Transactions on, 55*(9), 4487-4496. doi: 10.1109/TSP.2007.896108

Hunskaar, S., Burgio, K., Clark, A., Lapitan, M., Nelson, R., Sillen, U., & Thom, D. (2005). Epidemiology of urinary (UI) and faecal (FI) incontinence and pelvic organ prolapse (POP). *Incontinence, 1*, 255-312.

Imamura, M., Abrams, P., Bain, C., Buckley, B., Cardozo, L., Cody, J., Cook, J., Eustice, S., Glazener, C., & Grant, A. (2010). Systematic review and economic modelling of the effectiveness and cost-effectiveness of non-surgical treatments for women with stress urinary incontinence. *Health Technology Assessment*.

Itani, M., Kielar, A., Menias, C. O., Dighe, M. K., Surabhi, V., Prasad, S. R., O'Malley, R., Gangadhar, K., & Lalwani, N. (2016). MRI of female urethra and periurethral pathologies. *International Urogynecology Journal, 27*(2), 195-204.

Ives, C. T., & Doherty, T. J. (2014). Influence of needle electrode depth on DE-STA motor unit number estimation. *Muscle Nerve, 50*(4), 587-592. doi: 10.1002/mus.24208

Jácome, C., Oliveira, D., Marques, A., & Sá-Couto, P. (2011). Prevalence and impact of urinary incontinence among female athletes. *International Journal of Gynecology & Obstetrics, 114*(1), 60-63.

Jing, D., Ashton-Miller, J. A., & DeLancey, J. O. (2012a). A subject-specific anisotropic visco-hyperelastic finite element model of female pelvic floor stress and strain during the second stage of labor. *Journal of biomechanics, 45*(3), 455-460.

Jing, D., Ashton-Miller, J. A., & DeLancey, J. O. L. (2012b). A subject-specific anisotropic visco-hyperelastic finite element model of female pelvic floor stress and strain during the second stage of labor. *Journal of biomechanics, 45*(3), 455-460. doi: http://dx.doi.org/10.1016/j.jbiomech.2011.12.002

Kadrie, H., Yates, S., Milner-Brown, H., & Brown, W. (1976). Multiple point electrical stimulation of ulnar and median nerves. *J Neurol Neurosurg Psychiatry, 39*(10), 973-985.

Karateke, A., Haliloglu, B., Cam, C., & Sakalli, M. (2009). Comparison of TVT and TVT-O in patients with stress urinary incontinence: Short-term cure rates and factors influencing the outcome. A prospective randomised study. *Australian and New Zealand journal of obstetrics and gynaecology, 49*(1), 99-105. doi: 10.1111/j.1479-828X.2009.00957.x

Kelly, H. A., & Dumm, W. M. (1914). Urinary incontinence in women, without manifest injury to the bladder: A report of cases. *Surg Gynecol Obstet, 18*, 444–450.

Keshwani, N., & McLean, L. (2015). State of the art review: intravaginal probes for recording electromyography from the pelvic floor muscles. *Neurourology and urodynamics, 34*(2), 104-112.

Kleine, B. U., van Dijk, J. P., Lapatki, B. G., Zwarts, M. J., & Stegeman, D. F. (2007). Using two-dimensional spatial information in decomposition of surface EMG signals. *J Electromyogr Kinesiol, 17*(5), 535-548.

Kociszewski, J., Rautenberg, O., Kolben, S., Eberhard, J., Hilgers, R., & Viereck, V. (2010). Tape functionality: position, change in shape, and outcome after TVT procedure—mid-term results. *International Urogynecology Journal, 21*(7), 795-800.

Kociszewski, J., Rautenberg, O., Perucchini, D., Eberhard, J., Geissbühler, V., Hilgers, R., & Viereck, V. (2008). Tape functionality: sonographic tape characteristics and outcome after TVT incontinence surgery. *Neurourology and urodynamics, 27*(6), 485-490.

Krcmar, M., Krofta, L., Urbankova, I., Reisl, J. F., Havelkova, L., & Hyncik, L. (2015). *BIOMECHANICAL PROPERTIES OF LEVATOR ANI MUSCLE USED FOR VIRTUAL MODEL OF PELVIC FLOOR.* Paper presented at the International Urogynecology Journal.

Kruger, J., Dietz, H., & Murphy, B. (2007). Pelvic floor function in elite nulliparous athletes. *Ultrasound in obstetrics & gynecology, 30*(1), 81-85.

Li, S., Liu, J., Bhadane, M., Zhou, P., & Rymer, W. Z. (2014). Activation deficit correlates with weakness in chronic stroke: evidence from evoked and voluntary EMG recordings. *Clin Neurophysiol, 125*(12), 2413-2417. doi: 10.1016/j.clinph.2014.03.019

Li, X., Holobar, A., Gazzoni, M., Merletti, R., Rymer, W. Z., & Zhou, P. (2015). Examination of Poststroke Alteration in Motor Unit Firing Behavior Using High-Density Surface EMG Decomposition. *IEEE Trans Biomed Eng, 62*(5), 1242-1252. doi: 10.1109/TBME.2014.2368514

Li, X., Nandedkar, S. D., & Zhou, P. (2016). Modified motor unit number index: A simulation study of the first dorsal interosseous muscle. *Med Eng Phys, 38*(2), 115-120. doi: 10.1016/j.medengphy.2015.11.002

Li, X. Y., Rymer, W. Z., & Zhou, P. (2012). A Simulation-Based Analysis of Motor Unit Number Index (MUNIX) Technique Using Motoneuron Pool and Surface Electromyogram Models. *Ieee Transactions on Neural Systems and Rehabilitation Engineering, 20*(3), 297-304. doi: 10.1109/Tnsre.2012.2194311

Liu, Y., Ning, Y., He, J., Li, S., Zhou, P., & Zhang, Y. (2014). Internal muscle activity imaging from multi-channel surface EMG recordings: a validation study. *Conf Proc IEEE Eng Med Biol Soc, 2014*, 3559-3561. doi: 10.1109/EMBC.2014.6944391

Liu, Y., Ning, Y., Li, S., Zhou, P., Rymer, W. Z., & Zhang, Y. (2015). Three-Dimensional Innervation Zone Imaging from Multi-Channel Surface EMG Recordings. *Int J Neural Syst, 25*(6), 1550024. doi: 10.1142/S0129065715500240

Luber, K. M. (2004). The definition, prevalence, and risk factors for stress urinary incontinence. *Reviews in urology, 6*(Suppl 3), S3.

Luginbuehl, H., Greter, C., Gruenenfelder, D., Baeyens, J., Kuhn, A., & Radlinger, L. (2013). Intra-session test–retest reliability of pelvic floor muscle electromyography during running. *International Urogynecology Journal, 24*(9), 1515-1522.

Luginbuehl, H., Naeff, R., Zahnd, A., Baeyens, J. P., Kuhn, A., & Radlinger, L. (2016). Pelvic floor muscle electromyography during different running speeds: an exploratory and reliability study. *Arch Gynecol Obstet, 293*(1), 117-124. doi: 10.1007/s00404-015-3816-9

Luo, J., Chen, L., Fenner, D. E., Ashton-Miller, J. A., & DeLancey, J. O. (2015). A multi-compartment 3-D finite element model of rectocele and its interaction with cystocele. *J Biomech, 48*(9), 1580-1586. doi: 10.1016/j.jbiomech.2015.02.041

Madill, S. J., & McLean, L. (2008). Quantification of abdominal and pelvic floor muscle synergies in response to voluntary pelvic floor muscle contractions. *J Electromyogr Kinesiol, 18*(6), 955-964. doi: 10.1016/j.jelekin.2007.05.001

Mangera, A., Bullock, A. J., Chapple, C. R., & MacNeil, S. (2012). Are biomechanical properties predictive of the success of prostheses used in stress urinary incontinence and pelvic organ prolapse? A systematic review. *Neurourology and urodynamics, 31*(1), 13-21.

Marateb, H. R., McGill, K. C., Holobar, A., Lateva, Z. C., Mansourian, M., & Merletti, R. (2011). Accuracy assessment of CKC high-density surface EMG decomposition in biceps femoris muscle. *J Neural Eng, 8*(6), 066002.

Martinez-Valdes, E., Laine, C. M., Falla, D., Mayer, F., & Farina, D. (2016). High-density surface electromyography provides reliable estimates of motor unit behavior. *Clin Neurophysiol, 127*(6), 2534-2541. doi: 10.1016/j.clinph.2015.10.065

Mayeur, O., Witz, J. F., Lecomte, P., Brieu, M., Cosson, M., & Miller, K. (2016). Influence of Geometry and Mechanical Properties on the Accuracy of Patient-Specific Simulation of Women Pelvic Floor. *Ann Biomed Eng, 44*(1), 202-212. doi: 10.1007/s10439-015-1401-9

McComas, A., Fawcett, P. R. W., Campbell, M., & Sica, R. (1971). Electrophysiological estimation of the number of motor units within a human muscle. *J Neurol Neurosurg Psychiatry, 34*(2), 121-131.

Merletti, R., Botter, A., Troiano, A., Merlo, E., & Minetto, M. A. (2009). Technology and instrumentation for detection and conditioning of the surface electromyographic signal: state of the art. *Clin Biomech, 24*(2), 122-134.

Merletti, R., Bottin, A., Cescon, C., Farina, D., Gazzoni, M., Martina, S., Mesin, L., Pozzo, M., Rainoldi, A., & Enck, P. (2004). Multichannel surface EMG for the non-invasive assessment of the anal sphincter muscle. *Digestion, 69*(2), 112-122. doi: 10.1159/000077877

Merletti, R., Holobar, A., & Farina, D. (2008). Analysis of motor units with high-density surface electromyography. *J Electromyogr Kinesiol, 18*(6), 879-890. doi: 10.1016/j.jelekin.2008.09.002

Minardi, D., Piloni, V., Amadi, A., El Asmar, Z., Milanese, G., & Muzzonigro, G. (2007). Correlation between urodynamics and perineal ultrasound in female patients with urinary incontinence. *Neurourology and urodynamics, 26*(2), 176.

Minassian, V. A., Drutz, H. P., & Al-Badr, A. (2003). Urinary incontinence as a worldwide problem. *International Journal of Gynecology & Obstetrics, 82*(3), 327-338.

Minassian, V. A., Stewart, W. F., & Wood, G. C. (2008). Urinary incontinence in women: variation in prevalence estimates and risk factors. *Obstetrics & Gynecology, 111*(2, Part 1), 324-331.

Molden, S. M., & Lucente, V. R. (2008). New minimally invasive slings: TVT Secur. *Current urology reports, 9*(5), 358-361.

Nandedkar, S. D., Barkhaus, P. E., & StÅlberg, E. V. (2010). Motor unit number index (MUNIX): principle, method, and findings in healthy subjects and in patients with motor neuron disease. *Muscle Nerve, 42*(5), 798-807.

Neshatian, L., Peng, Y., Zhang, C., Khavari, R., Boone, T., Quigley, M., & Zhang, Y. (2016). *Assessment of pelvic floor neuromuscular integrity by high-density surface electromyography.* Paper presented at the NEUROGASTROENTEROLOGY AND MOTILITY.

Neuwirth, C., Nandedkar, S., Stålberg, E., Barkhaus, P. E., de Carvalho, M., Furtula, J., van Dijk, J. P., Baldinger, R., Castro, J., & Costa, J. (2011). Motor Unit Number Index (MUNIX): A novel neurophysiological marker for neuromuscular disorders; test–retest reliability in healthy volunteers. *Clin Neurophysiol, 122*(9), 1867-1872.

Neuwirth, C., Nandedkar, S., StåLberg, E., & Weber, M. (2010). Motor unit number index (MUNIX): a novel neurophysiological technique to follow disease progression in amyotrophic lateral sclerosis. *Muscle Nerve, 42*(3), 379-384.

Ning, Y., Zhu, X., Zhu, S., & Zhang, Y. (2015). Surface EMG decomposition based on K-means clustering and convolution kernel compensation. *IEEE J Biomed Health Inform, 19*(2), 471-477. doi: 10.1109/JBHI.2014.2328497

Noblett, K., Jensen, J., & Ostergard, D. (1997). The relationship of body mass index to intra-abdominal pressure as measured by multichannel cystometry. *International Urogynecology Journal, 8*(6), 323-326.

Nygaard, I. E., & Heit, M. (2004). Stress urinary incontinence. *Obstetrics & Gynecology, 104*(3), 607-620.

Oliveira, R., Resende, A., Silva, C., Dinis, P., & Cruz, F. (2014). Mini-arc for the treatment of female stress urinary incontinence: long-term prospective evaluation by patient reported outcomes. *ISRN Urol, 2014*, 659383. doi: 10.1155/2014/659383

Osman, N. I., Marzi, V. L., Cornu, J. N., & Drake, M. J. (2016). Evaluation and Classification of Stress Urinary Incontinence: Current Concepts and Future Directions. *European Urology Focus*.

Parente, M., Jorge, R. N., Mascarenhas, T., Fernandes, A., & Martins, J. (2008). Deformation of the pelvic floor muscles during a vaginal delivery. *International Urogynecology Journal, 19*(1), 65-71.

Peng, Y., Dai, Z., Mansy, H. A., Sandler, R. H., Balk, R. A., & Royston, T. J. (2014). Sound transmission in the chest under surface excitation: an experimental and computational study with diagnostic applications. *Med Biol Eng Comput, 52*(8), 695-706. doi: 10.1007/s11517-014-1172-8

Peng, Y., He, J., Khavari, R., Boone, T., & Zhang, Y. (2015). PD24-03 IDENTIFICATION OF INNERVATION ZONES OF THE PELVIC FLOOR MUSCLE FROM NONINVASIVE HIGH-DENSITY INTRA-VAGINAL/RECTAL SURFACE EMG RECORDINGS. *The Journal of urology, 4*(193), e491.

Peng, Y., He, J., Khavari, R., Boone, T. B., & Zhang, Y. (2016). Functional mapping of the pelvic floor and sphincter muscles from high-density surface EMG recordings. *Int Urogynecol J, 27*(11), 1689-1696. doi: 10.1007/s00192-016-3026-4

Peng, Y., He, J., Yao, B., Li, S., Zhou, P., & Zhang, Y. (2016). Motor unit number estimation based on high-density surface electromyography decomposition. *Clin Neurophysiol, 127*(9), 3059-3065. doi: 10.1016/j.clinph.2016.06.014

Peng, Y., Khavari, R., Nakib, N. A., Boone, T. B., & Zhang, Y. (2016). Assessment of urethral support using MRI-derived computational modeling of the female pelvis. *Int Urogynecol J, 27*(2), 205-212. doi: 10.1007/s00192-015-2804-8

Peng, Y., Khavari, R., Nakib, N. A., Stewart, J. N., Boone, T. B., & Zhang, Y. (2015). The Single-Incision Sling to Treat Female Stress Urinary Incontinence: A Dynamic Computational Study of Outcomes and Risk Factors. *J Biomech Eng, 137*(9), 091007. doi: 10.1115/1.4030978

Peng, Y., Khavari, R., Stewart, J., Boone, T., & Zhang, Y. (2015). *COMPARISON OF FEMALE PELVIC FLOOR DEFORMATION BETWEEN JUMPING AND VALSALVA MANEUVER.* Paper presented at the Neurourology and urodynamics.

Peng, Y., Neshatian, L., Khavari, R., Boone, T., & Zhang, Y. (2016). *A Fluid-Structure Interaction Simulation of Fecal Incontinence.* Paper presented at the JOURNAL OF UROLOGY.

Peng, Y., Neshatian, L., Quigley, E. M., & Zhang, Y. (2016). Tu1782 Computational Modeling and Simulation of Fecal Incontinence-The Effect of Stool Consistency on Leakage. *Gastroenterology, 150*(4), S944.

Petros, P. E. P. (2011). *The female pelvic floor: function, dysfunction and management according to the integral theory*: Springer Science & Business Media.

Petros, P. E. P., & Ulmsten, U. I. (1990). An integral theory of female urinary incontinence. *Acta Obstetricia et Gynecologica Scandinavica, 69*(S153), 7-31.

Peyrat, L., Haillot, O., Bruyere, F., Boutin, J., Bertrand, P., & Lanson, Y. (2002). Prevalence and risk factors of urinary incontinence in young and middle-aged women. *BJU international, 89*(1), 61-66.

Pregazzi, R., Sartore, A., Bortoli, P., Grimaldi, E., Troiano, L., & Guaschino, S. (2002). Perineal ultrasound evaluation of urethral angle and bladder neck mobility in women with stress urinary incontinence. *BJOG: An International Journal of Obstetrics & Gynaecology, 109*(7), 821-827.

Ren, S., Xie, B., Wang, J. L., & Rong, Q. G. (2015). Three-Dimensional Modeling of the Pelvic Floor Support Systems of Subjects with and without Pelvic Organ Prolapse. *BioMed research international, 2015*. doi: Artn 845985

10.1155/2015/845985

Revicky, V., & Tincello, D. G. (2014). New surgical approaches for urinary incontinence in women. *Maturitas, 77*(3), 239-242. doi: 10.1016/j.maturitas.2013.12.008

RICHARDSON, A. C., EDMONDS, P. B., & WILLIAMS, N. L. (1981). Treatment of stress urinary incontinence due to paravaginal fascial defect. *Obstetrics & Gynecology, 57*(3), 357-362.

Richardson, A. C., Lyon, J. B., & Williams, N. L. (1976). A new look at pelvic relaxation. *American journal of obstetrics and gynecology, 126*(5), 568-571.

Rivlin, R. S., & Saunders, D. (1951). Large elastic deformations of isotropic materials. VII. Experiments on the deformation of rubber. *Philosophical Transactions of the Royal Society of London A: Mathematical, Physical and Engineering Sciences, 243*(865), 251-288.

Rogers, R. G. (2008). Urinary stress incontinence in women. *New England Journal of Medicine, 358*(10), 1029-1036.

Rostaminia, G., & Abramowitch, S. (2015). Finite Element Modeling in Female Pelvic Floor Medicine: a Literature Review. *Current Obstetrics and Gynecology Reports, 4*(2), 125-131.

Salvatore, S., Serati, M., Laterza, R., Uccella, S., Torella, M., & Bolis, P. (2009). The impact of urinary stress incontinence in young and middle-age women practising recreational sports activity: an epidemiological study. *British journal of sports medicine, 43*(14), 1115-1118.

Sendag, F., Vidinli, H., Kazandi, M., Itil, I. M., Askar, N., Vidinli, B., & Pourbagher, A. (2003). Role of perineal sonography in the evaluation of patients with stress urinary incontinence. *Australian and New Zealand journal of obstetrics and gynaecology, 43*(1), 54-57.

Sim, K., Chen, S., Li, Y., Kammoun, M., Peng, Y., Xu, M., Gao, Y., Song, J., Zhang, Y., Ardebili, H., & Yu, C. (2015). High Fidelity Tape Transfer Printing Based On Chemically Induced Adhesive Strength Modulation. *Sci Rep, 5*, 16133. doi: 10.1038/srep16133

Stafford, R. E., Sapsford, R., Ashton-Miller, J., & Hodges, P. W. (2010). A novel transurethral surface electrode to record male striated urethral sphincter electromyographic activity. *The Journal of urology, 183*(1), 378-385.

Systèmes, D. (2012). Abaqus v6. 12 Documentation-ABAQUS analysis user's manual. *Abaqus Inc, 6*.

Tunn, R., Goldammer, K., Neymeyer, J., Gauruder-Burmester, A., Hamm, B., & Beyersdorff, D. (2006). MRI morphology of the levator ani muscle, endopelvic fascia, and urethra in women with stress urinary incontinence. *European Journal of Obstetrics & Gynecology and Reproductive Biology, 126*(2), 239-245.

Van Dijk, J., Lowery, M., Lapatki, B., & Stegeman, D. (2009). Evidence of potential averaging over the finite surface of a bioelectric surface electrode. *Ann Biomed Eng, 37*(6), 1141-1151.

Van Dijk, J., Verhamme, C., Van Schaik, I., Schelhaas, H., Mans, E., Bour, L., Stegeman, D., & Zwarts, M. (2010). Age-related changes in motor unit number estimates in adult patients with Charcot–Marie–Tooth type 1A. *Eur J Neurol, 17*(8), 1098-1104.

Van Dijk Johannes, P. (2012). High-density surface EMG: Techniques and applications at a motor unit level. *Biocybern Biomed Eng, 32*(3), 3-27.

van Dijk, J. P., Blok, J. H., Lapatki, B. G., van Schaik, I. N., Zwarts, M. J., & Stegeman, D. F. (2008). Motor unit number estimation using high-density surface electromyography. *Clin Neurophysiol, 119*(1), 33-42.

van Dijk, J. P., Schelhaas, H. J., Van Schaik, I. N., Janssen, H. M., Stegeman, D. F., & Zwarts, M. J. (2010). Monitoring disease progression using high-density motor unit number estimation in amyotrophic lateral sclerosis. *Muscle Nerve, 42*(2), 239-244.

Verelst, M., & Leivseth, G. (2007). Force and stiffness of the pelvic floor as function of muscle length: A comparison between women with and without stress urinary incontinence. *Neurourology and urodynamics, 26*(6), 852-857.

Voorham-van der Zalm, P. J., Voorham, J. C., van den Bos, T. W., Ouwerkerk, T. J., Putter, H., Wasser, M. N., Webb, A., DeRuiter, M. C., & Pelger, R. C. (2013). Reliability and differentiation of pelvic floor muscle electromyography measurements in healthy volunteers using a new device: the Multiple Array Probe Leiden (MAPLe). *Neurourol Urodyn, 32*(4), 341-348. doi: 10.1002/nau.22311

Wang, Q., Zeng, H., Best, T. M., Haas, C., Heffner, N. T., Agarwal, S., & Zhao, Y. (2014). A mechatronic system for quantitative application and assessment of massage-like actions in small animals. *Ann Biomed Eng, 42*(1), 36-49. doi: 10.1007/s10439-013-0886-3

Wang, S., Zhou, Y., Tan, J., Xu, J., Yang, J., & Liu, Y. (2014). Computational modeling of magnetic nanoparticle targeting to stent surface under high gradient field. *Comput Mech, 53*(3), 403-412. doi: 10.1007/s00466-013-0968-y

Whitehead, W. E., Rao, S. S., Lowry, A., Nagle, D., Varma, M., Bitar, K. N., Bharucha, A. E., & Hamilton, F. A. (2015). Treatment of fecal incontinence: state of the science summary for the National Institute of Diabetes and Digestive and Kidney Diseases workshop. *Am J Gastroenterol, 110*(1), 138-146; quiz 147. doi: 10.1038/ajg.2014.303

Wu, J. M., Kawasaki, A., Hundley, A. F., Dieter, A. A., Myers, E. R., & Sung, V. W. (2011). Predicting the number of women who will undergo incontinence and prolapse surgery, 2010 to 2050. *American journal of obstetrics and gynecology, 205*(3), 230. e231-230. e235.

Yamada, H., & Evans, F. G. (1970). Strength of biological materials.

Yao, B., Zhang, X., Li, S., Li, X., Chen, X., Klein, C. S., & Zhou, P. (2015). Analysis of linear electrode array EMG for assessment of hemiparetic biceps brachii muscles. *Front Hum Neurosci, 9*, 569. doi: 10.3389/fnhum.2015.00569

Zhang, H., Nussbaum, M. A., & Agnew, M. J. (2015). A new method to assess passive and active ankle stiffness during quiet upright stance. *J Electromyogr Kinesiol, 25*(6), 937-943. doi: 10.1016/j.jelekin.2015.10.011

Zhang, H., Nussbaum, M. A., & Agnew, M. J. (2016). Development of a sliding mode control model for quiet upright stance. *Med Eng Phys, 38*(2), 204-208. doi: 10.1016/j.medengphy.2015.11.019

Zhang, J., Koo, B., Subramanian, N., Liu, Y., & Chattopadhyay, A. (2015). An optimized cross-linked network model to simulate the linear elastic material response of a smart polymer. *Journal of Intelligent Material Systems and Structures*, 1045389X15595292.

Zhang, Y., Kim, S., Erdman, A. G., Roberts, K. P., & Timm, G. W. (2009). Feasibility of using a computer modeling approach to study SUI induced by landing a jump. *Annals of biomedical engineering, 37*(7), 1425-1433.

Zhang, Y., Sweet, R. M., Metzger, G. J., Burke, D., Erdman, A. G., & Timm, G. W. (2009). Advanced finite element mesh model of female SUI research during physical and daily activities.

Zhou, D., Peng, Y., Bai, J., & Rosandich, R. G. (2014). CONTACT EFFECT EVALUATION USING STRESS DISTRIBUTION IN VISCOELASTIC MATERIAL UNDER GENERALIZED LOADING. *International Journal of Modelling and Simulation, 34*(4).